

USING TRANSIENT ELECTRICAL RESISTIVITY  
TO CHARACTERIZE AN ACTIVE  
HEAP LEACH SITE

By

JULIE A. TURRENTINE

Bachelor of Science

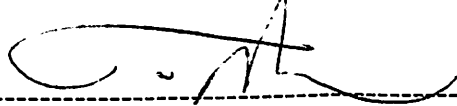
Oklahoma State University

2001

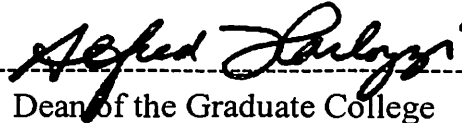
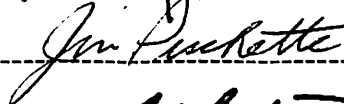
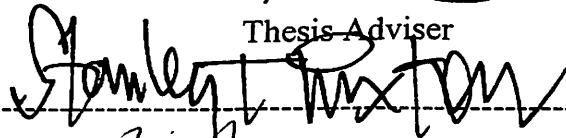
Submitted to the Faculty  
of the Graduate College of  
Oklahoma State University  
in Partial fulfillment of  
the requirements for  
the Degree of  
MASTER OF SCIENCE  
May, 2004

USING TRANSIENT ELECTRICAL RESISTIVITY  
TO CHARACTERIZE AN ACTIVE  
HEAP LEACH SITE

Thesis Approved:



Thesis Adviser



Dean of the Graduate College



## ACKNOWLEDGEMENTS

This research was made possible by the cooperation and funding assistance of Cortez Gold Mines. I would especially like to thank Jim Collord and Natalie Deringer for their availability and efforts to keep this project going despite long delays. Funding assistance from a GSA student research grant is also greatly appreciated.

A number of collaborators participated in this research effort. I particularly appreciate the help from Tom Fenstermaker, Geoff Webb, and Dr. Scott Tyler of the University of Nevada, Reno for helping set up the equipment and organizing the project so that I could fly in and quickly start collecting data.

I would also like to thank my advisor, Dr. Todd Halihan, for finding additional funding and projects for me over the last two years so that I could make this project into a thesis. Finally, I would like to thank my committee members, Dr. Puckette and Dr. Paxton, my friends, and family for their advice and support.

## TABLE OF CONTENTS

Chapter	Page
I. INTRODUCTION .....	1
Purpose and Goals.....	3
Objectives .....	3
Study Area .....	5
Lift Construction.....	5
Ore Geology.....	7
Leaching Solution Chemistry and Application.....	12
II. LITERATURE REVIEW .....	13
Electrical Resistivity .....	13
Traditional Applications .....	14
Resistivity Measurements of Saturated Fluid Flow .....	15
Resistivity of the Vadose Zone.....	16
Transient Electrical Resistivity.....	17
Solution Infiltration and Flow.....	18
Geochemical Processes.....	21
III. METHODOLOGY .....	23
Field Equipment and Setup.....	23
Electrode Cables .....	25
Additional Electrodes.....	29
Data Collection .....	30
Contact Resistance Tests.....	31
Command Files.....	31
Pole-Pole Arrays .....	32
Pole-Dipole Arrays .....	32
ERT Arrays .....	32
Dipole-Dipole Arrays.....	32
Additional Arrays and Induced Potential.....	33
Data Inversion.....	33
Inversion of the Apparent Resistivity Data.....	34
Transient Inversion .....	34

Chapter	Page
Resistivity Data Analysis and Editing .....	35
Color Scales .....	35
Model Sensitivity .....	37
Statistical Parameters .....	40
Data Trimming .....	40
Geochemical Analysis .....	42
IV. RESULTS .....	45
Data Repeatability and Dependability .....	46
Background Resistivity .....	49
Identification of Preferential Flow .....	51
Cable C Wetting Front Data .....	53
Transient Resistivity .....	58
Cable A .....	58
Cable B .....	60
Cable A Induced Polarization Files .....	62
Geochemical Comparisons .....	64
Gold Content and Solution Conductivity .....	64
Gravimetric and Volumetric Water Content .....	65
Fluid Velocity .....	65
V. DISCUSSION .....	67
Surface Effects .....	67
Inversion Interpretation Considerations .....	68
Wetting Front Analysis .....	69
Steady State Flow .....	70
Geochemistry Comparisons .....	71
Suggestions for Further Study and Lessons Learned .....	72
VI. CONCLUSIONS .....	74
BIBLIOGRAPHY .....	76
APPENDIXES .....	81
APPENDIX A – Table of Resistivity Files Collected and Inversion Statistics .....	81
APPENDIX B – Transient Inversion Data Sets .....	87

LIST OF TABLES

Table	Page
1. Positions of Subsurface and Infinity Electrodes .....	30
2. Type of Files Collected .....	46

## LIST OF FIGURES

Figure	Page
1. Study Area Location Map .....	6
2. Site Location Map of Geoelectrical Study .....	8
3. Cortez Gold Acres Facility .....	9
4. Grain Size Variability .....	11
5. Preferential Flow Patterns Schematic .....	19
6. Electrical Resistivity Equipment.....	24
7. Cable A Setup .....	26
8. Cable Positioning and Setup Schematic.....	27
9. Cable B and C Setup .....	28
10. Custom Resistivity Color Scale .....	36
11. Color Scales for Sensitivity and Percent Difference Images .....	38
12. Model Sensitivity Plots .....	39
13. Data Misfit Histogram.....	42
14. Change in Apparent Resistivity through Time.....	47
15. Change in Apparent Resistivity with Horizontal Distance .....	48
16. File C27DDF3 from Cable B .....	49
17. File C27PD1.....	50
18. File C27PD13a.....	52

Figure	Page
19. File C36PP25 .....	52
20. File C27PD7.....	54
21. File C27PP8 .....	54
22. File C27PP12 .....	55
23. File C27PP14 .....	55
24. File C27PP18 .....	56
25. File C27PP20 .....	56
26. Transient Inversion Set from C36pp12 to C36pp27 .....	61
27. File C36PP22a Induced Polarization .....	62
28. File C36PP22a Resistivity .....	63
29. File C36PP22a Sensitivity Plot .....	63

## CHAPTER I

### INTRODUCTION

Heap leach mining of low-grade precious metal ores has become a critically important industry in the western United States, mostly in arid environments. Heap leach mining has become the second largest industry in the state of Nevada. The heaps that are created are very large structures (hundreds of acres) of heterogeneous composition and grain size (ranging from clay to meter-scale boulder) in which the flow properties are largely unknown. As such, it is important to study these structures so that water and chemical transport through the heap and any potentially significant environmental impacts on long-term infiltration, water quality, and native vegetation can be anticipated. The mining industry is also interested in determining whether the regulations governing heap leaching procedures can be improved to better manage ore and waste rock rinsing and disposal.

Most of these mines employ the same basic mining procedures. Run-of-mine ore is most commonly used. Run-of-mine is ore that is first blasted using explosives and then extracted from large pits resulting in a highly unsorted ore pile. Ores with higher mineral content may also be sent through a crushing process. The ore for the bottommost lift (a single leaching layer of the heap) is placed on an impermeable polymer liner that slopes for drainage. The ore is piled in stages, allowing each lift (7 – 16 meters in height) to be individually leached before the next lift is added to the top (Bartlett, 1992). The final

heap can exceed 100 meters in height and may cover 10 to 300 acres of land. The primary leaching agent is usually a low concentration sodium cyanide solution, at an elevated pH, delivered through sprinkler or drip hose irrigation systems. The solution complexes with metals in the ore and is gravity drained through the heap to a processing plant where the metals are removed and the solution is recycled. Following active leaching, these piles are rinsed, drained, and closed. Ultimately, remaining ore is typically stored on-site as waste rock (often as unlined fill).

Such heap leach pads provide an opportunity to study controlled infiltration and unsaturated flow through highly heterogeneous materials in arid environments. Solution inputs and outputs can be measured, so in many respects, the heaps function as field scale lysimeters that can be used to simulate flow within the vadose zone. With this additional knowledge of the site conditions and structure, fluid flow interpretations using geophysically acquired data can be improved. Since this is a relatively untested application of electrical imaging methods, this research is of interest to academic, mining, and environmental communities and may provide a greater understanding of the subsurface physical and chemical hydrologic processes involved. In particular, the mining industry is interested in developing a conceptual model of solution flow to improve application procedures and gold extraction rates.

This study conducted electrical resistivity surveys during the application of leaching solution on the final lift of a heap at Cortez Gold Acres Facility in northeastern Nevada. Changes in wetting throughout the leaching period were imaged until a steady-state was achieved. Data were collected from the heap in four basic flow phases including: 1) prior to wetting, 2) during the initial wetting front progression, 3) during the



initial development of flow patterns, and 4) as the heap approached steady-state flow conditions.

### Purpose and Goals

Knowledge regarding the factors controlling flow within the vadose zone is currently limited. Many of the current theories and flow models are untested at a field scale. Even in highly homogeneous field conditions, many questions remain concerning unsaturated flow and the development of flow fields. The flow conditions in a heap are even more complex in that they involve a chemically and physically active flow field under unsaturated conditions in a highly heterogeneous and reactive medium.

It is known that fluid migration in the subsurface causes changes in electrical properties of materials (Kean et al., 1987). This allows electrical resistivity to be a useful fluid flow monitoring technique in some situations (Binley et al., 2002; Daily et al., 1992; French et al., 2002; Reynolds, 1997). This study intends to test the ability of electrical resistivity surveys to image an active heap leach pile with the basic goal of monitoring, interpreting, and characterizing site flow conditions in an effort to begin development of a conceptual model of unsaturated flow in heap leach ores based on electrical resistivity data.

### Objectives

The objectives of this study were refined based on their ability to be tested with field data, data quality, and applicability to mining, academic, and environmental interests. They are:

1. Design a system and methodology for data collection. This involved constructing adaptations for the electrical resistivity data collection system to protect the system from the leaching solution for the duration of the study. By developing an algorithm using variable array types, infinity electrodes, electrode lines, and command files, a more extensive set of data could be collected. It was thought that by using this type of collection algorithm the study would also have the greatest chance of success under the extreme conditions for the equipment.
2. Develop a data processing methodology. Changes in resistivity were observed and processed using transient analysis software. Error statistics and more traditional geochemical parameters were used to determine whether the measured resistivity data could be considered consistent, repeatable, and comparable to other methods. In particular, by analyzing the lysimeter flow times and additional geochemical data taken at the site in conjunction with the geophysical measurements, interpretations of the electrical images were improved. These comparisons may also reveal inconsistencies in the data due to electrical interference caused by additional electrical potentials within the heap. The reactive constituents in the ore may generate electrical potentials that could mask or overlay the electrical signature of the fluid and ore. Additionally, the fluid flow itself is capable of generating an electrical current by streaming potential processes.
3. Test the ability to identify preferential pathways and flow signatures. Transient electrical resistivity imaging was used to identify areas within the heap with time-variable electrical signatures due to changes in fluid flow, moisture content, and

metal dissolution. Can the wetting of the ore be interpreted as a steadily decreasing trend in resistivity? Can this data determine if preferential flow and ineffective leaching occur within the heap? Can this data be useful in constraining causal factors of expected heterogeneous flow patterns and evaluating the effectiveness of current wetting practices?

4. Evaluate the detection of geochemical processes within the heap. A number of chemical reactions and processes occur within an active heap due to the presence of reactants like gold, carbonate, nitrates, sodium cyanide, and other trace constituents. Since these reactions may cause variable electrical properties, the electrical resistivity data were evaluated for indications that chemical processes could be identified. The detection of gold release into solution was of particular interest.

### Study Area

Cortez Gold Mines is a large-scale mining operation in Lander County in northeastern Nevada near the towns of Crescent Valley and Beowawe (Figure 1 Inset). This research focused on the uppermost lift of a heap in the Gold Acres section of the mine which was added primarily for geophysical and geochemical research.

#### Lift Construction

Twenty-four gravity drained lysimeters of varying sizes and dimensions and four graphite electrodes were installed at the bottom of the lift prior to piling the ore by the standard loading method. Five 1500 ft<sup>2</sup> (139.3 m<sup>2</sup>) lysimeters and nineteen 28 ft<sup>2</sup> (2.6 m<sup>2</sup>) lysimeters were placed to maximize coverage area and better determine flow

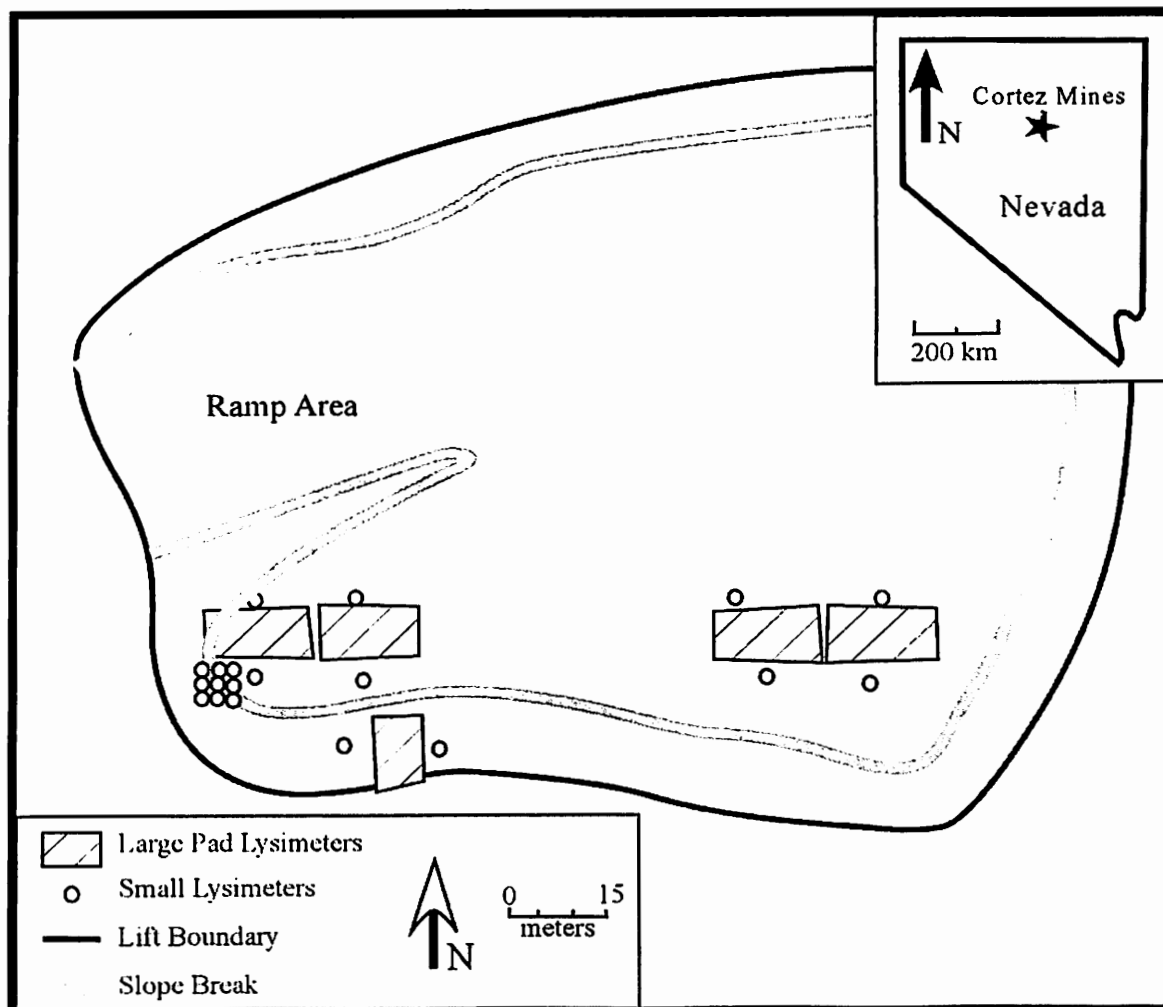


Figure 1. Study Area Location Map. The map illustrates the boundaries of the uppermost lift of the Gold Acres heap as well as the location of the mine in reference to the state of Nevada (inset). The 24 lysimeters within the heap are concentrated in the southern half of the lift. This study was concentrated on the southwestern corner of the lift, south of the ramp area.

heterogeneities. Four of these lysimeters near the western edge of the heap contained electrodes that were used with surface electrodes to collect resistivity data. After lift construction, locations of the subsurface electrodes were plotted, but it should be noted that there is a lateral uncertainty of up to 3 meters associated with these placements due to GPS position resolution (Figure 2).

Approximately 150,000 tons of ore were used in construction of the lift. Total lift surface area exceeds 10,680 m<sup>2</sup> (115,000 ft<sup>2</sup>). The lift itself was a roughly rectangular pile 8.3 meters (27 feet) high at the easternmost end and 6.1 meters (20 feet) at the western end. Since the base slopes to the east, this allowed for a top surface of roughly equal elevation and a sloping base. The top surface itself was textured by a process called “ripping.” Surface area was increased and infiltration improved by cultivating the ore and forming a series of troughs and ridges measuring less than one meter across (Figure 3).

### Ore Geology

The ore for the study area of the lift was composed of 10-20% lower Devonian Wenban limestone mixed into 80-90% Upper Silurian Roberts Mountain Formation. These are Carlin-type carbonate hosted oxidized ores with approximately 0.03% gold content, which is disseminated. The Wenban limestone has variable recrystallization, marbleization, and clay alteration. Goethite, limonite, and manganese oxides are also present (Hart, 2002). The Roberts Mountain ore found here is typical in that it is a dolomitic limestone with quartz silt. As in the Wenban, traces of goethite, limonite, and manganese oxides are common (Armstrong et al., 1998).

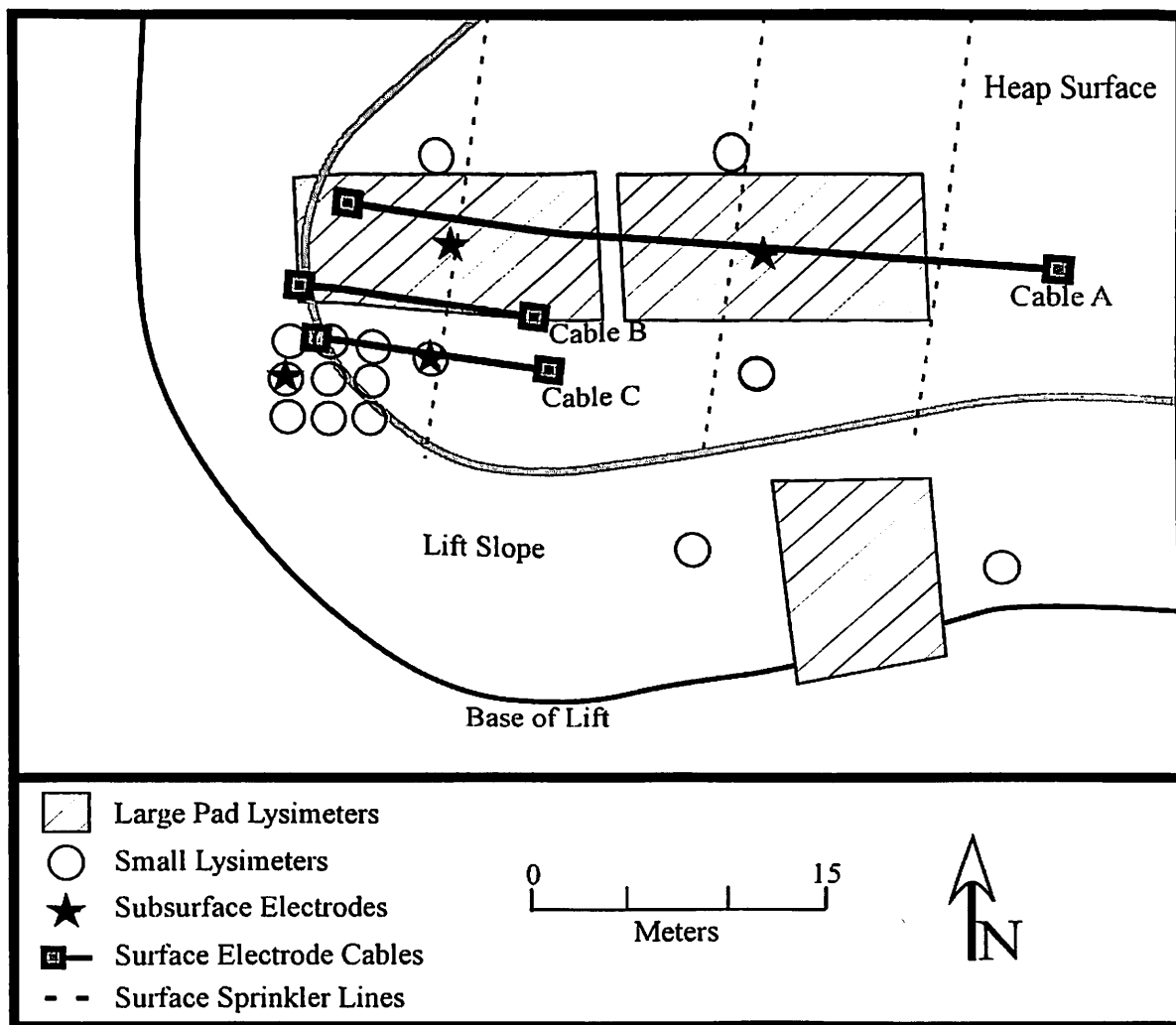


Figure 2. Site Location Map of Electrical Resistivity Study. This enlargement of the previous figure depicts the locations of the 3 fixed position electrical resistivity electrode lines, the lysimeters below them, the 4 subsurface graphite electrodes, and the surface sprinkler system lines. Note that the locations of objects below the top lift are within +/- 3 meters of their correct location.

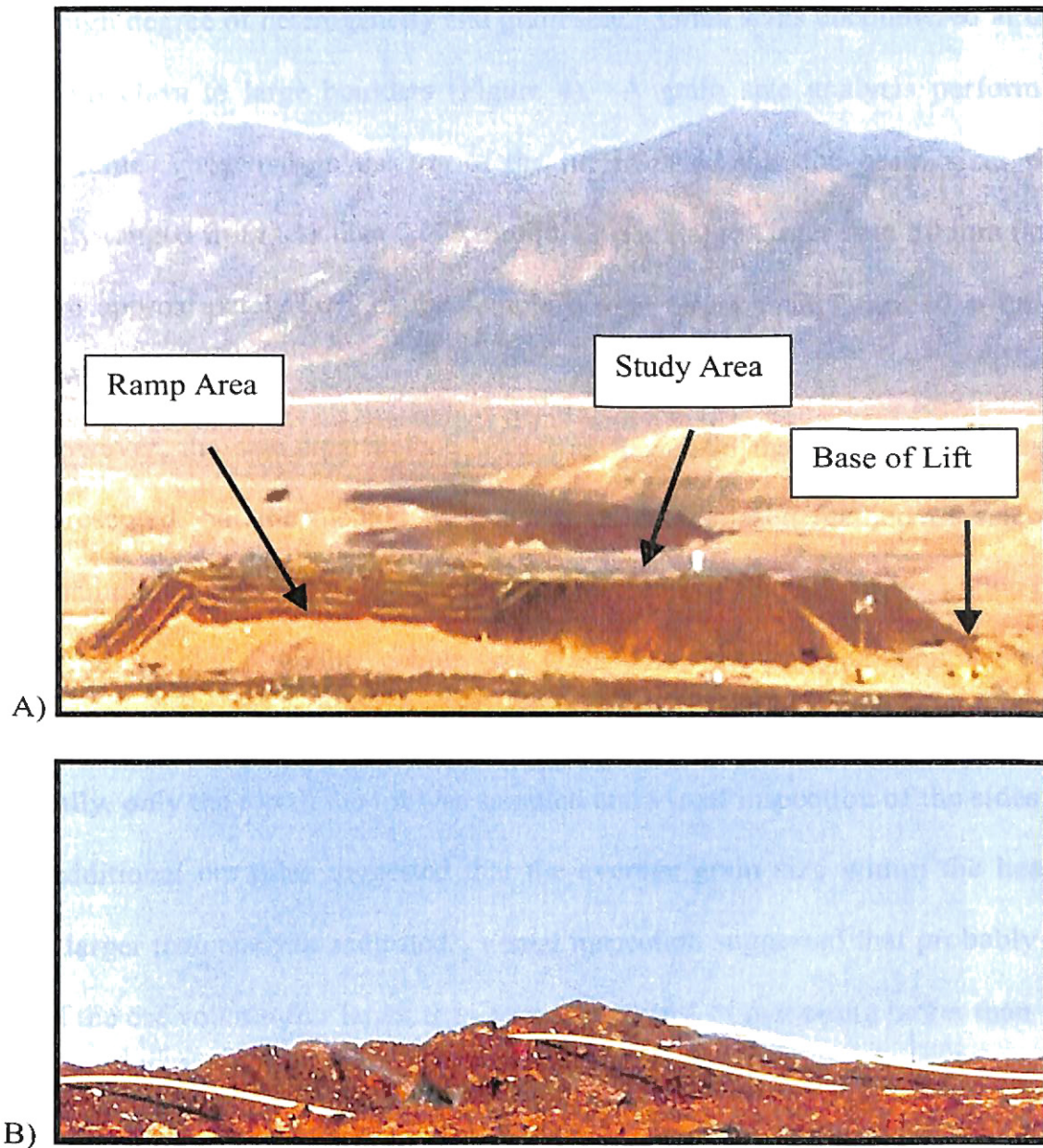


Figure 3. Cortez Gold Acres Facility.

- A) This photo, looking east, shows the heap in study in the foreground. Notice the sprinkler system strung across the ramp area of the lift.
- B) This photo depicts uneven, “rippled” texture at the edge of the heap surface. Sprinklers oscillate and were connected to the yellow PVC piping.

The lift used for this study was constructed using run-of-mine crushed ore, which lead to a high degree of heterogeneity and grain size. Grain sizes encountered at the site ranged from clays to large boulders (Figure 4). A grain size analysis performed on sample volumes chosen from the top of the lift revealed that the grain sizes present consistently ranged from less than 0.075 mm (0.42  $\phi$  units) to larger than 50 mm (-5.64  $\phi$  units) with approximately 80% of the sample weight larger than 1 mm (0  $\phi$  units) on average (Webb, 2003).

However, the sampling method used was flawed in that large grain sizes were under-represented, but the method was chosen as an unbiased method of selecting a standard sample volume. Grains larger than the diameter of a standard five gallon bucket could not be sampled. Smaller cobble size grains were generally un-sampled because they preferentially fell off of the shovel, only partially resided in the sample volume, etc. Additionally, only the top of the lift was sampled and visual inspection of the sides of the lift and additional ore piles suggested that the average grain size within the heap was probably larger than analysis indicated. Visual inspection suggested that probably closer to 90% of the ore volume was larger than 1 mm with most of that being larger than 1 cm.

Additionally, this degree of variability in grain size increases the probability of a large variability in pore sizes. The heap material was relatively uncompacted (particularly before wetting began) and the small grains were not of a large enough fraction to completely infill large void spaces. This type of scenario increases the potential for preferential flow and the development of faster flow paths. It is likely that the flow system evolved as the leaching solution was applied and heap materials compacted, reacted, infilled, and dissolved (Berkowitz et al., 2001).



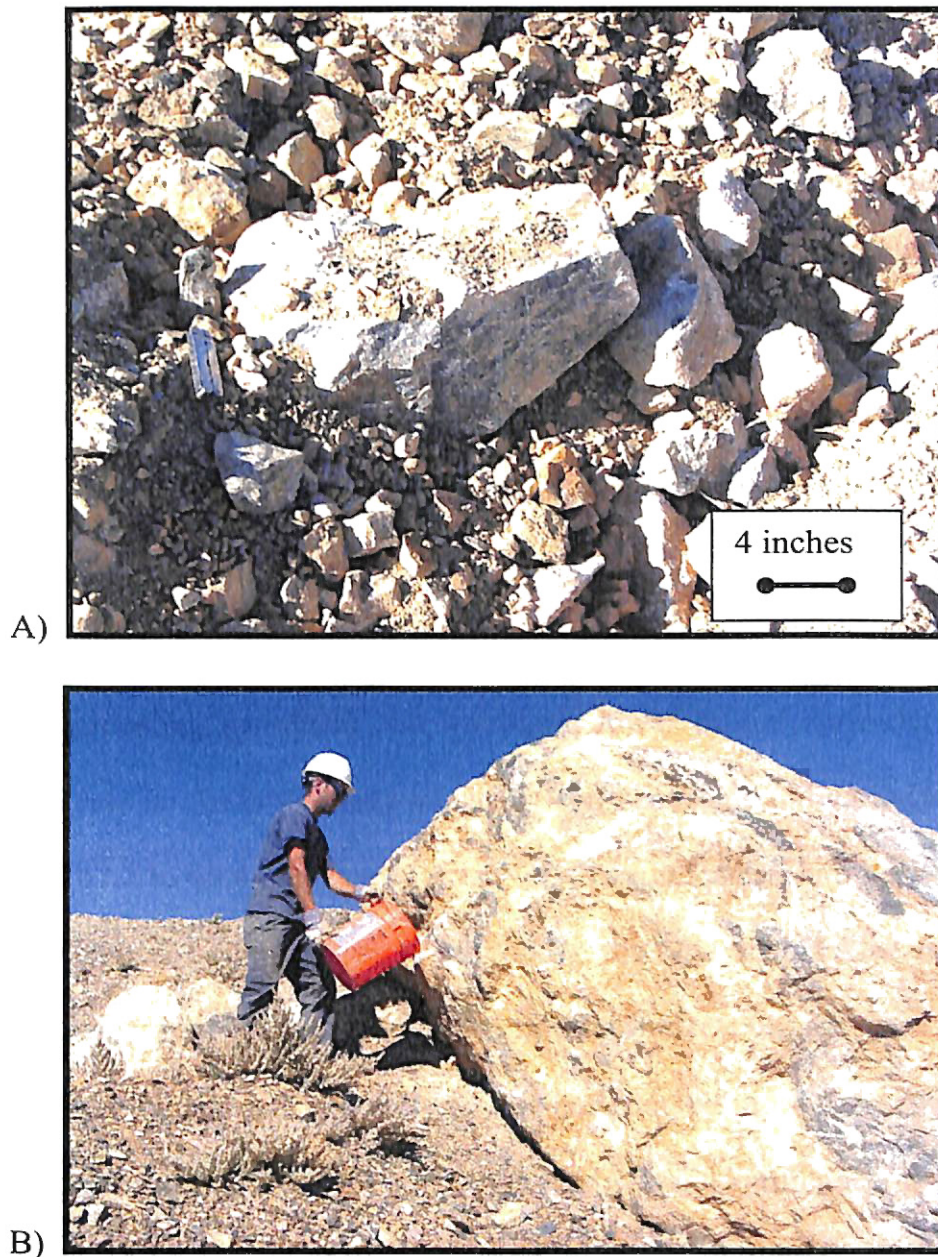


Figure 4. Grain Size Variability.

- A) Ore on the top of the lift most commonly resembled this combination of grains. Silt and clay infilled spaces between gravels and boulders. (Note: Leatherman for scale.)
- B) Several compact car-size boulders protruded from the sides of the heap. These large grains were not accurately represented by the grain size analysis sampling, but are expected to be present within the heap. As the photo shows, some grains were simply too large to fit into the sample volume for grain size analysis.

## Leaching Solution Chemistry and Application

The leaching solution consisted of a dilute sodium cyanide solution (approximately 0.0375 %) with lime (calcium carbonate) added to raise the pH to above 10. This elevated pH prevented the cyanide solution from vaporizing. Values of pH measured from lysimeter outflows generally ranged from 11-13 after flow stabilized. The electrical conductivity of the solution exiting the heap ranged from 1-4 mS/cm. Throughout the study, the cyanide concentration in solution taken from the lysimeters was near 0.2 lbs/ton or 0.01% (Webb, 2003).

This solution was applied to the heap via a network of sprinklers. A combination of oscillating, streaming sprinklers and wobbling, lower output sprinklers were used. The application rate for the entire heap was held nearly constant and varied between 1073 and 1084 gpm (67.7 to 68.4 liters/sec). However, the application rate varied by location on top of the heap based on proximity to a sprinkler, the type of sprinkler used, and wind conditions. Temperature variation also affected sprinkler output, since there was a possibility for freezing at night, and daily temperature ranged more than 15.5° C (60° F). Application rates measured on top of the lift gave an average application flux of  $3.3 \times 10^{-3}$  liters/sec/m<sup>2</sup> within a range of  $2.5 \times 10^{-4}$  to  $8.7 \times 10^{-3}$  liters/sec/m<sup>2</sup> (Webb, 2003).

## CHAPTER II

### LITERATURE REVIEW

This study incorporates the use of electrical resistivity into the study of unsaturated flow and transport. Basic resistivity theory will be presented and discussed in terms of its general applications and studies performed to measure the resistivity of saturated and unsaturated fluid flow. Unsaturated zone fluid infiltration, flow, and chemistry will also be discussed to provide a fundamental understanding of the physical and chemical processes in the heap and some of the complications involved with using electrical resistivity to study them.

#### Electrical Resistivity

Resistance [ohms] is a fundamental and inherent property of a volume of material and is defined as the material's opposition to the flow of electrical current (Burger, 1992). Given a uniform cubic volume with length (L) and cross-sectional area (A), the resistance of the material will be proportional to the potential drop of an applied current (V/I). Resistivity [ohm-m] is related to this property and is expressed as a resistance through a distance, which makes it independent of material geometry. Resistance (R) and resistivity ( $\rho$ ) can be expressed by the following equations (Reynolds, 1997):

$$(1) R = V / I \text{ } [\Omega] \text{ (Ohm's Law)}$$

$$(2) \rho = VA / IL \text{ } [\Omega\text{-m}].$$

Electrical resistivity is most commonly measured by applying a known direct or low frequency alternating current through two electrodes and measuring the potential field with another pair of electrodes (Burger, 1992). Modern technology allows this process to be controlled by automated systems with command files directing which combinations of source and potential electrodes are used and when (Ramirez et al., 1993). Automated systems are often capable of collecting hundreds to thousands of data points within an hour. Additionally, advancements in inversion software allow field data to be quickly inverted and interpreted (Loke and Barker, 1996).

Resistivity is considered to be a function of the rock porosity, volumetric fraction of saturated pores, and the resistivity of the pore water (Archie, 1942). Since in many cases, it is the pore fluids that contribute more to the overall resistivity signature than the host rock, this may be a more intuitive way of thinking of resistivity for this study. As the fluid infiltrates the heap, it is expected to provide the dominant electrical signature.

### Traditional Applications

Electrical resistivity methods were first developed and used in the early 1900s. It has often been used to denote changes in lithology or fluid type in the subsurface. For most of the 20<sup>th</sup> century, resistivity was considered to be a useful mapping tool, but also involved tedious data collection and interpretation (Spicer, 1952). With the advancement of computers in the 1970s, electrical resistivity gained widespread use in environmental applications. Since that time, data collection capabilities improved and resistivity measurements could be obtained as true two or three dimensional data rather than simple, one dimensional data sets. Electrical resistivity has since been used for groundwater exploration, detection of subsurface structural features, and subsurface mapping.

Resistivity also has a long history used for downhole logging in oil and gas exploration (Reynolds, 1997).

Resistivity methods have been utilized for many decades to detect variations in water quality, especially in slow moving systems. In the 1980s, a comprehensive electrical resistivity study was used to help characterize the groundwater potential in hundreds of Nigerian villages. These data were used to plan drilling locations and were successful in decreasing the borehole failure rate from 82% without the use of geophysics to 17% after geophysical interpretation (Reynolds, 1987). This type of technology continues to be used today in exploring for potable groundwater resources and mapping salt-water intrusion (Reynolds, 1997).

#### Resistivity Measurements of Saturated Fluid Flow

Electrical resistivity methods have also become valuable tools to delineate pollution migration in groundwater. Resistivity has become a commonly used method to map leachate plumes below buried waste, landfills, and underground storage tanks (USTs) (Reynolds, 1997). Resistivity methods have been found to be effective in mapping the extent and transport of chemical contamination and monitoring the progress of remediation efforts.

Cahyna et al. (1990) used resistivity and induced potential to monitor leakage of cyanide complexes below a landfill. They determined that field geophysical investigations can be difficult when the natural rock heterogeneity is as pronounced as the measured geophysical anomalies. This study was complicated by the natural decay of the contaminant and a resultant change in electrical signature, but the authors were confident that they were able to map the groundwater plume. While this type of study is

fairly common and may provide helpful insight into the migration of the cyanide solution in this study, these studies tend to focus on saturated flow conditions that occur within an aquifer and do not translate well to unsaturated flow.

#### Resistivity of the Vadose Zone

Using resistivity to study flow in the vadose zone is an emerging field. Currently, studies conducted in the vadose zone are less common and the field of knowledge is less comprehensive than in saturated flow conditions. Kean et al. (1987) used electrical resistivity sampling techniques to study the effect of different lithology and soil moisture content on electrical signatures under unsaturated flow conditions. They determined that there is no absolute relationship between resistivity values and moisture content, but rather a general trend for decreasing resistivity with increasing moisture. Clay content and temperature variations were found to somewhat control the changes in resistivity. Park (1998) used resistivity data collected on heterogeneous alluvial material to conclude that the fluid flow in the study occurred by capillary action. He also deduced that the flow was controlled by the distribution of the finest grains (clays and silts).

In 1992, Daily et al. performed one of the first field tests of a controlled infiltration event using an automated electrical resistivity system. The test site geology was a complex interbedding of heterogeneous materials, and the resistivity images showed that flow did not occur until the fine materials were nearly saturated and that lithology changes were distinguishable by differing electrical signatures.

Al Hagrey et al. (1999) found that even when studying unsaturated, homogeneous sand, flow is somewhat preferential and concentrated. They attributed these variations in flow to small scale heterogeneities and the presence of in situ structures, as well as a

lithologic change to gravel below the sand layer. Preferential flow was also detected by Faybishenko et al. (2000) while they studied flow through unsaturated, fractured basalt. They observed vertical and horizontal rapid flow of a solution through large fractures, but as water was slowly redistributed between fractures and matrix, the larger fractures desaturated.

### Transient Electrical Resistivity

Time lapse electrical resistivity surveys are useful when studying dynamic systems. These types of surveys are a relatively recent variation on traditional resistivity measurements. Transient analysis involves taking identical measurements at the same location at two different times and comparing the results (Loke, 1999). This comparison can reveal changes in the water table or moisture content due to extraction or infiltration, flow of water through the unsaturated zone, flow and transport of chemicals, steam, or pollutants, and leaks from dams, tanks, or hydraulic barriers (al Hagrey and Michaelson, 1999; Barker and Moore, 1998; Johansson and Dahlin, 1996; Ramirez et al., 1993; Titov et al., 2000).

Barker and Moore (1998) were able to repeat a series of resistivity measurements during an infiltration test in Birmingham, England. A water hose supplied a constant wetting source for 10 hours and the site was monitored for two weeks. Their transient resistivity approach successfully imaged the initial application and flow of water through the unsaturated zone, as well as the dispersion of the water through the following weeks.

French et al. (2002) used borehole electrical resistivity cables to monitor flow and transport of snowmelt infiltration into soil and sand sediments. They found that with weekly monitoring, electrical resistivity imaging yielded comparable results to data from



a suction cup lysimeter grid. Flow of the snowmelt tracer within the roughly 3 meters of vadose zone was found to be preferential and bypassed some of the lysimeters (which could not be installed without disturbing the soil structure), but was detected by the electrical resistivity equipment. A similar experiment found that electrical resistivity was a suitable technique for measuring changes in moisture content after a controlled tracer injection into a sandstone aquifer (Binley et al., 2002).

### Solution Infiltration and Flow

The academic areas of soil science and hydrology have studied unsaturated flow in porous media extensively over the last 60 years (Orr, 2002). However, infiltration into and fluid flow within the heterogeneous vadose zone are currently poorly understood phenomena. It is generally not known which processes control flow and transport at particular fractured or heterogeneous porous field sites. In general, it is thought that a number of processes contribute to flow characteristics such as matrix – pore interaction, preferential flow (non-uniform distribution of fluids), film flow, fluid velocity, fingering, funneling, flow instability, sediment transport, and the interplay of advection and diffusion with the matrix (Figure 5). In the past, these unsaturated flow conditions have been primarily studied in laboratory settings. Through the use of column tests and small scale experiments, numerous models of unsaturated flow have been developed, but they are often unsuccessfully applied at a field scale due to upscaling problems (NRC, 2001). As Figure 4 illustrates, field scale heterogeneities are present at this field site that can not be replicated at a smaller scale.



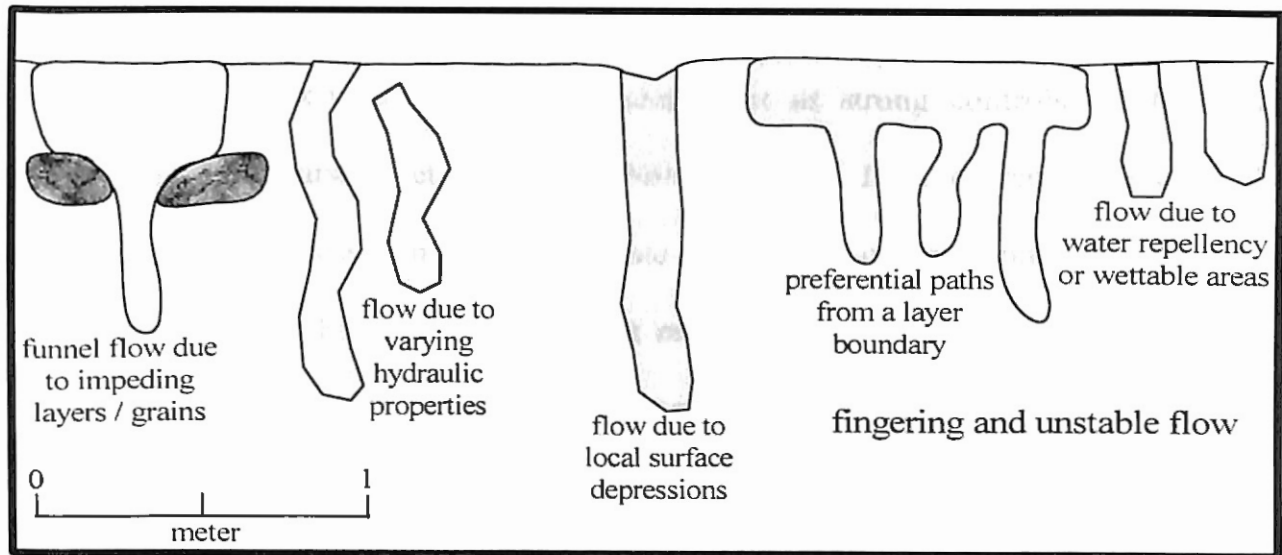


Figure 5. Preferential Flow Patterns Schematic. These patterns were observed in heterogeneous and homogenous soils at a Darcian scale, but these terms can also be applied to this study (after Hendrickx and Flury, 2001).

However, several flow characteristics in the vadose zone are well documented and applicable to this research. Flow in a gravity drain heap acts as two phase flow with the components of air and the leaching solution. For the solution to flow downward, it must essentially push the air within the heap also. This can cause instabilities to develop (Orr, 2002). Uneven availability of moisture at the surface, which is the case at heap leach sites, may also instigate non-uniform flow (Davis, 1995). These factors and others suggest that flow from an infiltration event generally does not proceed as a single wetting front, but rather at some non-uniform rate (preferential flow) with some flow paths arriving much earlier than can be calculated using uniform flow rates (Kung, 1990; NRC, 2001; Orr, 2002; Pruess, 1999). This non-uniform flow has been documented at varying scales and through different flow patterns in the vadose zone (Figure 5). For instance, unstable flow is common in coarse grains and may be caused by continuous infiltration,

air entrapment, and textural layering (Hendrickx and Flury, 2001). Also, fluid velocity variation and matrix-void interaction generally act as strong controls on flow path development (Bodvarsson et al., 2001; NRC, 2001). It is currently thought that preferential flow processes in heaps and waste dumps are a common phenomenon, rather than the exception. Field investigations at numerous mines suggest that the leaching solution usually bypasses some of the ore, but more study is needed to predict where and why (Orr, 2002).

Considering the variability in grain size, there are a number of reasons why this system will behave quite differently than either a saturated system or a smaller scaled study. First, in unsaturated systems permeability is a function of saturation and capillary forces. Finer grained areas tend to have higher suction, which means that materials like clays may act as fluid passages rather than barriers where capillary forces dominate flow. Secondly, coarse grains with larger air filled pores may act as capillary barriers that lead to flow diversion or funnel flow (Orr, 2002). Finally, this suggests that as application and saturation varies so will the preferred flow paths size. This is consistent with Bakshi and Nelson (1995). They performed column tests simulating rinsing of leached gold ore. Through intermittent rather than continuous rinsing, they were able to better rinse more of the heap and develop a more effective cyanide removal procedure.

Additionally, numerous references can be found for flow of conservative contaminants in individual fractures or for contaminants in unsaturated porous media, but flow of reactive solutions in fractured or highly heterogeneous porous media has been given little attention. The ability to quantitatively predict or model responses to chemical transport is even more limited (Berkowitz et al., 2001).

## Geochemical Processes

This study is also concerned with identifying the chemical reactions and flow processes occurring within the heap because of their potential to generate electrical impulses, particularly redox and streaming potentials. Reduction and oxidation (redox) reactions are simply chemical reactions that involve the transfer of electrons between involved chemical elements (Runnells, 1995). An electric current can be generated if regions of varying redox potentials are connected by a conductor which would create the equivalent of a galvanic cell. This is an electrical property that is most often discussed with attempts to locate ore bodies at depth using electrical methods. Such potential fields have been labeled “geobatteries” (Stoll et al., 1995; Timm and Moller, 2001). With all of the active constituents contained in the heap, it is probable that various redox reactions will occur simultaneously with the leaching process. Additionally, the flow of subsurface water may induce electrical current flow creating streaming potentials which can also generate self potential anomalies (Kilty, 1984; Stoll et al., 1995).

These electrical potentials are additive and are designated as self potentials (SP) at the field scale (Timm and Moller, 2001). Solid rock self potential measurements in the previous field studies are the result of weak potential fields on a large scale (many are larger than a kilometer). While prospecting for ore bodies using SP, anomalies are most commonly only 20 – 50 mV due to galvanic connection between minerals (Vagshal and Belyaev, 2001). SP measurements used to study water seepage fell in the same range, and varied with rock properties (degree of fracturing and porosity) and fluid properties such as the total head (Bogoslovsky and Ogilvy, 1970).

Self potential anomalies may interfere with the resistivity data collection by creating excess noise, but it is unlikely that the voltages generated will be large enough to compromise resistivity data quality. The voltage generated by such self potential anomalies is dependent on factors such as the available surface area for electron transfer, surface chemistry of the material, the resistance of the current path in the ore, the competing redox reactions, and electron transport conditions at the surface of the material (Kilty, 1984). Since the heap materials consist of a variety of minerals in close proximity, much of the potential to generate SP will “cancel out.”

## CHAPTER III

### METHODOLOGY

This project required the standardization of several procedures such as: 1) setup of field equipment, 2) field data collection, 3) data analysis, and 4) presentation of results. Procedures were developed allow for high quality, repeatable resistivity data that can be correlated to other available geochemistry and hydrologic data.

#### Field Equipment and Setup

An 8 channel automated resistivity/induced polarization instrument (SuperSting R8 IP™), an electrode switchbox, a 36 electrode cable, and two 27 electrode cables manufactured by Advanced Geosciences, Inc. were used for data collection, file storage, and switching between electrodes (Figure 6). Three electrode cables (A, B, and C) were placed in position prior to wetting to collect resistivity measurements of background conditions and during wetting. Each cable was retrofitted with housing to protect metal parts from the caustic leaching solution. Six additional graphite electrodes were installed. Four were subsurface electrodes (PL1, PL2, TL5, and LA4) installed at 6.1 meters depth within the heap prior to lift construction and used to collect borehole resistivity electrical files (also referred to as Electrical Resistance Tomography or ERT). Two graphite electrodes were infinity electrodes at the surface (IEE and IEW) used in pole-dipole and pole-pole surveys.



Figure 6. Electrical Resistivity Equipment. (A) 8 channel resistivity/induced polarization instrument (SuperSting R8 IP™) and (B) switchbox with connector cable manufactured by Advanced Geosciences, Inc.

## Electrode Cables

The electrode cable locations were chosen to maximize coverage over the two 1500 ft<sup>2</sup> pan lysimeters and an array of 10 smaller lysimeters on the western edge of the heap. This provided a better spatial comparison with the geochemistry data. The electrodes cables were placed in troughs in the surface material created by the “ripping” process to increase the contact area with the ore. Troughs in locations above the subsurface electrodes were chosen.

Cable A consisted of 36 stainless steel electrodes inside polyvinyl chloride (PVC) housings (Figure 7). These electrodes were placed at the base of the heap beyond the leaching solution sprinklers. The bare ends of the copper wire extensions were secured to each electrode inside the PVC. Joints and holes in the PVC were liberally sealed with silicone caulking to prevent intrusion of the cyanide solution and resultant corrosion of the wiring or electrodes inside. Each insulated copper extension wire was then reeled to the top of the heap with care given to ensure that wires from neighboring electrodes were separated and weighted to prevent electrical interference or wind movement. The free end of the wire was screwed into a graphite rod electrode. The point of attachment was generously plastic coated to protect the screw and wire ending. Each graphite rod electrode was then buried approximately 0.3 meters into the ore material at a one meter spacing allowing for a total survey line length of 35 meters (Figure 8).

Cables B and C consisted of 27 graphite electrodes each at a constant spacing of 0.46 meters (1.5 feet) for a total cable length of 11.96 meters each. These cables were placed directly on the heap surface in parallel troughs created by the ripping process (Figure 8). A conductive bentonite grout was used as a coupling agent (Figure 9). This



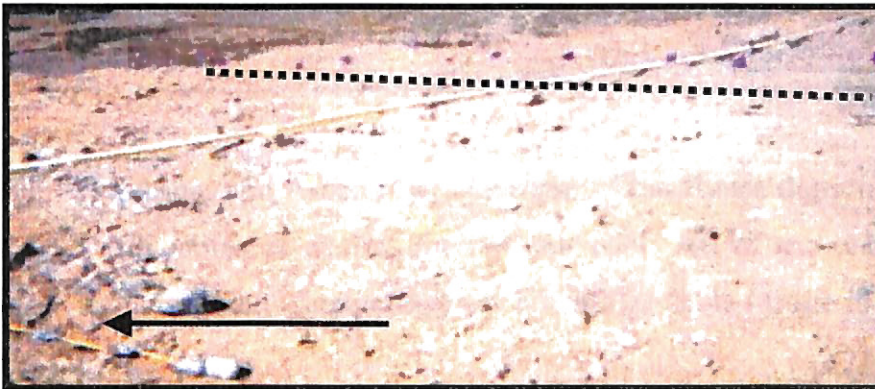
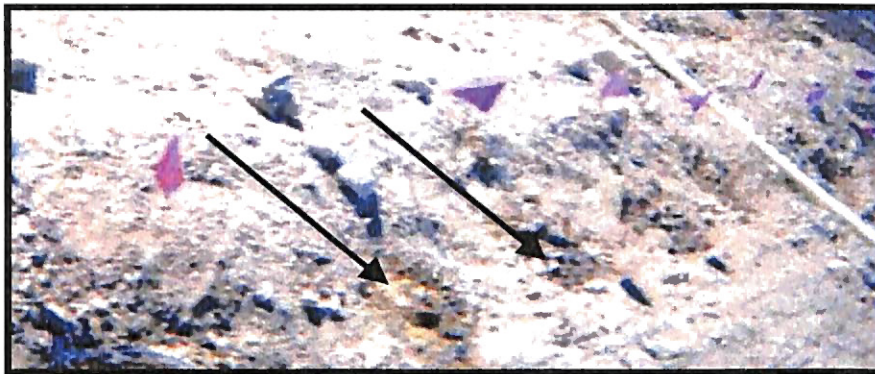


Figure 7. Cable A Setup. The cable with 36 electrodes was placed at the base of the heap in PVC and under plastic sheeting (top). Flags were used to mark the locations of the 36 buried graphite electrodes indicated by arrows (middle). The 36 electrode line ( ---- ) and the northernmost 27 electrode line (arrow) were approximately 5 meters apart (bottom).



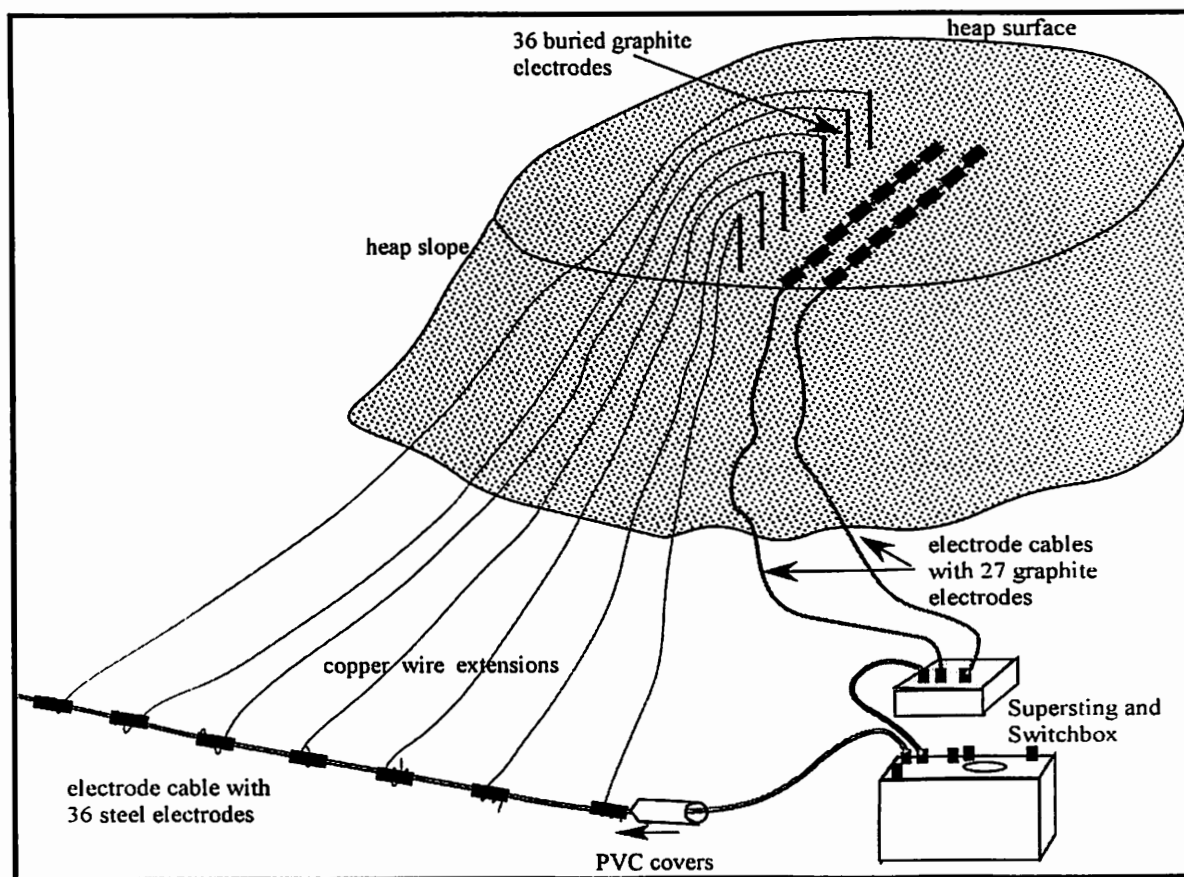


Figure 8. Cable Positioning and Assembly Schematic. This figure depicts the layout and assembly of the cables as well as their extensions. All of the cables attached to the resistivity instrument (Supersting) or switchbox. This image is not to scale.

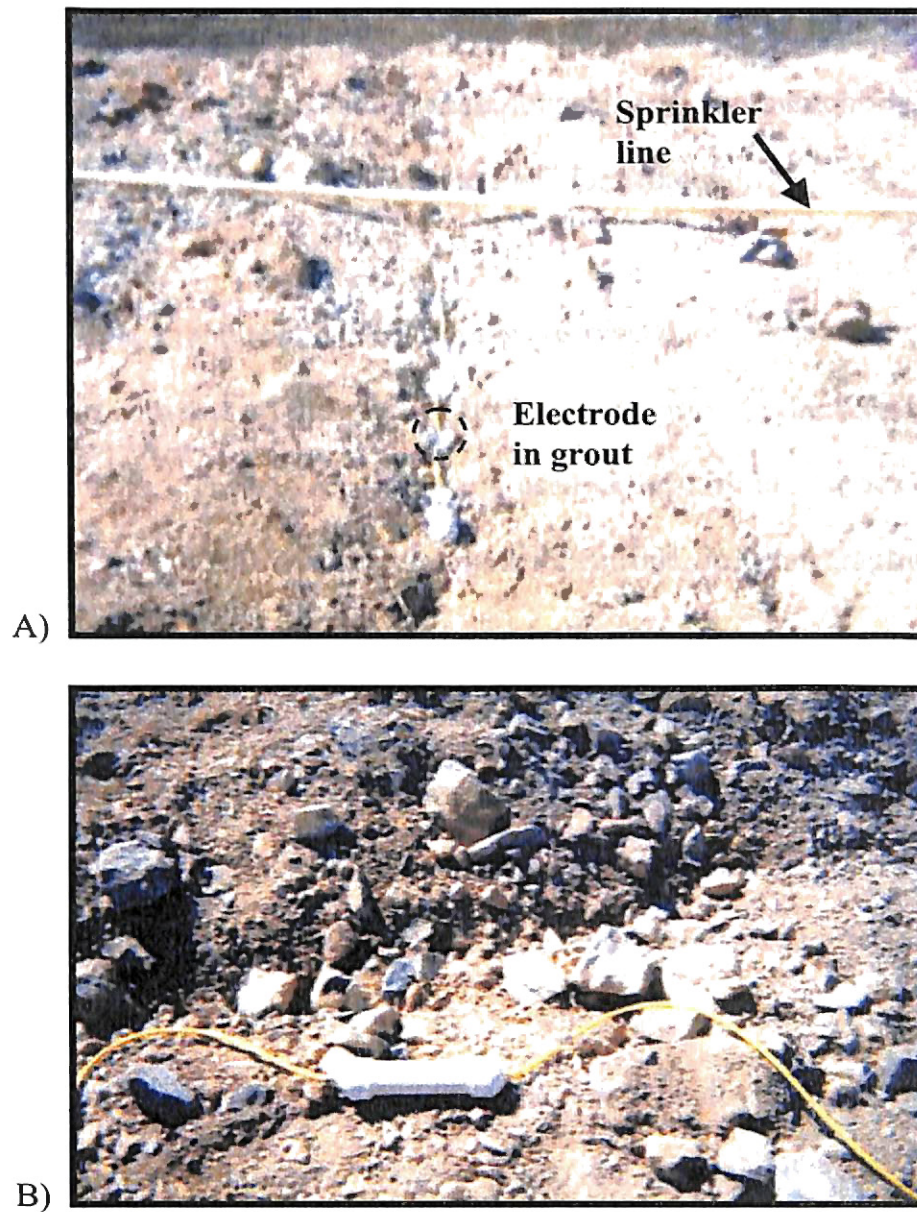


Figure 9. Cable B and C Setup.

- A) View of Cable B towards the edge of the heap. Each electrode rested in conductive bentonite grout in a small trough in the lift surface.
- B) Connectors were housed in PVC casings and sealed for protection.

is a common method of ensuring that current is applied directly into the surrounding media (Reynolds, 1997). These cables were connected to the switchbox by extension cables whose connectors were also encased in PVC for protection.

#### Additional Electrodes

Two of these graphite rod electrodes were placed on the surface with roughly 180° of separation with one on the eastern (IEE) and the other on the western (IEW) side of the heap (Table 1). These electrodes were used as infinity electrodes with the term infinity indicating that the distance separating the electrode line and graphite electrode is approximately ten times the length of the electrode line itself.

The four subsurface graphite rod electrodes were placed in lysimeters before lift construction at what would become the base of the top lift (Table 1). This introduced the potential for damage to the electrodes or the connecting wires during construction, but the three that survived were used to improve data resolution at the base of the heap, especially in and near the lysimeters. The 4 subsurface electrodes function as single borehole electrodes that increase the quality of data collected near their location. In this sense, data collected using these electrodes can be considered ERT. When these electrodes were used in conjunction with the surface electrode cables, data were collected using standard pole-pole or pole-dipole command files, treating the subsurface electrodes as infinity electrodes, but inverting the data as the equivalent of borehole electrodes.

Each of these electrodes had a unique location (Table 1). The combination of electrode cable, subsurface electrodes, and infinity electrodes in use determines the image plane for each data set. Subsurface electrodes may not be directly in-line with the surface electrode cable and any angular or directional relationship was considered when

interpreting the final inverted image. In these situations, the system measured the 2-D slice of the heap containing the cable and the electrode accurately, but it must be understood that the image represents a tilted “slice” of the heap in relation to the surface electrode cable.

<b>Electrode</b>	<b>Depth Below Surface (m)</b>	<b>Horizontal from Cable A (m)</b>	<b>Horizontal from Cable B (m)</b>	<b>Horizontal from Cable C (m)</b>
<b>PL1</b>	6.1	30.0	7.6	8.4
<b>PL2</b>	6.1	16.1	23.1	24.7
<b>TL5</b>	6.1	37.0	7.0	8.4
<b>LA4</b>	6.1	-3.0	0	-0.3
<b>IEE</b>	0.0	350	350	350
<b>IEW</b>	0.0	-127	-124	-125

Table 1: Positions of Subsurface and Infinity Electrodes. Horizontal distances are given as the lateral distance from the first electrode in the surface electrode cable (0 meters).

### Data Collection

Data are collected and stored via communication between the 8-channel resistivity equipment and electrodes. As the first stage in data collection, the contact resistance between electrodes was tested to detect possible electrode problems *a priori*. Then, data files were collected using command files that encode measurement sequences. Measurements were taken using standard array types.

### Contact Resistance Tests

Contact resistance is a good indicator of overall electrode condition. To perform this test the instrument sends a current between a designated electrode pair and simultaneously measures the voltage between the electrodes. This returns a value representing the electrodes' contact with the surrounding ore (Advanced Geosciences, Inc., 2001). This test is repeated for each electrode pair on the cable. A failed test indicates either a poor contact between the electrode and surrounding ore or a problem with cable connections or extensions. Since the electrodes could not be visually inspected often during leaching, contact resistance tests were conducted daily on each cable to monitor any change in electrode functionality.

### Command files

Command files are created and transferred to the measurement instrument to control how and when individual measurements are taken. These command files contain information regarding the location of current and potential electrodes and the type of array used. Each array type has inherent advantages, disadvantages, and sensitivities due to the electrode configuration and measurement technique (Reynolds, 1997). Varying electrode arrays were used to increase overall data set quality by minimizing the overall contribution of any one possibly malfunctioning electrode or array type. For this project, preprogrammed standard command files were also stacked so that many of the data files contain multiple executions of a single standard command file. These combined command files produce several data sets that can be separated and used for transient analysis in time change increments of 25 to 40 minutes.

### Pole-Pole Arrays

Pole-pole surveys collect data using the standard electrode cable as well as two mutually perpendicular infinity electrodes (IEE and IEW). For this study, pole-pole command files were used to increase depth of investigation and quality of data at depth. The correct locations of the additional electrodes were used during the inversion process to produce spatially accurate images.

### Pole-Dipole Arrays

Pole-dipole surveys use one infinity electrode in addition to the electrode cable. Pole-dipole data sets measured to an intermediate depth of investigation and resolution. Since these files collect fewer data points than pole-pole surveys, they can be completed in a shorter period of time. This was useful when changes in fluid flow were rapid at the start of wetting.

### ERT Arrays

These surveys were collected using one or two subsurface electrodes with an electrode cable. These surveys were collected using pole-pole and pole-dipole command files, but because of electrode locations they should be thought of as ERT data. These files contain more data points than dipole-dipole surveys, and also increase data density at the base of the top lift.

### Dipole-Dipole Arrays

Dipole-dipole arrays are widely used and accepted, but have the shallowest depth of investigation since no additional electrodes are used. Dipole-dipole surveys were used to give high resolution data near the surface at the point of infiltration. These

surveys were particularly useful when imaging the initial wetting front because they require the least amount of time and give the highest surface detail.

#### Additional Arrays and Induced Potential

Two other array types (Schlumberger inverse and Wenner) were tested for comparison. However, it was decided that these arrays did not produce significantly better data than the other arrays. Therefore, pole-pole, pole-dipole, and dipole-dipole command files were performed for the duration of the study for reliability and consistency.

Induced polarization (IP) arrays were also taken concurrently with two resistivity data sets. IP is a measure of the chargeability of a geologic material. IP is a phenomenon that occurs as a current is injected into the ground causing some materials to become polarized or charged. IP has been used successfully in the past to detect clay units and is generally sensitive to changes in lithology and pore fluid chemistry (Slater and Lesmes, 2002; Buselli and Lu, 2001). However, interpretation of IP data is much less quantifiable than resistivity and so these files were simply used as a comparison.

#### Data Inversion

The instrument (Figure 6) collects a file of raw voltage and current data in the field. Apparent resistivities can be calculated using this raw data. These apparent resistivity plots must be inverted to produce a model of resistivity values in the form of 2-D pseudosections. Transient inversions were also used to compare files with identical collection methods and show changes in resistivity through time.

### Inversion of the Apparent Resistivity Data

For this study, AGI EarthImager 2D™ version 1.5.0 was used to perform these inversions. Smooth-model inversion algorithms with noise suppression were run to provide smooth, gradational changes in resistivity rather than “blocky” images. considering the abrupt differences in resistivity that can occur in the heap, smooth-model is also a more stable inversion process than robust or damped least squares inversion algorithms.

### Transient Inversion

Time-lapse or transient inversions were performed to give a quantitative measure of changes in resistivity in the heap over time. This analysis can be used to show dramatic changes in resistivity or negligible changes as the heap reached steady-state flow conditions. Files taken back-to-back can also be used to show data repeatability.

Transient inversions require that files are collected in the same location with the same electrode configuration and command file. Since numerous combinations of infinity and subsurface electrodes and command files were used to create an overall robust data set, many of the transient inversion subsets were irregularly timed.

The transient inversion process begins by inverting the first file in the subset. This inverted file is then used as a starting point for inverting the next file in the series. Then, by comparing the two files, the software calculates the percent difference in resistivity and conductivity between the two files and generates additional representative images. This gives a total of four images in each transient inversion. The process continues by using the second data file in the series as a template for the third and so on.



## Resistivity Data Analysis and Editing

To preserve data integrity and consistently present resistivity results, data analysis and editing techniques must be standardized. Color scales should be justified and held constant when possible to allow for comparison of similar data sets. Files should be sparingly edited using analysis from sensitivity, statistical and trim data.

### Color Scales

2-D electrical resistivity results are highly visual. This means that color scale manipulations affect perceptions of the data itself. Color scales can be chosen to make the data look entirely homogeneous or heterogeneous. To avoid these data misrepresentations, standardized color scales were chosen and applied to each resistivity pseudosection (Figure 10). Color ranges were chosen based on the fact that the maximum resistivity early in the study was quite high (over 1,000,000  $\Omega$ -m) and later in the study the minimum was near 1  $\Omega$ -m. The initial scale for the dry heap had to have a range of several orders of magnitude in the 100-1,000,000  $\Omega$ -m range, while smaller changes in resistivity in the 1-300  $\Omega$ -m range were more common near the end of the study. For this reason, two color scales were chosen, one representing dry heap conditions and the other wet. Neither logarithmically nor linearly chosen color intervals could be created that would demonstrate these changes. Instead, customized color scales were created using the requirements that the interval size be continually increasing and the color contours on resistivity images approximate an even spacing. These scales would approximate a constant gradient scale for the data.

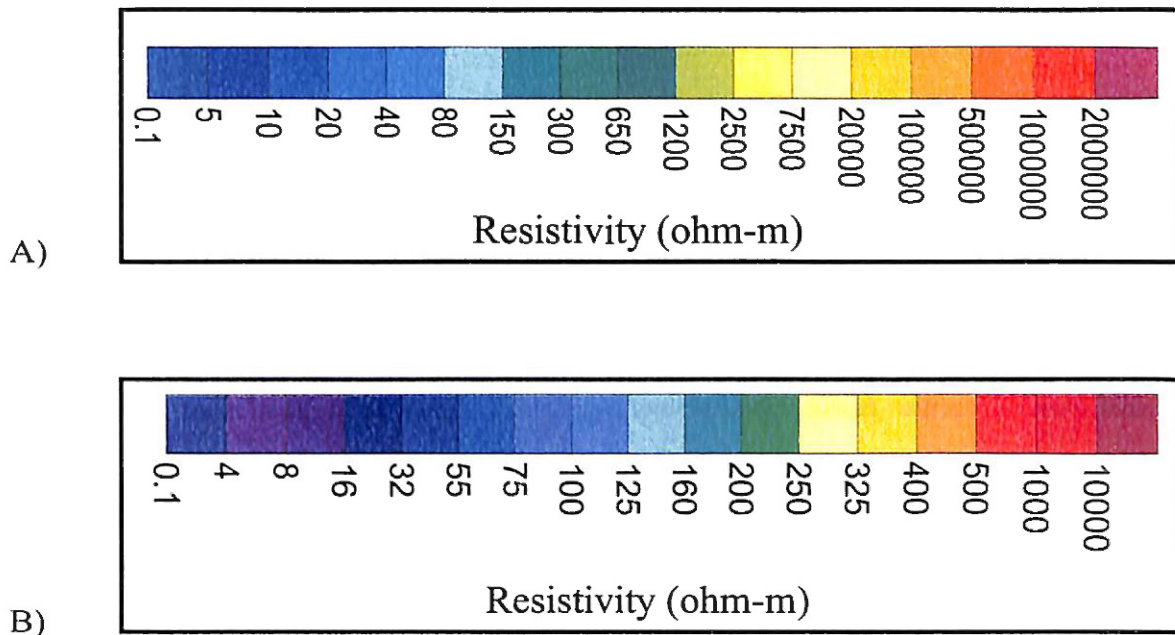


Figure 10. Custom Resistivity Color Scale.

- A) This color scale was applied to each inverted file during the initial wetting front to accommodate dry heap conditions. The levels or color intervals are not regular, but rather reflect the broad range of resistivity values (in ohm-m) that were present at the beginning of the study. Blue color hues also reflect areas of the heap affected by wetting.
- B) As the heap became wetter, resistivities dropped and the resultant range of values became smaller. This second color scale was applied to data taken after the initial wetting front reached the base of the lift. As with the first color scale, blue hues reflect areas that have been wetted to some degree and warmer color hues reflect an area with some degree of dryness.

Additionally, much of this study is concerned with showing the changes in resistivity between two images. Percent difference in conductivity images were also plotted for comparison to the percent difference in resistivity plots. With the use of percent difference calculations, large changes in percent may occur with insignificant changes of resistivity or conductivity values (i.e. not a 100% change from 1  $\Omega$ -m to 2  $\Omega$ -m). Standard color scales were chosen to show the positive and negative percent changes in resistivity and conductivity (Figure 11). Since conductivity is inversely proportional to resistivity, the color scales for these two properties were inverted, which allows blue hues to be interpreted as increasing conductivity using either scale, whereas red hues represent increasing resistivity. The use of inverted color scales allows for quick identification of areas with highly different percent differences that may be attributed to minimal changes in absolute values.

### Model Sensitivity

As with all potential techniques, the best resistivity data are collected nearest the electrodes. Plots of model sensitivity quantify the change in data collection ability as the data location increases away from the electrodes (Figures 11 and 12). Sensitivity is also a function of electrode geometry, apparent resistivity, and array type, so individual files have unique sensitivities (Zhou and Greenhalgh, 2002). For this study, the data seemed repeatable above a minimum sensitivity of 0.01. Below this value, the data appeared to reflect the signal strength rather than the signature of the heap.

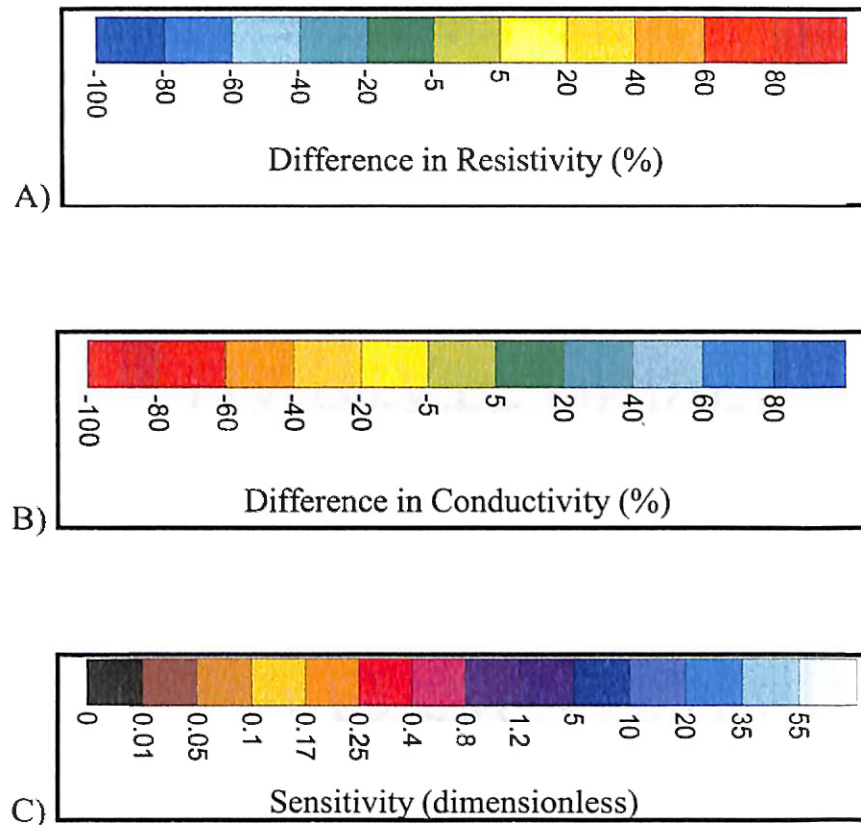


Figure 11. Color Scales for Sensitivity and Percent Difference Images.

- A) This color scale was applied to all percent difference resistivity plots calculated from transient inversions.
- B) Percent difference in conductivity images were plotted using this color scale. By using this inverted color scale, the percent difference in resistivity and conductivity images should be approximately identical.
- C) The color scale for sensitivity was chosen to represent a range in values from 0 to 55.

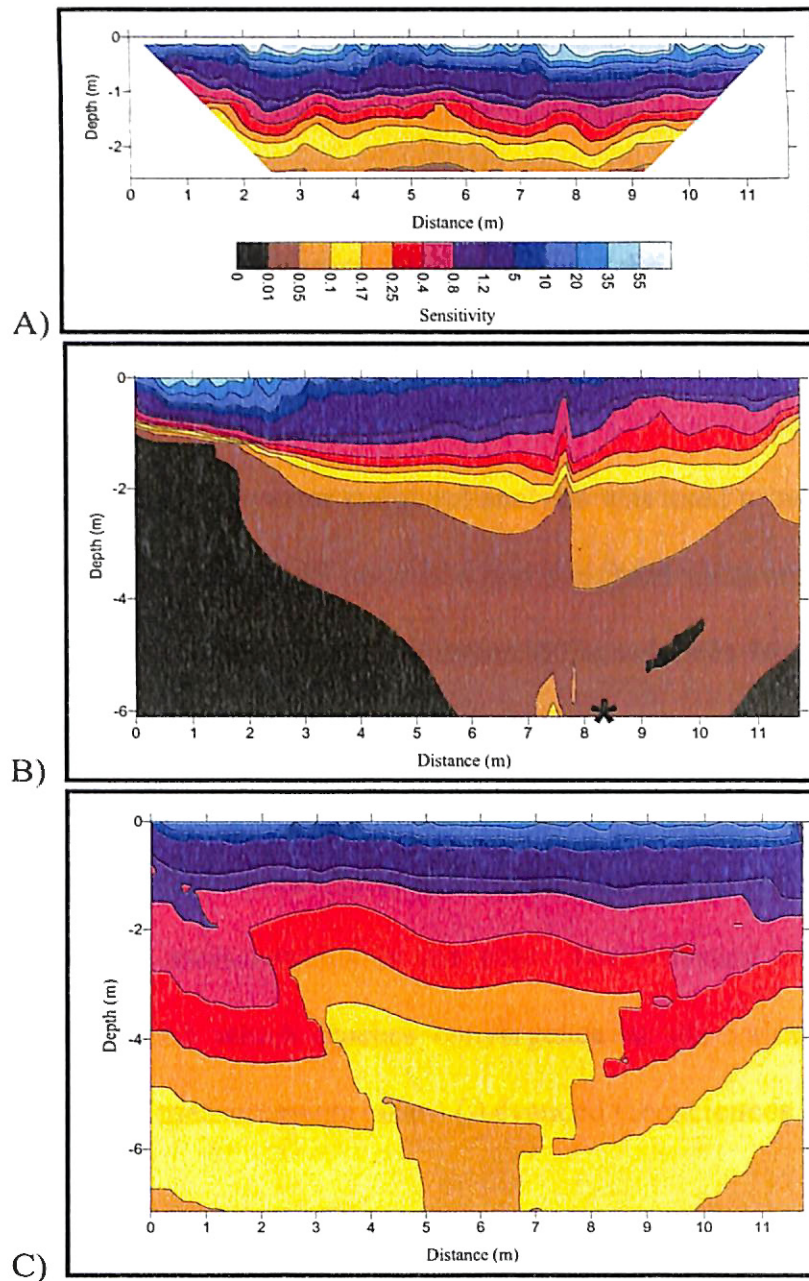


Figure 12. Model Sensitivity Plots.

- A) A sensitivity plot of file C27DDF3, which was a dipole-dipole file taken prior to wetting.
- B) A sensitivity plot of ERT file C27PD7 (wetted heap) has an increased depth, but has a poor sensitivity away from the single subsurface electrode (represented with an asterisk).
- C) A sensitivity plot of this ERT file (C27PP34, wetted) has increased sensitivity with depth through the use of two infinity electrodes.

The sensitivity function is a useful tool to use to establish degrees of confidence in areas of data. These images can help in deciding whether sections of data should be reliable or if the data may contain sources of error. Sensitivity plots were also used to help determine reliable depths of investigation in some of the drier and noisier data sets. These plots were often used to “blank” or trim data outside of the 0.01 sensitivity range.

### Statistical Parameters

Root mean square (RMS) error statistical analysis was used to evaluate data misfit relative to the inverted model. RMS error is a non-weighted measure of how well the data converges with the modeled solution (Advanced Geosciences Inc., 2003). Thus as the data becomes less noisy, the RMS error percentage decreases.

L2 Norm is another measure of data misfit that is defined as the normalized sum of the squared weighted data errors. Ideally, L2 values converge when the L2 value is equal to the number of measurements in the file. The software used in this study calculates a normalized L2 which reaches convergence at the value of 1 (L2 value divided by the number of measurements taken) (Advanced Geosciences Inc., 2003).

### Data Trimming

As with any geophysical technique, not all measured data are usable. In this study, command files were programmed to collect excessive data with the idea that any resultant poor data could be eliminated during processing. Special attention was given to the RMS percentage, L2 Norm value, Data Misfit Histogram, and model sensitivity during this process. It would be easy to over-trim and possibly misrepresent the data, so a protocol was established to be used for trimming each file:

- 1) Remove negative apparent resistivity values and noisy raw data points (points with greater than 3% error) prior to the first inversion. This resulted in a loss of 0% to 9% of the data with an average of 5%.
- 2) Check RMS error and Normalized L2 for their proximities to the goals of 10% or less and 1, respectively. Decide whether the file needs to be trimmed.
- 3) If trimming is necessary, proceed to the Data Misfit Histogram (Figure 13) and remove trailing and outlying points. Using this histogram the data should form a smooth continually decreasing curve. Spikes from this trend represent data that was trimmed. For this study, not more than 20% of the measurements were removed during any one trim, and a limited number of trims (not more than four) were performed. Generally, data points with RMS error less than 50% were not removed. On average, the final inversion retained 85.2% of the initial data with a range of 71% to 100% retained.
- 4) Remove areas of data with low sensitivities (less than 0.01) by blanking or “whiting out” the final image.



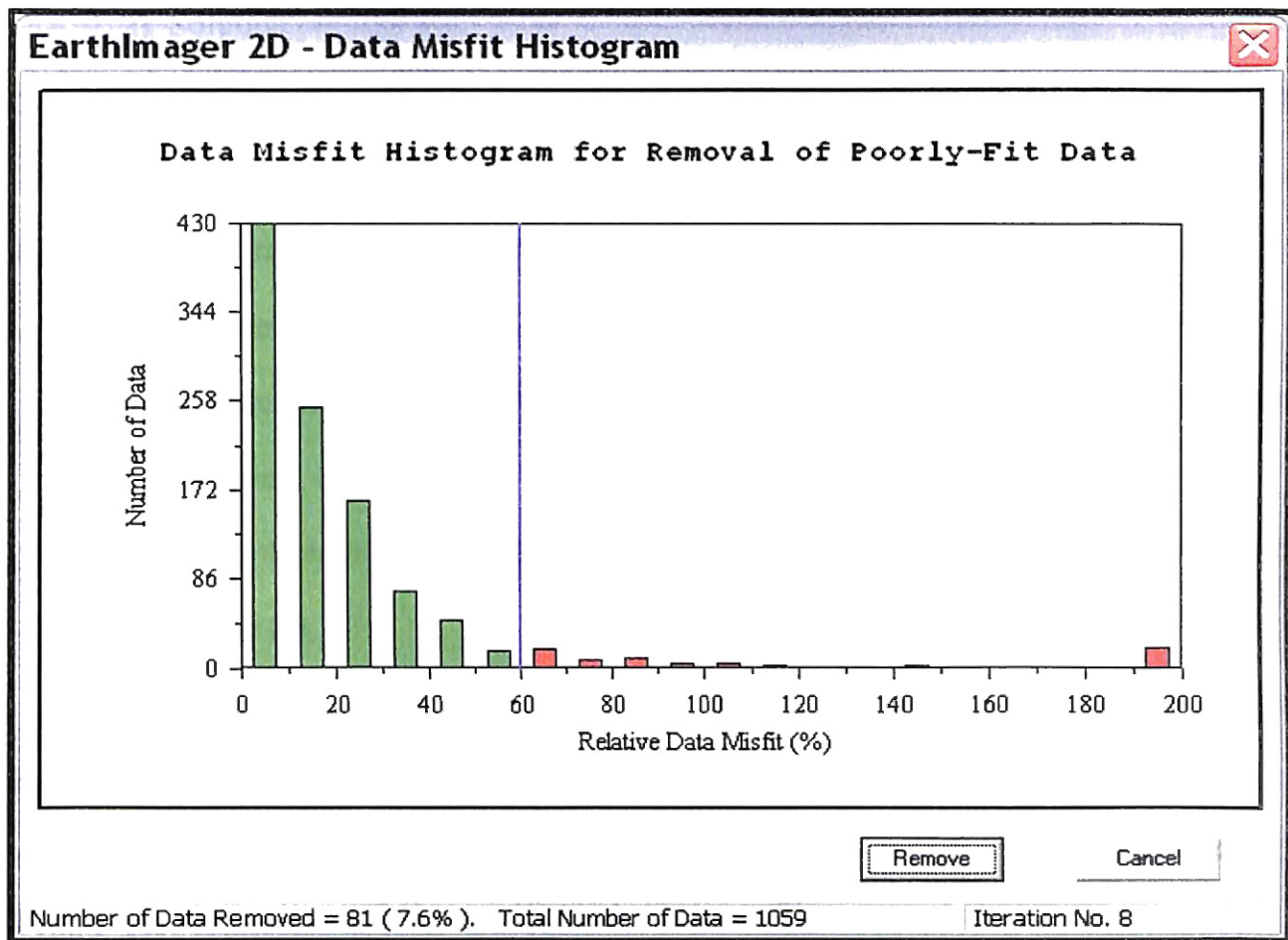


Figure 13. Data Misfit Histogram. EarthImager software allows for the trimming of data based on the data misfit error percentage. The blue line can be moved to the left to establish the error percentage beyond which the data will be removed (in red).

### Geochemical Analysis

A companion study was conducted to geochemically analyze the flow properties of the heap (Webb, 2003). These data were collected simultaneously with the geophysical surveys. Much of the data collected for that study will be helpful in constraining interpretations of the resistivity study, such as:

- 1) Daily solution application rates at 5 known locations on the heap surface,



- 2) Solution outflow rates from each of the 24 subsurface lysimeters,
- 3) Twice-daily field measurements of pH, TDS, EC, temperature, and DO of the solution as it flowed from the lysimeters,
- 4) Lab measurements of  $\text{CN}^-$  content and gold assays from solutions exiting lysimeters,
- 5) Measurements of gravimetric water content on ore samples before and after leaching, and
- 6) First observed flow times for solution outputs from the lysimeters at the base of the lift.

Some of these geochemical parameters were also used for comparison to the resistivity data. Since electrical conductivity (EC) is the inverse of electrical resistivity, fluid EC measurements were compared to resistivity measurements. The measured EC values were converted to electrical resistivity using Equation 3:

$$(3) \rho_a = (1/\text{EC}) * 10 [\Omega\text{-m}].$$

When electrical conductivity was entered in the units mS/cm, apparent resistivity ( $\rho_a$ ) resulted in the units of  $\Omega\text{-m}$ .

Velocities calculated using the inverted resistivity pseudosections were compared to calculated fluid flows using the lysimeter data. Resistivity pseudosection velocities were calculated using the change in depth of wetting over the time change between the two pseudosections at multiple, randomly chosen locations. Fluid flow rates from the lysimeters were calculated using the calculated fluid flux (Webb, 2003) using Equation 4:

$$(4) v = q / n_e [\text{m/s}].$$

When flux in m/s ( $q$ ) is divided by the effective porosity (dimensionless) ( $n_e$ ) the average linear velocity ( $v$ ) results in m/s. The effective porosity of the heap was estimated using values measured from gravimetric and volumetric water contents after the end of the leaching cycle. These values were calculated for five ore samples and the average linear velocities were calculated using the range of values present.

## CHAPTER IV

### RESULTS

The heap was nearly continually sampled over 9 days, resulting in the collection of over 177,000 resistivity data points. It was beneficial to collect a data set of that size to ensure repeatability of the data as well as to detect gradual changes. A total of 239 individual data files were collected during this study (Table 2; Appendix A). All images in this chapter are presented looking north, from west (left margin) to east (right margin).

Results are presented in order of the topic of study. Collected data files were first examined for data repeatability and dependability. Background resistivity prior to solution application was examined at each electrode cable location. A technique for identifying preferential flow was developed and applied in the presentation of results of wetting from Cable C and transient resistivity inversions. Induced polarization files were inverted and compared to concurrently collected resistivity files. Finally, resistivity results were compared to geochemical data.

<b>Cable Name</b>	<b>ERT Files</b>	<b>Pole-Pole Files</b>	<b>Pole-Dipole Files</b>	<b>Dipole-Dipole Files</b>	<b>Total</b>
Cable A	42	33	6	19	100
Cable B	17	11	16	13	57
Cable C	25	11	30	14	80

Table 2. Type of Files Collected. 237 total files were collected. Aside from those listed in the table, one Schlumberger Inverse file, one Wenner file, and four resistivity files containing induced polarization data were collected.

### Data Repeatability and Dependability

Data files with identical electrode configurations were often collected with small time changes (less than 4 hours). Transient inversions of such data sets show that the resistivity equipment was able to reproduce almost identical results when time did not change enough to allow for significant resistivity changes in the ore (Appendix B: Plates B-6, B-7, B-8, B-13, and B-26). These data sets provide good evidence for the repeatability of the collected data.

Since transient inversions are not an independent comparison of each data set, a series of graphs were plotted to determine if the trends of wetting in the transient inversion pseudosections correlate with the apparent resistivity and inverted resistivity of individual files. One dimensional line graphs of resistivity with depth taken from the same location along cable A (below electrode 19 at 18 meters and below electrode 20 at 19 meters) were plotted at variable times (Figure 14). Resistivity at differing locations within the same time interval were also compared (Figure 15). The graphs show that the data measured are variable, but repeatable after the first three days of wetting.

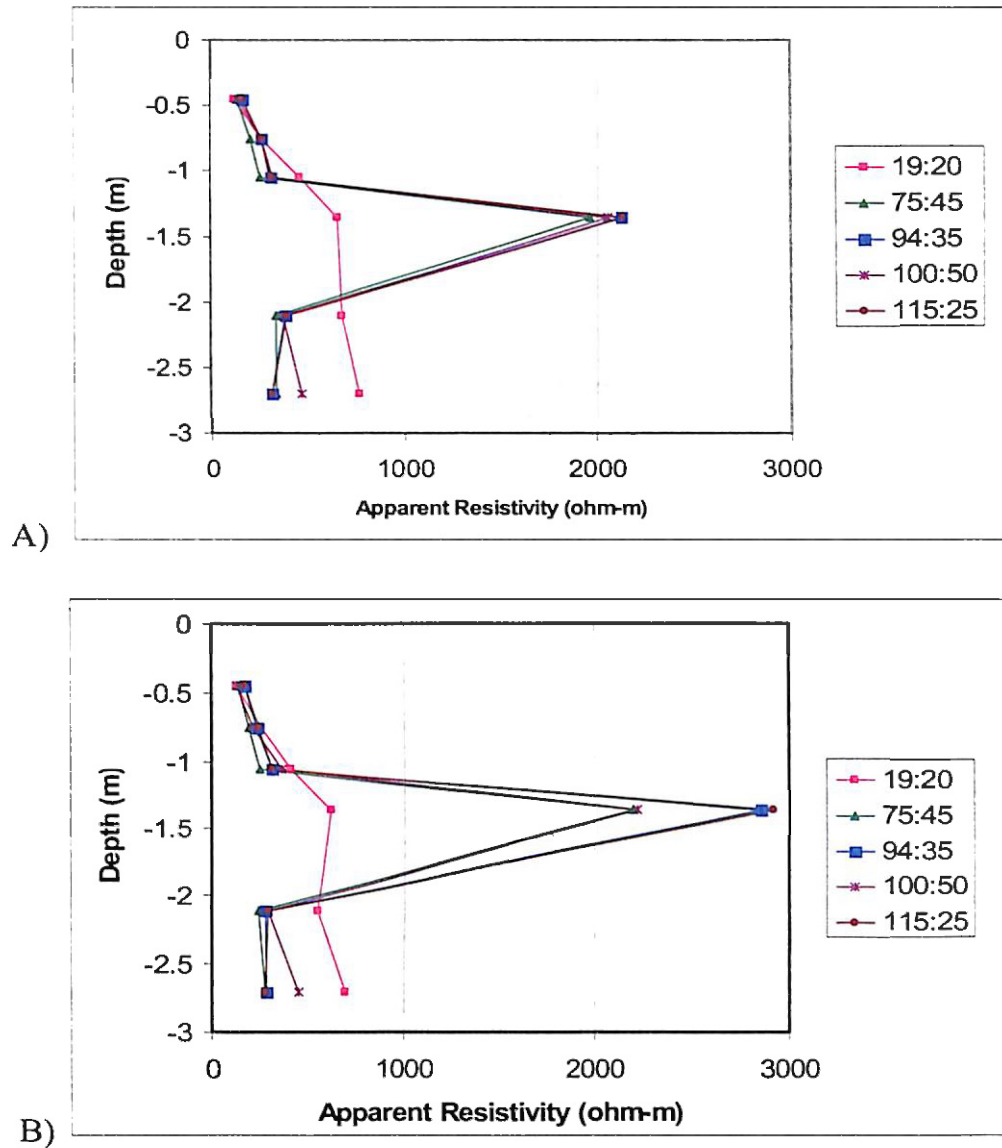


Figure 14. Change in Apparent Resistivity through Time. Each of these graphs represents a single 1-Dimensional profile of apparent resistivity at a fixed location. Each curve is identified by the start time of the file after the start of wetting in hrs:min. A) Resistivity profile below electrode 19 at 18 meters along cable A. B) Resistivity profile below electrode 20 at 19 meters. Both compare files at different time intervals from the Cable A dipole – dipole data series in Appendix B. The field locations of these profiles were separated by 1 meter, but the data shows similar resistivity trends through time. The graphs display the consistency of data collection at different locations through time.

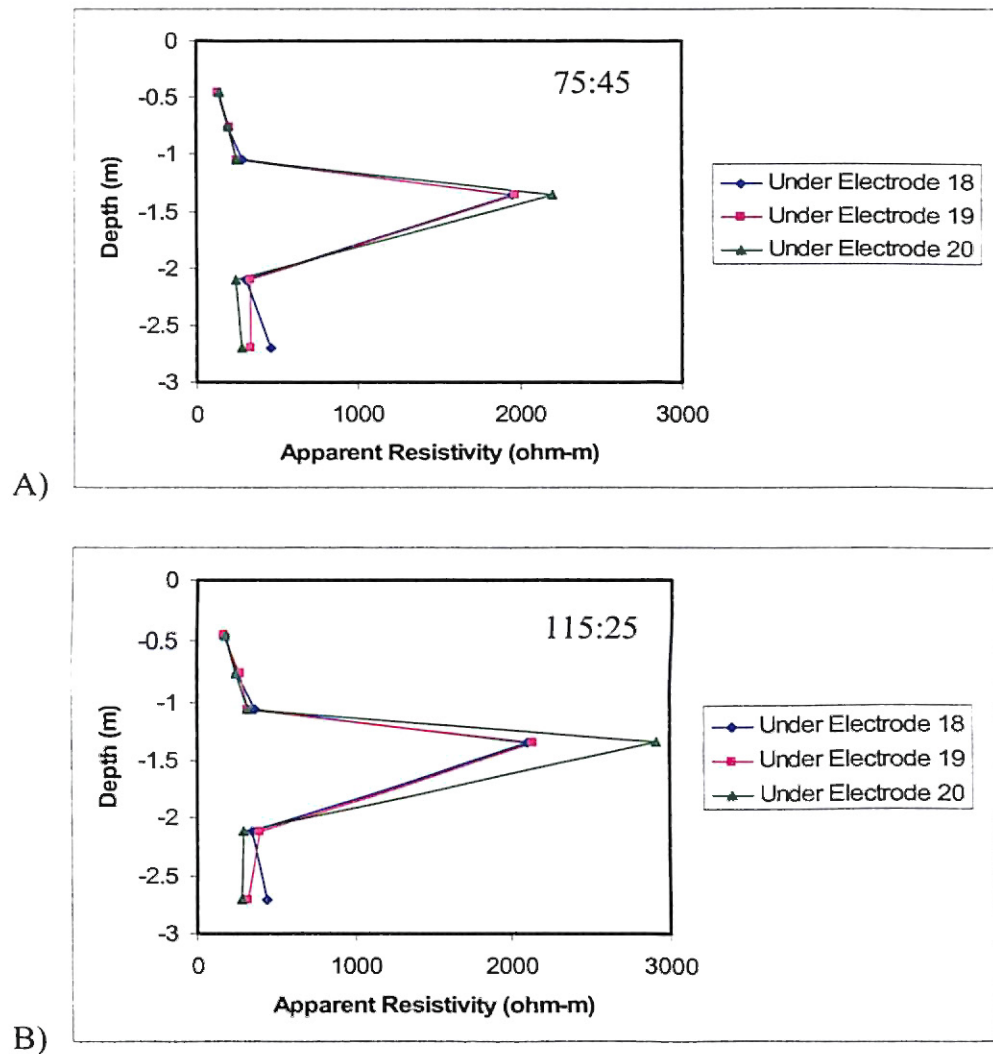


Figure 15. Change in Apparent Resistivity with Horizontal Distance. These graphs show 1-Dimensional profiles of apparent resistivity taken under the same surface electrodes with each graph representing a different time interval (A) File C36dd3 at 75:45 and B) File C36dd8 at 115:25 after the start of wetting). The graphs show that collected data were very similar, but later data tends to be more resistive (B) than earlier data (A).

## Background Resistivity

After setup of the resistivity equipment, eight preliminary resistivity files were taken to measure the resistivity of the dry heap at the locations of the three cables. These files were intended to measure the electrical resistivity of the initially dry ore to compare to later times, and reveal any unexpected structures or features within the heap.

However, background data collection proved problematic due to the extreme dryness and high resistivities (1,000  $\Omega$ -m to 1,000,000  $\Omega$ -m) (Figures 16 and 17). RMS errors were commonly greater than 40%. L2 Norm values were as high as 340 (Figure 17). Signal strengths were generally poor, and sensitivities dropped below 0.1 at approximately 2 meters depth. The sensitivity image in Figure 17 shows that many of the resistivity contours correlate with the decrease in signal strength at depth (below 2 meters). Where data are most reliable, the image shows a resistive signature (greater than 650  $\Omega$ -m).

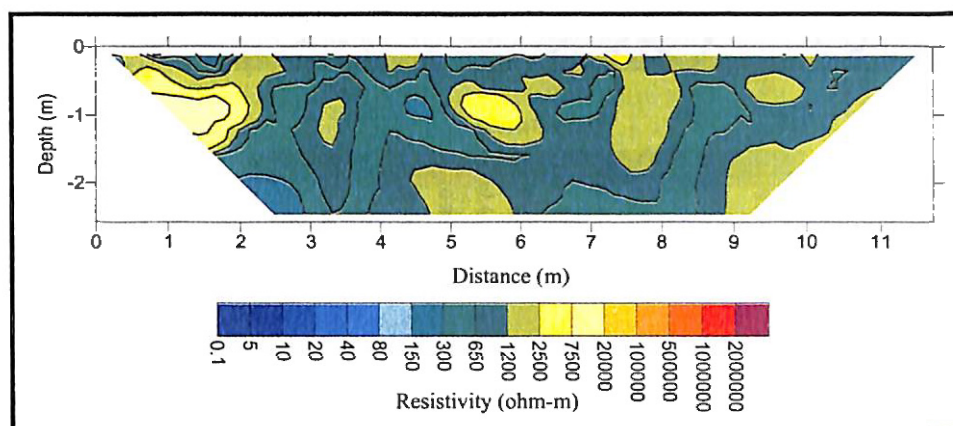


Figure 16. File C27DDF3 from Cable B. This dipole-dipole electrical resistivity image was taken as a background file and shows the even distribution of high resistivities prior to wetting. However, sensitivity degrades below about 2.5 meters depth (Figure 12A).



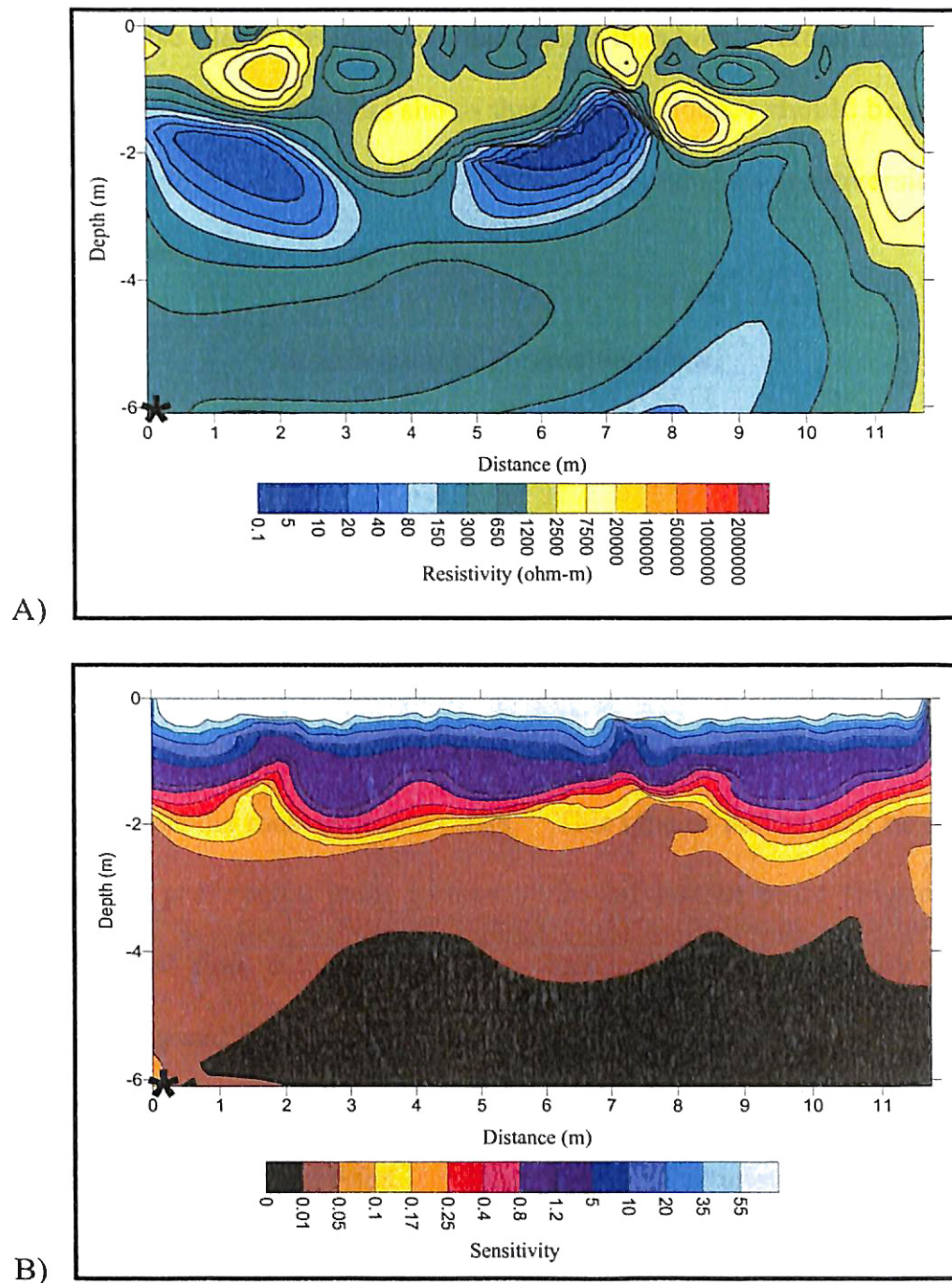


Figure 17. File C27PD1. A) This background electrical image was taken on Cable B with subsurface electrode LA4 (marked by an asterisk). Without further analysis, this image shows high conductivity areas prior to solution application. However, the sensitivity image for this file (B) indicates that sensitivity degrades below approximately 2 meters depth, and the true existence of those conductive regions was not supported.



Overall, these files collected fewer data points than later (wetter) files and the data was of poorer quality. Error analysis shows that little confidence should be placed in this data set. Direct comparisons to these files were avoided and transient inversions were not performed using these files as backgrounds.

### Identification of Preferential Flow

Several inverted resistivity images provide strong evidence for the presence of preferential flow. These data sets show definite spatial variability in electrical resistivity (Figures 18 and 19). Two points in the image plane within 1 meter or less may vary in resistivity by 100  $\Omega$ -m - 1000  $\Omega$ -m. When this uneven spatial distribution of resistivity follows a pattern of low resistivities (100  $\Omega$ -m or less) adjacent to higher values, preferential flow was the most probable cause. This type of pattern can be identified at the surface where preferential paths formed at the infiltration point (Figure 19) or as channelized vertical flow paths (Figure 18). Such patterns of resistivity that can be attributed to wetting and fluid migration constitute preferential flow.

The following inversions were taken after the initial wetting front and each shows variations in resistivity interpreted as fluid flow characteristics. Some of these characteristics include a potential for fingering, the development of linear conductive features (flow paths), zones of increasing conductivity (pockets of fluid collection), and zones of consistently higher resistivity (drier ore). White arrows were used to show some of the areas affected by linear conductive features (preferential flow) (Figures 18 and 19). These areas are often connected by narrow passageways similar to those observed in laboratory studies of heterogeneous flow (Figure 5).

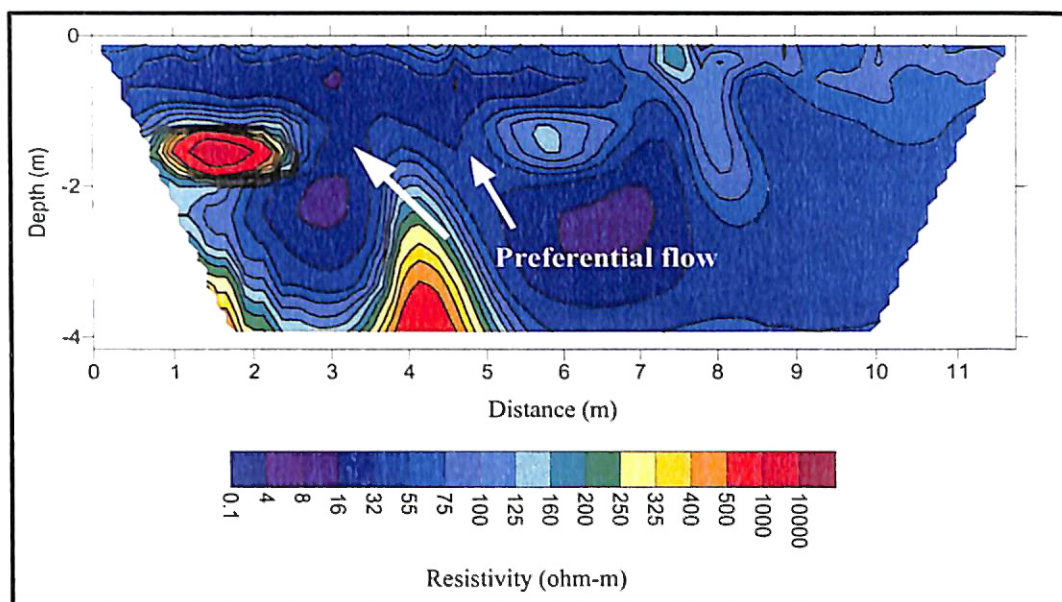


Figure 18. File C27PD13a. Inferred preferential flow paths are identified with white arrows on this pole-dipole file collected on cable B. It is also apparent that areas of high resistivity (dry ore) remain above 2 meters depth even after 2.5 days of wetting.

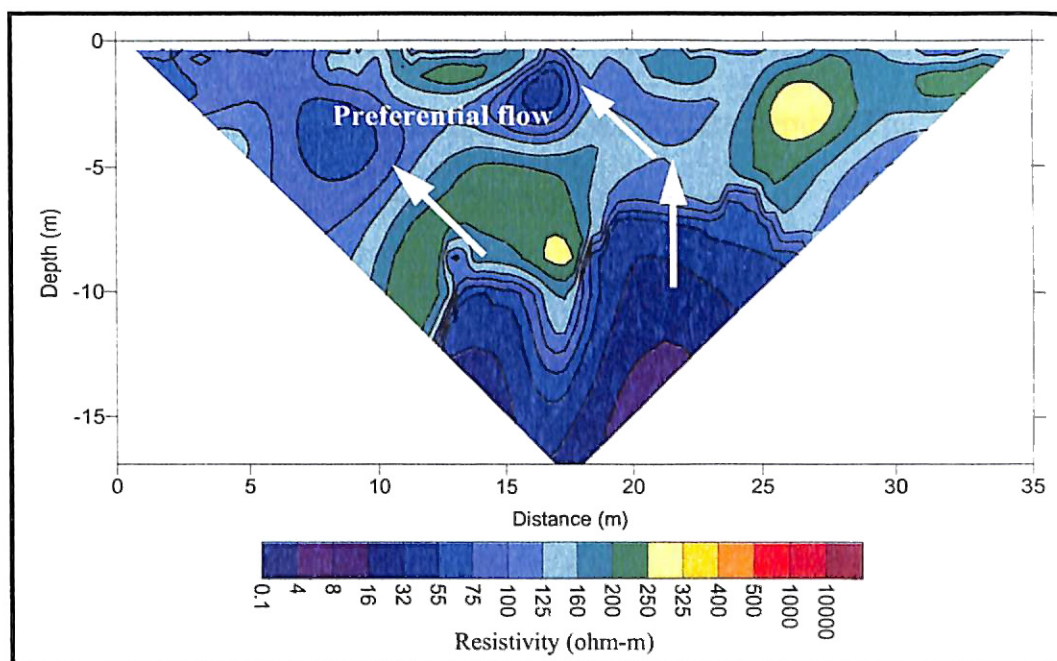


Figure 19. File C36PP25. This pole-pole file from cable A was taken on the last day of data collection (187:50) and zones of variable wetting still exist.

## Cable C Wetting Front Data

Analyzing the resistivity surveys from the first two days of the study can reveal effects from the start of leaching. These data can answer two important questions: “Do the interpretations of the resistivity images correlate with the fluid output of the lysimeters?” and “What pattern does the initial wetting front take as it flows through the top lift?”

A series of six data files is presented that shows the progression of the wetting front over the first three days of wetting (Figures 20, 21, 22, 23, 24, and 25). Figures 21, 22, 23, and 25 were all taken with the same combination of electrodes and measured the same volume of ore, so they can be directly compared. The additional figures fill gaps in time and show the general advancement of wetting through time.

All of these files were collected on Cable C with any additional subsurface electrodes depicted with an asterisk (Figure 2). The base of the top lift and the depths of the subsurface electrodes and lysimeters are at 6.1 meters depth. The file starting times are presented as “hours:minutes” after the start of wetting.

These surface resistivity surveys are interpreted to indicate the gradual, yet variable rate of fluid flow as the resistivity decreases over time. Pockets of low conductivity (wetted areas) developed throughout the top meter of the lift within 2 hours (Figure 20), but the top of the lift doesn’t appear to be thoroughly conductive (wetted) until 25:30 hours (Figure 21). A low resistivity zone (high moisture content) was consistently retained around 2.5 meters depth on the eastern side of the image plane for the second day of wetting (Figures 21, 22, and 23). Then, on the third day of wetting, the resistivity

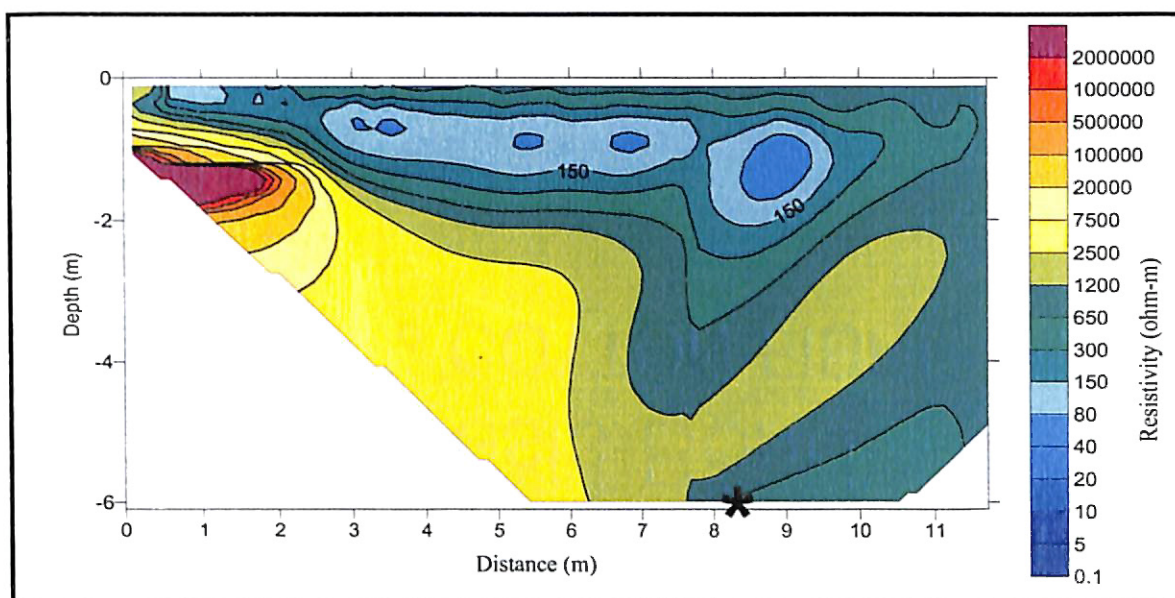


Figure 20. File C27PD7. This file began at 02:25 and used the subsurface electrode PL1. Within that time a conductive zone (some wetting) has progressed to approximately 1 meter at depth.

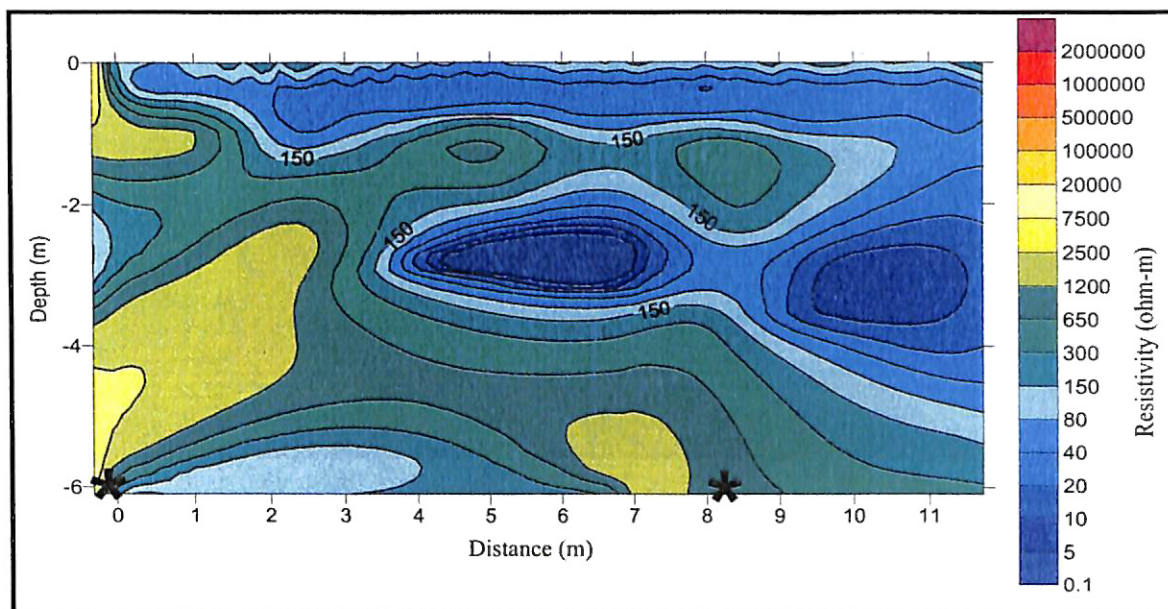


Figure 21. File C27PP8. This resistivity file began at 25:30 and used the subsurface electrodes TL5 and LA4. This data shows the top meter of the lift to be uniformly more conductive (wetted) with less uniform zones of resistivity (pockets of wetting) developing to 4 meters.



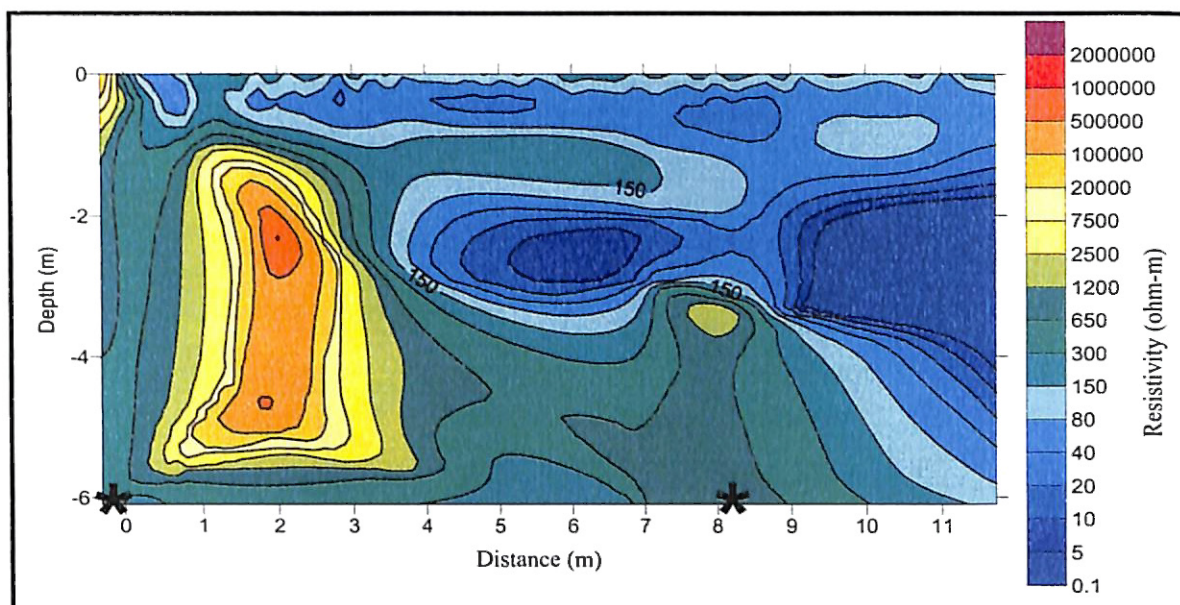


Figure 22. File C27PP12. This file began at 45:05 and used the subsurface electrodes TL5 and LA4. Although 19 hours have passed, Figures 21 and 22 are similar.

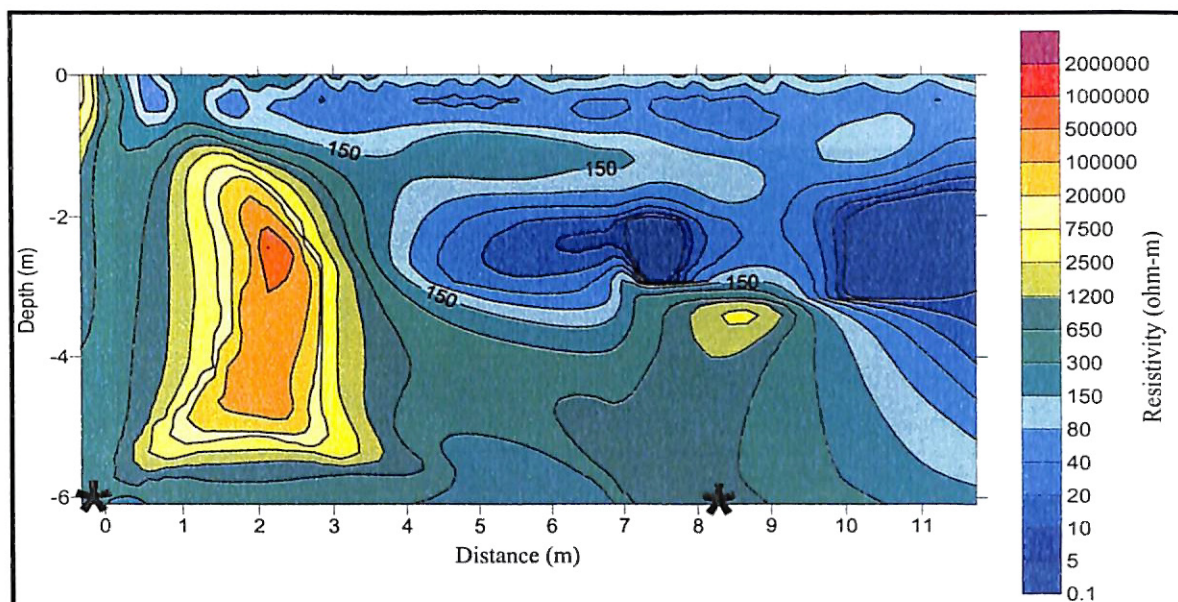


Figure 23. File C27PP14. This file started at 46:55 and used subsurface electrodes TL5 and LA4. In the two hours between this file and the previous (Figure 22), the eastern portion of the image (to the right) has grown more conductive (solution has increasingly flowed eastward).

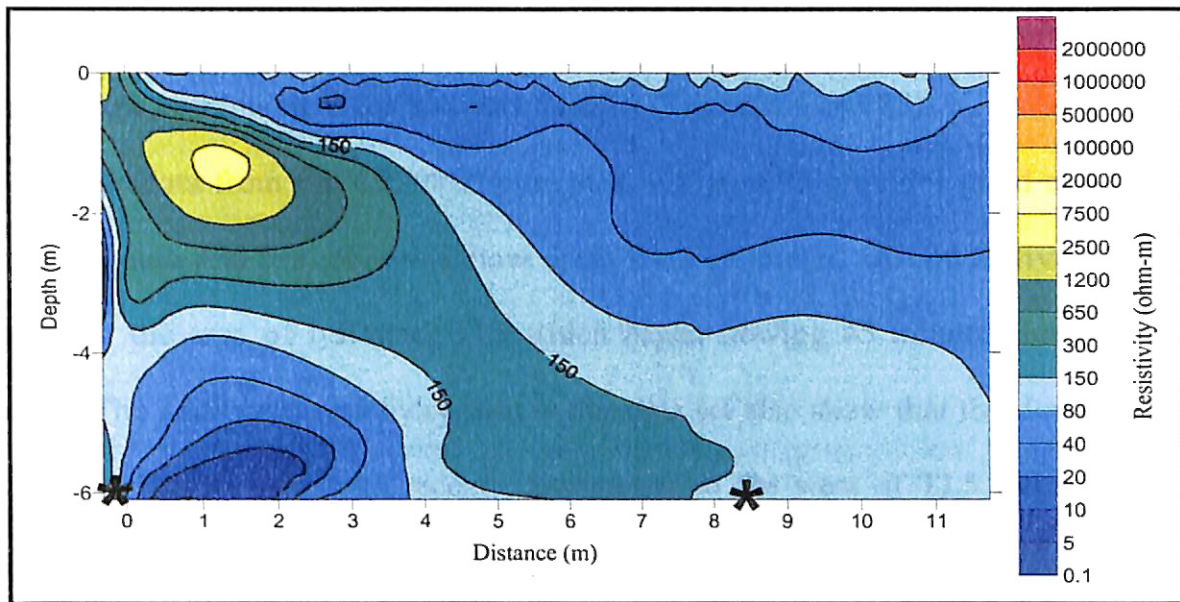


Figure 24. File C27PP18. This resistivity file began at 53:45 and used subsurface electrodes LA4 and PL1. The resistivity changes here were more horizontally distributed potentially indicating that wetting was more evenly distributed in this more northern image plane.

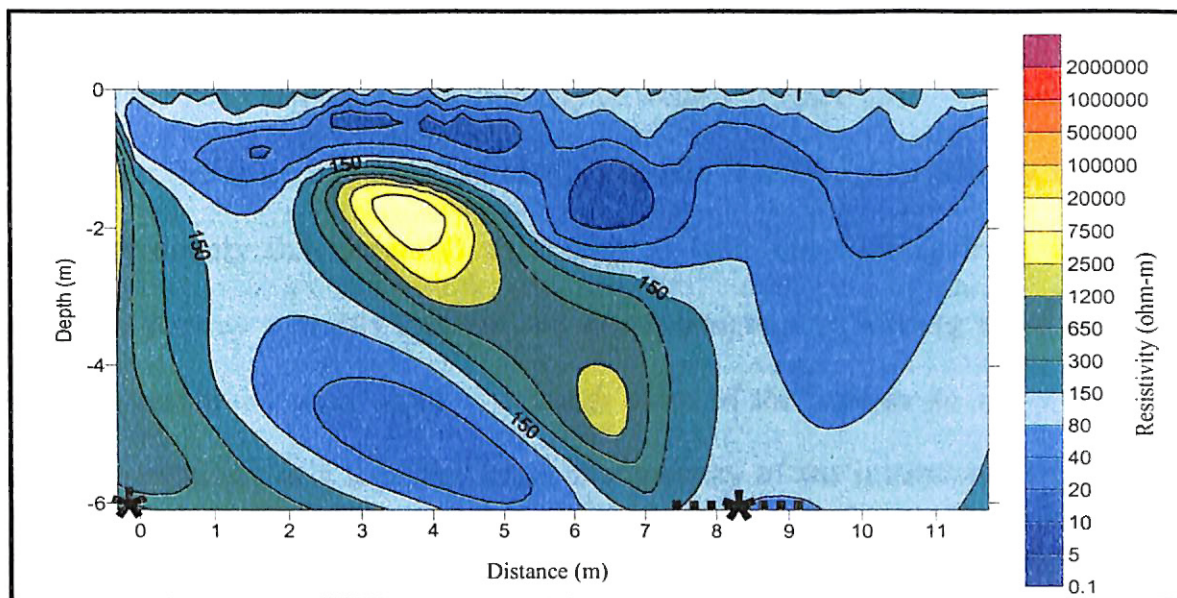


Figure 25. File C27PP20. This resistivity file began at 69:20 and used the subsurface electrodes LA4 and TL5 (marked by asterisks). The lysimeter TL5 is also labeled ( ..... ). This is the first data file collected after lysimeter TL5 began to flow.



of this area went back up and conductivity increased below it, which has been interpreted as fluid flow continuing to the bottom of the lift (Figures 24 and 25).

The data from file C27PP20 presented in Figure 25 provides good correlation of resistivity data and first observed flow times from lysimeter. A conductive region was imaged in the area of lysimeter TL5 which began flowing 45 minutes before this file started. The additional resistivity files in this data set also show that the development of the low resistivity zone was recent. Lysimeters to the west of TL5 did not flow for another day, and are still in a zone of higher resistivity (dry) in this image.

This series of images also shows the effect of variable solution application on the development of preferential flow paths. Cable C was located near the western edge of the lift (Figure 2). During the first few days of the study, this slope remained dry due to an eastward wind affecting the sprinklers and poor sprinkler coverage (which was later modified). Resistivity data support these observations by showing flow predominately away from the heap slope until the third day of wetting (Figure 25).

Since the scale of resolution that is possible from the data density in these files was approximately 0.5 meters (1 to 2 feet) at best, the wetting front images were expected to portray a mostly uniform and slowly progressing wetting front as a steadily decreasing resistivity with depth. Although some of the images do show this type of change in resistivity at a localized scale, the majority of the inversions depict irregular zones of high and low resistivity interpreted as preferential flow paths. It is apparent that resistivity drops due to fluid flow occur in distinct pathways.

## Transient Resistivity

Resistivity files were sorted into sets with identical command files and electrode configurations. Transient inversions were performed on these data sets to identify changes in flow through time. Four complete series of transient inversion sets are presented in Appendix B.

Individual transient inversions are presented as a group of four images. The first two images are inverted resistivity pseudosections. The first acted as a starting point and the second resulted from the transient inversion. These are followed by an image of the percent change in resistivity between the two, and then the percent change in conductivity for comparison. The start time of each image is given as the cumulative time after the start of wetting in “hours:minutes”.

### Cable A

Three extensive series of transient inversions taken on cable A are presented in Appendix B. These data series contain dipole-dipole, pole-dipole, and pole-pole data.

The dipole-dipole data series on cable A spans the entire period of time studied, but only provides reliable data to 5 meters depth. The first three transient inversions in this series were performed in reverse chronological order to account for poorer data quality at times with drier ore (Appendix B: Plates B-1, B-2, and B-3). Data from the first three days of wetting consistently showed an increase in resistivity as inversions were performed from wetter to drier times (Appendix B: Plates B-2 and B-3). Zones of increasing conductivity generally indicated poor signal strength below high resistivity zones (especially when the electrical resistivity was greater than 7500 ohm-m) (Appendix B: Plate B-3).



During the third day of wetting, resistivity of the ore dropped as moisture content increased and resistivity data quality improved to allow the remainder of the dipole-dipole transient inversions to be performed forward in time (Appendix B: Plates B-4, B-5, B-6, B-7, B-8, and B-9). This data series repetitively shows a somewhat continuous zone of resistive material between 2 and 3 meters depth. These inversions also show gradual changes in resistivity with percent difference in resistivity ranging  $\pm 40\%$ . Files taken within 2 hours of each other show negligible changes ( $\pm 5\%$  change in resistivity) and illustrate the level of data repeatability achieved (Appendix B: Plates B-6, B-7, and B-8).

The cable A pole-dipole data series was collected using infinity electrode IEE and images the top lift of the heap. However, this data series only contains three transient inversion sets and contains large gaps in time (Appendix B: Plates B-16, B-17, and B-18). These inversions contain resistivities generally below 200 ohm-m, suggesting some influence by fluid flow for most of the top lift. Even though most of the ore appears to have been somewhat wetted, resistivities continued to change with time, and much of the top 5 meters of ore increased in resistivity through time (Appendix B: Plates B-16, B-17, and B-18). This is an unexpected result of the study that will be further discussed in the next chapter.

The largest of the cable A transient inversion data series includes pole-pole data taken using infinity electrodes IEE and IEW. The sum total of resistivity changes for that series shows that significant increases and decreases in resistivity occurred during the last five days of the study (Figure 26). Smaller time change increments indicate more gradual changes in wetting (Appendix B).

The transient inversion from file C26pp12 to file C36pp27 (Figure 26) presents the total changes in resistivity from the first to the last file in the Cable A pole-pole data series spanning approximately 100 hours of wetting. The later resistivity image (C36pp27, Figure 26) shows the development of more defined conductive zones (flow paths) with abrupt contacts between zones of high and low resistivity. Zones of resistivity greater than 500 ohm-m are proximal to zones with resistivity less than 100 ohm-m. The low resistivity zone between 5m and 10m on the western side of file C36pp27 (Figure 26) does not appear to have a flowpath connecting the anomaly to the surface, yet the resistivity decreases in that area. Contrary to expectations, the earlier image from file C36pp12 (Figure 26) shows a more even distribution of wetting with a range in resistivity of approximately 35 ohm-m to 250 ohm-m.

#### Cable B

One series of transient inversion sets collected using Cable B is presented in Appendix B (Plates B-10 through B-15). This data set was the most statistically sound and mechanically repeatable type of file collected during the study. Each file contained the same number of data points and none of the files required any trimming, other than for sensitivity.

With this good data quality, a number of interesting observations can be made using this data set. The top two meters of the heap became more resistive through time starting with the 5<sup>th</sup> day of wetting, while the ore below four meters became more conductive (Appendix B: Plates B-10, B-12, B-14, and B-15). Also, some changes in resistivity appear to be isolated with respect to surrounding ore on the image plane (Appendix B: Plate B-11).

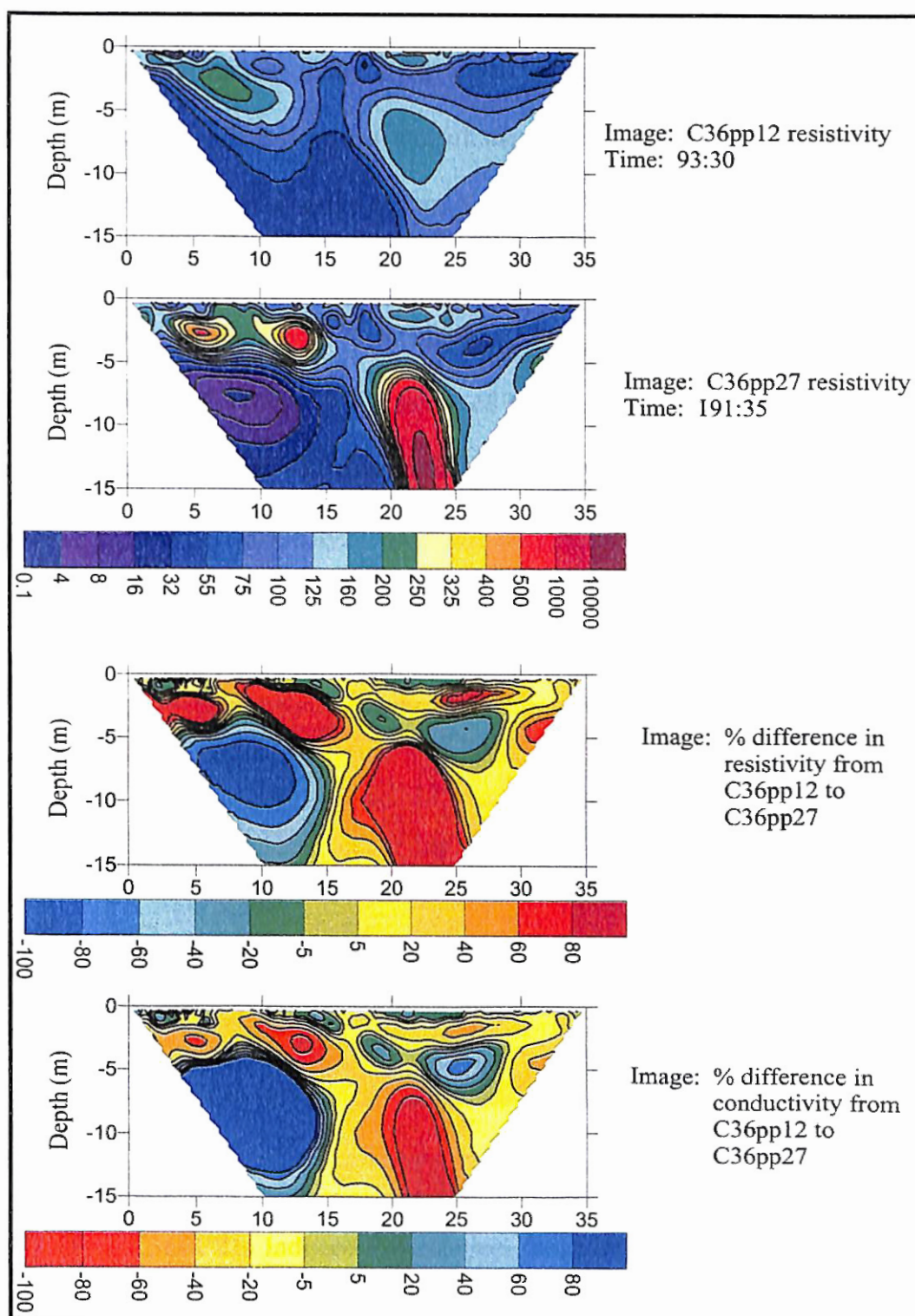


Figure 26. Transient Inversion Set from C36pp12 to C36pp27. This group of inversions represents the sum total of resistivity changes in the Cable A pole-pole transient inversion set.

## Cable A Induced Polarization Files

Induced polarization files were collected to help distinguish between the conductive signatures of clay versus that of the cyanide solution. The hypothesis was that areas with clay content would be more chargeable than those without. The following induced polarization pseudosection is presented with the concurrently measured resistivity section and sensitivity plot (Figures 27, 28, and 29). Although the IP signal was weak (changes of  $10^{-3}$  mV/V), zones of low chargeability tend to correlate with zones of poor sensitivity and high resistivity. Similarly, zones of low resistivity correlate with zones of higher chargeability.

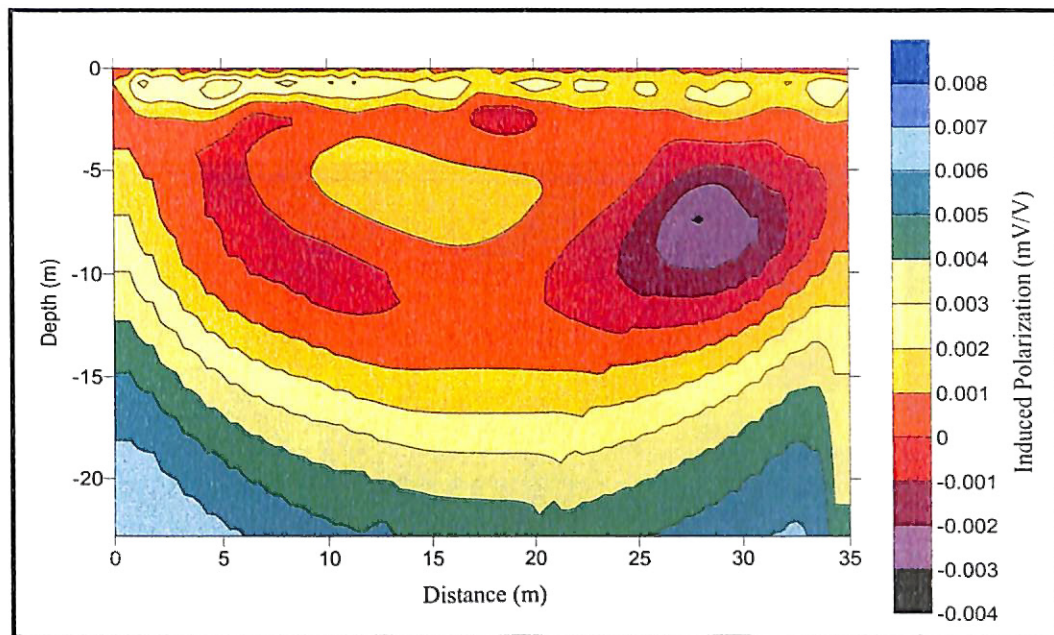


Figure 27. File C36PP22a Induced Polarization. Notice that the changes in chargeability are slight, and have a range of only 0.011 (or 11 mV/V).



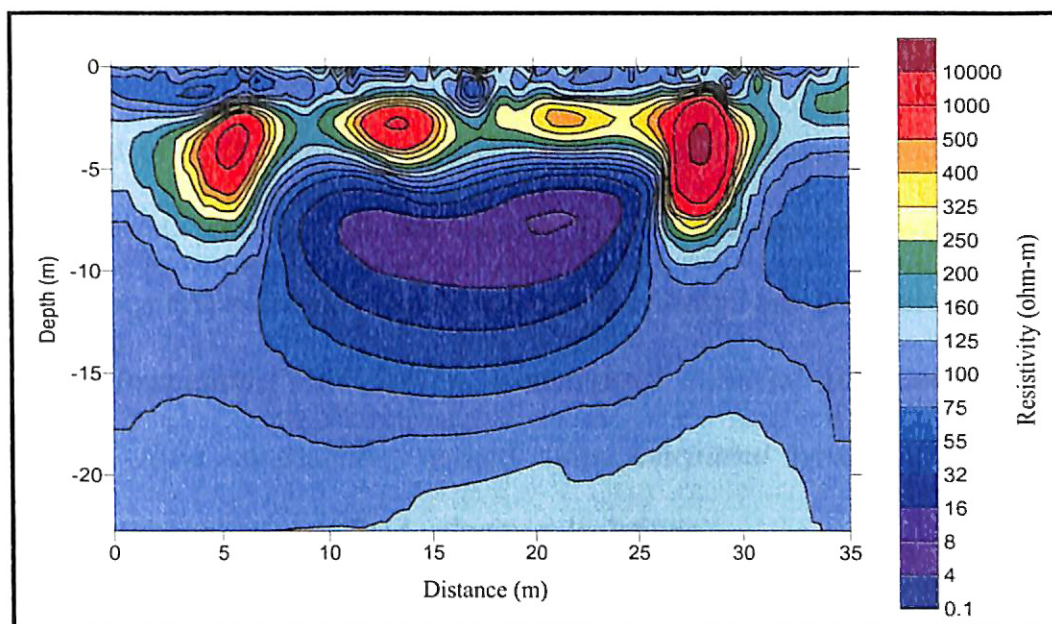


Figure 28. File C36PP22a Resistivity. Even though this pole-pole file was collected at 165:50 after the start of wetting, zones of high resistivity remain near 3 meters depth.

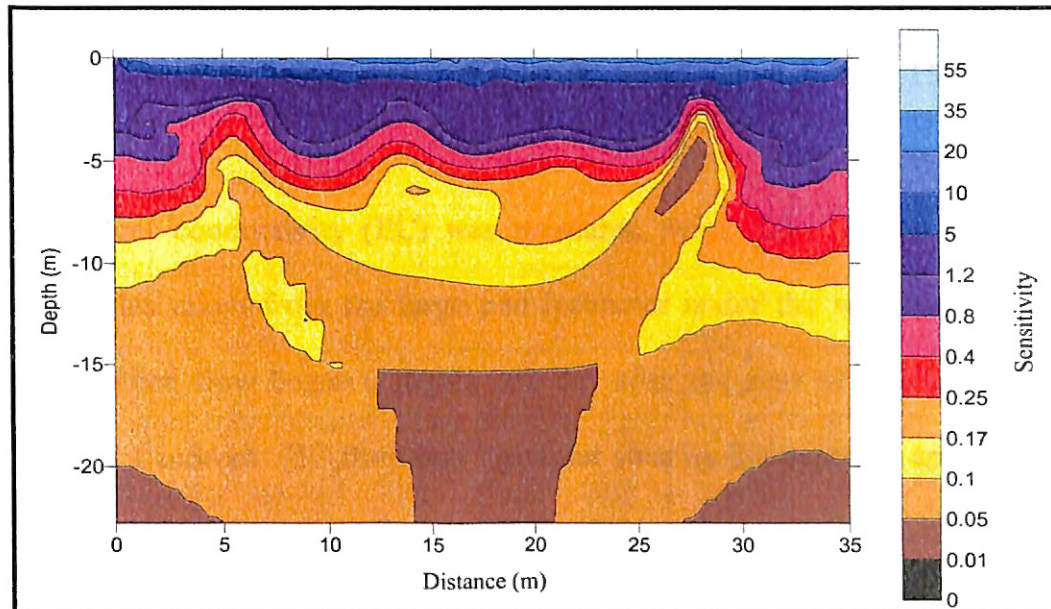


Figure 29. File C36PP22a Sensitivity Plot. Sensitivity for this file begins to degrade near 10 meters depth, especially in zones of high resistivity.

## Geochemical Comparisons

Several of the parameters used in a companion study were used as comparisons for resistivity data collected in this study. The comparison data were calculated or monitored using lysimeter flow rates, solution chemistry, ore grain sizes, and solution application information (Webb 2003). Comparisons included gold content in solution through time, fluid conductivity through time, calculated porosity, gravimetric and volumetric water content, and fluid velocity calculations.

### Gold Content and Solution Conductivity

Gold content in solution was measured throughout the study and by gold assays measured in ounces of gold per tonne of solution. Values ranged between 0.02 and 0.18 oz/tonne. Gold content in solution at the lysimeters peaked after approximately 2.4 days and again after 6 days (Webb, 2003). It should be noted that solution outputs from the large pad lysimeter are an average of solution properties over the 1500 feet<sup>2</sup> of ore covered.

Electrical conductivity (EC) was measured twice daily during the study from solution samples taken from the large pad lysimeter under the western end of the lift (Figure 2). When flow began (roughly one day after the start of wetting), the EC was approximately 1 mS/cm. EC from that lysimeter steadily increased to approximately 3.2 mS/cm at the end of the study (Webb, 2003). Calculations using Equation 3 to convert conductivity to resistivity resulted in a range in fluid resistivity of 3.1  $\Omega$ -m (end of study) to 10  $\Omega$ -m (first lysimeter solution sample).

The EC was expected to correlate with gold content peaks. However, no correlation could be determined. There was no noticeable change in the trend of EC

when the gold assays peaked. This suggests that gold in solution does not make a significant contribution to the fluid electrical properties.

#### Gravimetric and Volumetric Water Content

Surface samples were analyzed for water content before and after the leaching cycle. Previous to wetting, the ore contained  $0.01 \text{ g}_{\text{water}}/\text{g}_{\text{dry ore}}$ . This was increased to an average of  $0.1 \text{ g}_{\text{water}}/\text{g}_{\text{dry ore}}$  after the end of leaching. Volumetrically, water composed an average 3% of the ore before wetting and an average of 19% afterwards (with a range of 14% to 29% for the five sample volumes measured) (Webb, 2003).

These calculations show the increase in water content for the entire duration of the leaching cycle, and show that the increase in wetting was significant. This also indicates that measured porosity in the heap was at least 14% to 29%. However, additional samples were not analyzed during this study to be able to interpolate a trend in the moisture content to compare to the resistivity data which were only taken during the first 9 days of the leaching cycle.

#### Fluid Velocity

Fluid velocity was approximated using the vertical change in resistivity from inverted resistivity pseudosections. Pseudosections taken prior to wetting reaching the bottom of the lift with identical electrode configurations were chosen for comparison. Calculated velocities ranged from  $1.5 \times 10^{-5} \text{ m/s}$  to  $5.6 \times 10^{-5} \text{ m/s}$ . These velocity approximations remained consistent independent of which pseudosections were compared or the magnitude of time change represented.

During the same time intervals, the large pad lysimeter had recorded flow rates from 4 to 6.5 gpm. This was converted to a flux (flow rate over the area of the lysimeter)

of  $2 \times 10^{-6}$  m/s to  $3.2 \times 10^{-6}$  m/s (Webb, 2003). Average linear velocities were calculated using Equation 4 to yield a range of  $6.9 \times 10^{-6}$  m/s to  $9.3 \times 10^{-5}$  m/s. It was hypothesized that this velocity calculated from actual lysimeter outflow should be roughly equivalent to fluid velocities calculated from the resistivity data. In fact, the resultant calculations are of the same magnitude with the lysimeter values having a larger range of values.



## CHAPTER V

### DISCUSSION

Changes in resistivity could possibly be interpreted as changes in fluid movement, solution composition, or generated electrical potentials. Fluid movement and changes in wetting were determined to be the only significant causes of resistivity changes, since solution had a fairly constant electrical signature and interference from electrical potentials (SP) should have been minimal. As the heap was initially wetted, an overall decrease in resistivity was noted. Areas with lower resistivities were considered to be indications of increased fluid content. Such areas often appeared as channel-like patterns and were interpreted to be preferential flow pathways. Even with these certainties, it should be noted that resistivity methods can have errors, inherent difficulties, and interpretation problems.

#### Surface Effects

Near the surface of the heap, the resistivity was more variable from day to day than was expected. It was thought that since ore near the surface was close to the infiltration point, flow paths would develop quickly and remain consistent. This was not the case.

Even though solution supply to the heap was constant, areas on the surface were susceptible to changes in evaporation rates, local application rates, or drying and

hardening of surface materials on a daily basis due to changes in temperature, wind speed and direction, compaction, and mechanical functionality of the sprinkler system as calcium carbonate precipitated in the sprinkler heads and temperature varied. Temperature changes can also directly affect the electrical resistivity of the heap material. As fluid temperature increases, resistivity decreases (Ramirez et al., 1993). This could have a significant impact on resistivity at and near the surface since daily air temperature fluctuations were close to 15.5° C (60° F).

### Inversion Interpretation Considerations

It was also realized that locations of anomalies may be skewed vertically or horizontally. Due to the extreme heterogeneity in the heap, the flow of the injected electrical current may be distorted by the heterogeneous distribution of electrical resistivity (Skianis and Hernandez, 1999). So, imaged anomalies were not interpreted as absolute indicators of locations.

Inverted resistivity images may be influenced by noise, instrument drift, and a number of other problems. Since this is the case, anomaly size and location must be interpreted as best estimates rather than hard fact (Mauriello and Patella, 1999). These anomalies must also make sense within the range of possible flow processes and lift construction methods.

The transient resistivity pseudosections that were produced depict some phenomena that may be overstated in magnitude. The transient inversions after the initial wetting depicted some large resistivity increases and decreases in close proximity or with one below the other (Appendix B: Plate B-3). While gradual increases or decreases in

resistivity indicate changes in fluid content, the larger magnitude changes within the first few days of wetting (100  $\Omega$ -m or greater) may be a product of difficult data collection during one of the files. An inability to collect the same number of data points causes a mismatch of data or a change in the file sensitivity at depth, which alters the final transient models. This type of anomaly has been observed in other studies in cases where no geologic significance could be assigned (Park, 1998).

Several possible explanations for resistivity pseudosection anomalies were developed, but were not verified. Some large resistive anomalies were interpreted as being large grains, but these locations were not excavated for verification. Environments with high alkalinities are capable of dissolving many minerals. This leads to ions in solution and chemical reactions, which would alter the fluid resistivity. It was assumed that fluid resistivity would stabilize quickly and remain consistent throughout the study, but a detailed solution chemistry study was not performed to confirm this assumption.

However, despite these complications, resistivity methods are among the best tools currently available to image the subsurface and can be insightful when describing subsurface processes.

### Wetting Front Analysis

The inverted wetting front pseudosections depict flow that was mostly a steadily progressing front near the surface with a few pathways of faster or more concentrated travel surpassing 2 meters depth within the first 24 hours of wetting. After four or more days of wetting, most of the heap appeared to be wetted. The timing of the first flow out of the individual lysimeters supported these observations. The large pad lysimeters

began to flow within the first two days. With their large surface area, they had a much greater likelihood of intercepting zones of preferential flow. The smaller trough lysimeters began to flow at much more random times. Some showed flow by the second day, others didn't flow until four or five days after the start of wetting. This was most likely dependent on whether the lysimeter was influenced by preferential flow paths or the slower main wetting front.

### Steady State Flow

Changes in flow continued to occur on the last day of the study. However, near the end of the study, the rate of change in interpreted flow pattern differences remained consistent. Several transient inversion sets represent time changes of roughly one day (Appendix B: Plates B-17, B-18, and B-20). For each of these images, percent differences in resistivity and conductivity were approximately 20%, positive or negative, which is less dramatic than changes for previous times. Plates B-17 and B-18 show changes in comparable zones, as if the start of a pattern of wetting. This was initially interpreted as steady-state flow within the heap.

However, additional transient inversions show rapid resistivity changes that occurred in less than 10 hr increments of time during the 5<sup>th</sup> through 9<sup>th</sup> days of wetting (Appendix B: Plates B-21, B-22, and B-31). These inversions do not support the existence of steady-state flow within the heap, yet these files can not be discredited statistically or otherwise.

The combination of these two types of files suggests that flow within the heap was highly complex. Changes in resistivity did not follow a determinable trend. Flow

often appeared to enter the 2-D profile through horizontal, not vertical, flow paths (Appendix B: Plates B-21, B-22, and B-31). It is possible that flow within the heap was not constant, but rather acted in surges. Such flow may have gathered in pockets, building potential energy until that energy was sufficient to force gravitational flow. With this type of flow, it would be difficult to determine if the flow in the heap could ever reach a steady-state.

### Geochemistry Comparisons

Electrical resistivity was a complementary measurement technique for lysimeter and solution chemistry data. Rather than being a point specific method such as the lysimeters, the resistivity equipment should observe heap activity in the volume of material under the surface electrodes. While it is a great benefit to be able to analyze a larger area of the heap, electrical resistivity images are non-unique solutions to the measured electrical responses of the rock and fluid. This means that using an additional measurement technique, such as the lysimeters, to collect physical flow and chemistry data is critical to being able to interpret the resistivity pseudosections.

The use of lysimeters also gave clues to processes within the heap that were not anticipated. For example, sediment was occasionally found in lysimeter solution samples. This suggests that flow at times must have been significant enough to carry or flush out sediments.

## Suggestions for Further Study and Lessons Learned

The known constraints on this study were limited and a number of additional factors could be studied to reduce uncertainties associated with this research, such as:

1. A similar series of surveys could be conducted during the fresh water rinsing cycle and compared to this study. This may help determine the effect of the cyanide solution and gold dissolution on the measured resistivity. This also may reveal the permanence of the interpreted preferential flow pathways as well as their reproducibility.
2. Several questions concerning the degree to which the clay within the ore controls the flow remain. Hardened clay at the surface may contribute to channeled flow upon infiltration. Pockets of clay within the heap may act as pathways that hinder even distribution of the solution. A similar experiment with more homogeneous gravel to boulder sized sediments or crushed ore could help resolve this issue by eliminating some of the complications of dealing with this extreme range of grain sizes.
3. Since flow within the heap is essentially a two-phase flow problem with air and solution, it has been suggested that preferential flow may be decreased by wetting the ore prior to leaching (Orr, 2002). This makes the heap more of a single-phase flow problem since the solution and water have roughly equivalent densities. An initial wetting cycle may inhibit the formation of fingering or funnel flow.
4. More robust data collection algorithms that utilize a mixture of array types rather than standard measurement sequences would have improved data quality and decreased processing time for collected data files. This would have also increased

the quality of data taken while the heap was still dry. The standard files that were used to collect data during this phase had poor sensitivity and reliability below the top third of their depth of investigation, which limited their ability to function as background files during transient inversions.

5. Of the measurement types used for this study, some proved more useful than others. If this study were conducted again on a wet heap, mostly dipole-dipole and pole-pole data would be collected. These files showed the contrast between shallow and deep depths of investigation and variable resolutions. Additionally, by decreasing the number of different files used, more focus could be placed on creating large transient data sets representing smaller time increments.
6. The use of 3-D resistivity would also be beneficial in this application. Many of the transient inversions suggest that flow entered the profile through lateral pathways, but this can not be proved conclusively without 3-D imaging.
7. This type of study could also be used to determine the diurnal effects temperature and evaporation may have on electrical resistivity at the surface. These are especially important factors to understand in an arid environment. However, a less active site should be chosen so that causal factors can be directly linked to effects on resistivity.

## CHAPTER VI

### CONCLUSIONS

This study successfully applied electrical resistivity methods for subsurface characterization of cyanide solution migration at an active heap leach site. This research was conducted during initial fluid application and was able to resolve wetting of the ore and flow path development at a field scale.

This study addressed four major objectives. First, a reliable field system setup and data collection system was designed. Second, data collection and processing standards were developed. The reliability and repeatability of acquired resistivity data was tested using error statistics and comparisons to other available data. Final data sets were comparable to site conditions and physical observations, physical flow times from the lysimeters, and were often very similar to previous resistivity data. Third, the resolution of the resistivity data was tested. Inverted resistivity pseudosections were able to depict the development and changes in preferential flow paths and identify areas with varying degrees of wetting. Finally, the ability of electrical resistivity to identify geochemical reactions was tested. It was determined that no strong correlation between heap chemistry and electrical resistivity could be identified.

It was anticipated that resistivity could be used to identify wetting within the heap, but it was unexpected that the wetting would not occur as a continually decreasing trend in resistivity with increasing moisture content. In fact, this study can conclude that



resistivity varies with wetting rather than continually decreasing. Some zones actually increased in resistivity through time. Unfortunately, the flow mechanisms within the heap that cause this variation in resistivity could not be absolutely determined, but this type of phenomenon should spur additional research related to the development of preferential flow in heterogeneous materials.

## BIBLIOGRAPHY

- Advanced Geosciences, Inc. 2001. Instruction manual for the SuperSting R8 IP <sup>TM</sup> and Swift<sup>TM</sup>. 50 p. P.O. Box 201087, Austin, Texas 78720. Tel. (512) 335-3338, Fax (512) 258-9958, [www.agiusa.com](http://www.agiusa.com).
- Advanced Geosciences, Inc. 2003. EarthImager Version 1.5.0. 2D Resistivity and IP Inversion Software Instruction Manual. P.O. Box 201087, Austin, Texas 78720. Tel. (512) 335-3338, Fax (512) 258-9958, [www.agiusa.com](http://www.agiusa.com).
- al Hagrey, S. A. and Johannes Michaelson, 1999. Resistivity and percolation study of preferential flow in vadose zone at Bokhorst, Germany. *Geophysics*, v. 64, no. 3, 746-753.
- al Hagrey, S. A., T. Schubert-Klempnauer, D. Wachsmuth, J. Michaelson, and R. Meissner, 1999. Preferential flow: first results of a full-scale flow model. *Geophys. J. Int.* v. 138, 643-654.
- Archie, G. E., 1942. The electrical resistivity log as an aid to determining some reservoir characteristics. *Trans. A.I.M.E.*, v. 146, 389-409.
- Armstrong, Augustus K., Ted G. Theodore, Robert L. Oscarson, Boris B. Kotlyar, Anita G. Harris, Keith H. Bettles, Eric A. Lauha, Richard A. Hipsley, Gregory L. Griffin, Earl W. Abbott, and J. Kelly Cluer, 1998. Preliminary Facies Analysis of Silurian and Devonian Autochthonous Rocks that Host Gold along the Carlin Trend, Nevada, in Tosdal, R. M., ed., Contributions to the gold metallogeny of northern Nevada; U.S. Geological Survey Open-File Report 93-338 1998.
- Bakshi, A. K. and M. G. Nelson, 1995. Effect of Seasonal Work on Residual Cyanide Removal from Leach Heaps in Sub-Arctic Conditions. Chapter 20 in New Remediation Technology in the Changing Environmental Arena, SME, Littleton, CO.
- Barker, R. and Moore, J., 1998. The application of time-lapse electrical tomography in groundwater studies. *The Leading Edge*, v. 17, 1454-1458.
- Bartlett, R. W., 1992. *Solution Mining: Leaching and Fluid Recovery of Materials*. Gordon & Breach Science Publishers: The Netherlands.

- Berkowitz, Brian, Ronit Nativ, and Eilon Adar, 2001. Evaluation of Conceptual and Quantitative Models of Fluid Flow and Chemical Transport in Fractured Media. *in* Conceptual Models of Flow and Transport in the Fractured Vadose Zone. National Academy Press, Washington, D.C., 115-147.
- Binley, A., Cassiani, G., Middleton, R., and Winship, P., 2002. Vadose zone flow model parameterization using cross-borehole radar and resistivity imaging. *J. of Hydrogeology*, v. 267, 147-159.
- Bodvarsson, Gudmundur S., Hui Hai Liu, C. Frederick Ahlers, Yu-Shu Wu, and Eric Sonnenthal, 2001. Parameterization and Upscaling in Modeling Flow and Transport in the Unsaturated Zone of Yucca Mountain. *in* Conceptual Models of Flow and Transport in the Fractured Vadose Zone. National Academy Press, Washington, D.C., 335-365.
- Bogoslovsky, V. A. and A. A. Ogilvy, 1970. Natural potential anomalies as a quantitative index of the rate of seepage from water reservoirs. *Geophysical Prospecting*, v. 18, 261-268.
- Burger, H.R. 1992. *Exploration Geophysics of the Shallow Subsurface*. Prentice Hall, Englewood Cliffs, NJ, 489 p.
- Buselli, G. and K. Lu, 2001. Groundwater contamination monitoring with multichannel electrical and electromagnetic methods. *J. of Applied Geophysics*, v. 48, 11-23.
- Cahyna, Frantisek, Oldrich Mazac, and Daniela Venhodova, 1990. Determination of the extent of Cyanide Contamination by surface geoelectrical methods. *in* Geotechnical and Environmental Geophysics. Investigation in Geophysics no. 5. ed. Stanley H. Ward. Society of Exploration Geophysicists, Tulsa, OK. 97-99.
- Daily, W., Ramirez, A., LaBrecque, D., and Nitao J., 1992. Electrical resistivity tomography of vadose water movement. *Water Resources Research*, v. 28, 1429-1442.
- Davis, Stanley N., 1995. Vadose Zone Hydrogeology in the United States. *in* Handbook of Vadose Zone Characterization and Monitoring. ed. L. G. Wilson, L. G. Everett, and S. J. Cullen. CRC Press, 23-39.
- Faybishenko, Boris, Christine Doughty, Michael Steiger, Jane Long, Thomas Wood, Janet Jacobsen, Jason Lore, and Peter Zawislanski, 2000. Conceptual model of the geometry and physics of water flow in a fractured basalt vadose zone. *Water Resources Research*, v. 36, no. 12, 3499-3520.
- French, H. K., C. Hardbattle, A. Binley, P. Winship, and L. Jakobsen, 2002. Monitoring snowmelt induced unsaturated flow and transport using electrical resistivity tomography. *J. of Hydrogeology*, v. 267, 273-284.

- Hart, K. S., 2002. Cortez-Gold Acres Memorandum: Gold Acres Heap Leach Test Area Ore Characteristics. November 4, 2002.
- Hendrickx, Jan M. H., and Markus Flury, 2001. Uniform and Preferential Flow Mechanisms in the Vadose Zone. *in* Conceptual Models of Flow and Transport in the Fractured Vadose Zone. National Academy Press, Washington, D.C., 149-187.
- Johansson, S. and T. Dahlin, 1996. Seepage monitoring in an earth embankment dam by repeated resistivity measurements. *European J. of Engineering and Geophysics*, v. 1, 229-247.
- Kean, William F., Muriel Jennings Waller, and H. Richard Layson, 1987. Monitoring moisture migration in the vadose zone with resistivity. *Ground Water*, v. 25, no. 5, 562-571.
- Kilty, K. T., 1984. On the origin and interpretation of self-potential anomalies. *Geophysical Prospecting*, v. 32, 51-62.
- Kung, K.-J. S. 1990. Preferential flow in a sandy vadose zone. 1. Field observations. *Geoderma* v. 46, 51-58.
- Loke, M.H. and R.D. Barker, 1996. Rapid least-square inversion of apparent resistivity pseudosections using a quasi-Newton method. *Geophysical Prospecting*, v. 44, 131-152.
- Loke, M.H., 1999. Electrical imaging surveys for environmental and engineering studies: A practical guide to 2-D and 3-D surveys. Advanced Geosciences, Inc. Austin, TX. 59 p.
- Mauriello, Paolo and Domenico Patella, 1999. Resistivity anomaly imaging by probability tomography. *Geophysical Prospecting*, v. 47, 411-429.
- National Research Council (NRC), 2001. Conceptual Models of Flow and Transport in the Fractured Vadose Zone. National Academy Press, Washington, D.C., 374 p.
- Orr, Shlomo, 2002. Enhanced heap leaching; Part 1, Insights. *Mining Engineering*, vol. 54, no. 9, 49-56.
- Park, Stephen, 1998. Fluid migration in the vadose zone from 3-D inversion of resistivity monitoring data. *Geophysics*, v. 63, no. 1. 41-51.
- Pruess, K., 1999. A mechanistic model for water seepage through thick unsaturated zones in fractured rocks of low matrix permeability. *Water Resources Research*, v. 34, no. 4, 1039-1051.

- Ramirez, A.L., W. Daily, D. LaBrecque, E. Owen, and D. Chesnut, 1993. Monitoring an underground steam injection process using electrical resistivity tomography. *Water Resources Research*, v. 29, 73-87.
- Reynolds, J.M. 1987. The role of surface geophysics in the assessment of regional groundwater potential in northern Nigeria. *in* Planning and Engineering Geology, Geological Society Engineering Group Special Publication no. 4, ed. M.G. Culshaw, F.G. Bell, J.C. Cripps, and M. O'Hara, 185-190.
- Reynolds, J.M. 1997. *An Introduction to Applied and Environmental Geophysics*. John Wiley & Sons, Chichester, England, 796 p.
- Runnells, D. D., 1995. Basic Contaminant Fate and Transport Processes in the Vadose Zone – Inorganics. *in* Handbook of Vadose Zone Characterization and Monitoring. ed. L. G. Wilson, L. G. Everett, and S. J. Cullen. CRC Press, 79-92.
- Skianis, G. and M. Hernandez, 1999. Effects of transverse anisotropy on self-potential anomalies. *J. of Applied Geophysics*, v. 41, 93-104.
- Slater, L. and D. Lesmes, 2002. IP interpretation in environmental investigations. *Geophysics*, v. 67, no. 1, 77-88.
- Spicer, H. Cecil, 1952. Electrical resistivity studies of subsurface conditions near Antigo, Wisconsin. U. S. Geological Survey Circular 181. U. S. Dept. of the Interior. Washington, D. C. 19 p.
- Stoll, J., J. Bigalke, and E. W. Grabner, 1995. Electrochemical modeling of self-potential anomalies. *Surveys in Geophysics*, v. 16, 107-120.
- Timm, F. and P. Moller, 2001. The relation between electric and redox potential: evidence from laboratory and field measurements. *J. of Geochemical Exploration*, v. 72, 115-128.
- Titov, K., V. Loukhmanov, and A. Potapov, 2000. Monitoring of water seepage from a reservoir using resistivity and self polarization methods: case history of the Petergoph fountain water supply system. *First Break*, v. 18, 431-435.
- Vagshal, D. S. and S. D. Belyaev, 2001. Self-potential anomalies in Cerro de Pasco and Hualgayoc areas (Peru) revisited. *Geophysical Prospecting*, v. 49, 151-154.
- Webb, Geoff, 2003. Spatial Variability of Flow in Coarse, Unsaturated Mining Material: Results from Field-Scale Infiltration Experiments. M.S. thesis. University of Nevada, Reno. August 2003.

Zhou, B. and S. A. Greenhalgh, 2002. Rapid 2-D/3-D crosshole resistivity imaging using the analytic sensitivity function. *Geophysics*, v. 67, no. 3, 755-765.

# APPENDIXES

## APPENDIX A

Table of Resistivity Files Collected and Inversion Statistics

Figure #	File Name	Time from Start of Wetting (hrs:min)	Electrodes Used	Inversion Stats		Notes*
				RMS Error (%)	L2 Norm	
	C27DDF1	0:00	B			Inversion Error
	C27DDF2	0:00	C	49.11	1.67	
	C27DDF3	0:00	B	10.9	1.07	
	C27PD1	0:00	B, LA4	45.19	14.5	
	C27PD3	0:00	C, IEE	44	39	Inversion Error
	C27PP1	0:00	C, IEE, LA4			
	C27PP2	0:00	B, IEE, LA4			
	C36PP1	0:00	A, IEE, LA4			
	C36DD1	0:00	A	33.69	21.39	Start of wetting
	C36DD2	0:15	A	22.55	20.38	
	C27DD4	0:35	B	26	10.8	
	C27DD5	0:55	B	26.5	11	
	C27DD6	1:15	C	19	3.2	Electrode Error (PL2)
	C27DD7	1:35	C	13.58	1.02	
	C27PD5	1:55	C, IEE	31.7	11.8	
	C27PD6	2:10	C, LA4	17.2	32.7	
	C27PD7	2:25	C, PL1	15.32	0.79	
	C27PD8	2:45	C, PL2			
	C27PD9	3:05	C, TL5	33.93	9.13	
	C36PP2	3:25	A, TL5, LA4	9.2	9.4	
	C54PP1a	5:05	C, TL5, LA4			
	C54PP1b	5:35	B, TL5, LA4			
	C27DD8	17:05	B	8	0.64	
	C27PD10A	17:25	B, IEE	29	15	
	C27PD10B	17:45	B, IEE			
	C27PD10C	18:05	B, IEE			
	C27PD10D	18:25	B, IEE			
	C27PD10E	18:45	B, IEE			
	C27PD10F	19:05	B, IEE			

Figure #	File Name	Time from Start of Wetting (hrs:min)	Electrodes Used	Inversion	Stats	Notes*
				RMS Error (%)	L2 Norm	
	C36DD2-9	19:20	A	16.6	7.22	
	C36PP3-a	19:50	A, IEE, LA4	15.25	5.28	
	C36PP3-b	20:25	A, IEE, LA4	16.38	6.09	
	C36PP3-c	21:00	A, IEE, LA4	15.61	5.69	
	C36PP3-d	21:35	A, IEE, LA4	16.83	6.13	
	C27PD11	24:55	C, PL1	24.67	4.03	
	C27PD12	25:15	C, TL5	20	4.8	
	C27PP8	25:30	C, TL5, LA4	7.4	0.73	
	C36PP4	25:55	A, TL5, LA4	178	9.2	Noisy data
	C36PD3	26:35	A, TL5	28.4	2.9	
	C36PD4	27:15	A, LA4	21.4	7	
	C36PP5-a	27:50	A, PL1, IEE	21	11.6	
	C36PP5-b	29:05	A, PL1, IEE			
	C36PP5-c	30:20	A, PL1, IEE	26.91	4.31	
	C36PP5-d	31:35	A, PL1, IEE			
	C27PP10	33:05	B, PL1, IEE			Data Collection Error
	C36PP6-a	33:30	A, IEE, LA4	20.31	10.68	
	C36PP6-b	34:30	A, IEE, LA4	21	10.86	
	C36PP6-c	35:30	A, IEE, LA4	22.85	12.1	
	C36PP6-d	36:30	A, IEE, LA4	21.3	11.61	
	C36PP6-e	37:30	A, IEE, LA4	23.17	11.18	
	C36PP6-f	38:30	A, IEE, LA4	22.22	19.97	
	C36PP6-g	41:00	A, IEE, LA4	23.19	20.55	
	C27PP11	44:05	C, IEE, LA4	29.5	17.6	
	C27PP12	45:05	C, TL5, LA4	8.98	1.01	
	C27PP13	46:35	C, TL5, LA4	12	1.3	
	C27PP14	46:55	C, TL5, LA4	9.44	1.11	
	C27PP15	47:20	B, TL5, LA4	14	1.8	
	C27PP16	47:50	B, IEE, LA4	26.8	23.9	
	C36PP8a	49:05	A, IEE, PL1	8.5	0.8	
	C36PP8b	49:35	A, IEE, PL1			
	C36PP8c	50:05	A, IEE, PL1			
	C36PP8d	50:35	A, IEE, PL1			
	C36PP8e	51:05	A, IEE, PL1			
	C36PP8f	51:35	A, IEE, PL1			
	C36PP8g	52:05	A, IEE, PL1			
	C36PD5	52:20	A, IEE	16.07	1.88	
	C27PP17	53:15	B, LA4, PL1	14.1	1.9	
	C27PP18	53:45	C, LA4, PL1	7.59	0.49	
	C27PTNa	54:05	C, LA4	11.55	0.94	
	C27PTNb	54:25	C, LA4			
	C27PTNc	54:45	C, LA4			
	C27PTNd	55:05	C, LA4			



Figure #	File Name	Time from Start of Wetting (hrs:min)	Electrodes Used	Inversion	Stats	Notes*
				RMS Error (%)	L2 Norm	
	C27PTNe	55:25	C, LA4			
	C27PTNf	55:45	C, LA4	10.88	0.93	
	C36PP9a	56:35	A, LA4, IEE	34.5	11.5	
	C36PP9b	57:50	A, LA4, IEE			
	C36PP9c	59:05	A, LA4, IEE			
	C36PP9d	60:20	A, LA4, IEE			
	C36PP9e	61:35	A, LA4, IEE			
	C36PP9f	62:50	A, LA4, IEE			
	C36PP9g	64:05	A, LA4, IEE			
	C36PP9h	65:20	A, LA4, IEE			
	C36PP10	68:00	A, LA4, IEE	26.1	10.4	
	C27PP19	68:50	C, LA4, IEE	8.9	1.2	
	C27PP20	69:20	C, LA4, TL5	9.35	1.01	
	C27PP21	69:50	B, LA4, TL5	6.7	0.7	
	C27PP22	70:25	B, PL1, IEE	22.7	1.9	
	C36PD6	70:55	A, IEW	18	2.8	
	C27PD13a	71:50	B, IEW	17.3	2.1	
	C27PD13b	72:20	B, IEW			
	C27PD13c	72:50	B, IEW			
	C27PD13d	73:20	B, IEW			
	C27PD13e	73:50	B, IEW			
	C27PD13f	74:20	B, IEW			
	C27DD9	75:35	B	13.7	1.97	
	C36DD3	75:45	A	12.92	2.6	
	C36DD4	76:00	A	17.6	5.1	
	C27DD10	76:15	B	15	1.99	
	C27PP23	76:35	B, IEW, IEE	15	7.5	
	C27PP24	77:05	C, IEW, IEE	6.38	0.72	
	C27DD11	77:25	C	20	2.6	
	C27PD14a	77:35	C, IEE	11.5	1	
	C27PD14b	78:05	C, IEE			
	C27PD14c	78:35	C, IEE			
	C27PD14d	79:05	C, IEE			
	C27PD14e	79:35	C, IEE			
	C27PD14f	80:05	C, IEE			
	C36PP11	80:35	A, LA4, IEE	26	8	
	C27DD12	92:15	C	15.5	2.1	
	C27PD15	92:25	C, LA4	12.5	1	
	C27PD16	92:40	C, IEE			
	C27PP25	92:55	C, IEE, IEW	11	4.3	
	C36PP12	93:30	A, IEE, IEW	21.14	9.83	
	C36PD7	94:05	A, IEE	17.82	1.82	
	C36DD5	94:35	A	13.29	3.11	

Inversion Error

Figure #	File Name	Time from Start of Wetting (hrs:min)	Electrodes Used	Inversion	Stats	Notes*
				RMS Error (%)	L2 Norm	
	C36PD8	94:50	A, PL1	12.3	1.1	Inversion Error
	C27PD17a	95:35	B, PL1	12.1	0.72	
	C27PD17b	96:05	B, PL1			
	C27PD17c	96:35	B, PL1			
	C27PD17d	97:05	B, PL1			
	C27PD17e	97:35	B, PL1			
	C27PD17f	98:05	B, PL1			
	C27DD13	99:25	B	12.5	1.82	
	C27PP26	99:40	B, IEE, IEW	8.31	0.99	
	C36PP13	100:00	A, IEE, IEW	19.13	8.54	
	C36DD6	100:35	A	18.99	6.72	
	C36DD7	100:50	A	19.36	7.08	
	C27DD14	101:00	C	16.4	2.4	
	C27DD15	101:10	C	17.5	2.4	
	C27PD18a	101:20	C, IEE	15.7	3.9	
	C27PD18b	101:50	C, IEE			
	C27PD18c	102:20	C, IEE			
	C27PD18d	102:50	C, IEE			
	C27PD18e	103:20	C, IEE			
	C27PD18f	103:50	C, IEE			
	C36DD8	115:25	A	19.15	5.42	
	C27PD19	115:50	C, IEE			
	C36PD9	116:00	A, IEE	23.71	4.91	
	C27PP27	116:45	C, IEE, IEW	11.9	4.5	
	C36DD9	117:17	A	19.54	6.08	
	C27DD16	117:27	B	13	1.4	
	C27PD20	117:40	B, IEE	14.5	1.26	
	C27PP28	117:50	B, IEE, IEW	9.88	0.78	
	C27DD17	118:15	B	12.5	1.4	
	C36DD10a	118:25	A	17.26	3.79	
	C36DD10b	119:10	A	17.23	5.33	
	C36DD10c	119:55	A	17.59	5.27	
	C36DD10d	120:40	A	17.48	5.26	
	C36DD10e	121:25	A	17.76	5.3	
	C36DD10f	122:10	A	17.33	5.17	
	C27PP29	123:05	B, IEE, IEW	8.65	0.82	
	C36PP15	123:23	A, IEE, IEW	20.35	9.3	
	C27PD21	124:05	B, IEE	15	1.9	
	C36PD10	124:15	A, IEE	22.6	3.69	
	C27DD18	124:47	B	12.3	1.34	
	C27PP30	124:55	C, IEE, IEW	9	2.9	
	C27DD19	125:20	C	17.4	3.5	

Figure #	File Name	Time from Start of Wetting (hrs:min)	Electrodes Used	Inversion	Stats	Notes*
				RMS Error (%)	L2 Norm	
	C27PD22a	125:30	C, IEE	13	2.1	
	C27PD22b	126:00	C, IEE			
	C27PD22c	126:30	C, IEE			
	C27PD22d	127:00	C, IEE			
	C27PD22e	127:30	C, IEE			
	C27PD22f	128:00	C, IEE			
	C36PP16a	128:50	A, IEE, IEW	23.73	10.92	
	C36PP16b	129:50	A, IEE, IEW	20.46	6.56	
	C36PP16c	130:50	A, IEE, IEW	21.85	6.87	
	C36PP16d	131:50	A, IEE, IEW	21.56	6.86	
	C36PP16e	132:50	A, IEE, IEW	22.64	7.32	
	C36PP16f	133:50	A, IEE, IEW	21.31	7.09	
	C36PP16g	134:50	A, IEE, IEW	22.62	7.42	
	C36PP16h	135:50	A, IEE, IEW	22.45	7.4	
	C27PD23a	139:25	C, IEE	13.6	2.9	
	C27PD23b	139:55	C, IEE			
	C27PD23c	140:25	C, IEE			
	C27PD23d	140:55	C, IEE			
	C27PD23e	141:25	C, IEE			
	C27PD23f	141:55	C, IEE			
	C36PP17	142:35	A, IEE, IEW	17.7	5.5	
	C27PP31	143:05	C, IEE, IEW	12.9	7.4	
	C27DD20	143:25	C	19	3.4	
	C27PP32	143:45	B, IEE, IEW	10.59	1.03	
	C27PD24	144:05	B, IEE	12.6	1.2	
	C27PP33	144:20	B, IEE, IEW	10.2	2.26	
	C36PP18a	144:45	A, IEE, IEW	20.13	6.38	
	C36PP18b	145:20	A, IEE, IEW	19.61	6.27	
	C36PP18c	145:55	A, IEE, IEW	19.73	6.17	
	C36PP18d	146:30	A, IEE, IEW	18.51	5.57	
	C27PP34	146:55	B, IEE, IEW	9.38	0.82	
	C27DD21	147:25	B	11.5	1.16	
	C36PP19	147:35	A, IEE, IEW	17	5.2	
	C27PP35	148:20	C, IEE, IEW	10.8	5.5	
	C27PD25	148:35	C, IEE			Inversion Error
	C36PD11	148:50	A, IEE	17.16	2.19	
	C27PP37	163:25	C, IEE, IEW	17.5	10.4	
	C36PP21(IP)	163:50	A, IEE, LA4	18.13	20.13	
	C27PP38	165:10	C, IEE, LA4	25.5	3.8	
	C36PP22a (IP)	165:50	A, IEE, IEW	18.45	3.75	
	C36PP22b (IP)	167:35	A, IEE, IEW	22.76	3.99	
	C36PP22c (IP)	169:20	A, IEE, IEW	20.36	3.84	

Figure #	File Name	Time from Start of Wetting (hrs:min)	Electrodes Used	Inversion Stats		Notes*
				RMS Error (%)	L2 Norm	
	C27PP39	171:05	C, IEE, IEW	9.1	2.7	Inversion Error
	C36DD11	171:45	A	16.86	3.73	
	C36DD12	172:05	A	21.7	10.3	
	C27PP40	172:20	C, IEE, IEW	9.9	3.1	
	C36PP23	172:40	A, IEE, IEW	14.9	4.4	
	C27DD22	173:20	C	11.87	1.62	
	C36PP24a	173:45	A, IEE, IEW	21.15	6.41	
	C36PP24b	174:45	A, IEE, IEW	19.67	6.26	
	C36PP24c	175:45	A, IEE, IEW	20.81	6.25	
	C36PP24d	176:45	A, IEE, IEW	20.84	6.35	
	C36PP24e	177:45	A, IEE, IEW	20.73	6.4	
	C36PP24f	178:45	A, IEE, IEW	21.09	6.64	
	C36PP24g	179:45	A, IEE, IEW	21.05	6.59	
	C36PP24h	180:45	A, IEE, IEW	21.1	6.68	
	C36PP25	187:50	A, IEE, IEW	13.9	2.37	
	C27PP41	188:35	C, IEE, IEW	13.5	5.2	
	C27PD26	188:57	C, IEE			
	C27S11	189:15	C	12.5	3.6	
	C27WEN1	189:25	C	12.2	1.9	
	C36PP26	189:52	A, IEE, IEW	20.05	5.42	
	C27PP42	190:35	C, IEE, IEW	11.4	5.6	
	C36DD13	190:50	A	18.5	8.7	
	C27PP43	191:10	B, IEE, IEW	8.2	2	
	C36PP27	191:35	A, IEE, IEW	19.64	4.67	
	C27PP44	192:15	B, IEE, IEW	8.21	0.99	
	C27PD27	192:35	B, IEE	15.6	2.07	
	C36PP28	192:45	A, IEE, IEW			Data Collection Error
	C27PP45	192:55	B, IEE, IEW	9.2	0.9	
	C27PP46	193:40	B, IEE, IEW	5.18	0.79	
	C27DD23	194:10	B	5.5	0.68	

\* Files noted by "inversion error" could not be inverted using current software. These files had complex geometries due to the use of subsurface and/or infinite electrodes and could not be represented by a planar image. Files with a "data collection error" note were partial or incomplete.

## APPENDIX B

### Transient Inversion Data Sets

Each following page of figures represents one transient inversion set. The first two images are resistivity pseudosections. The first acted as a starting point and the second resulted from the transient inversion. These are followed by the percent change in resistivity between the two, and then the percent change in conductivity for comparison. The start time of each image is given as the cumulative time after the start of wetting in “hours:minutes”. Each image was blanked based on sensitivity plots. A chart listing the error statistics follows the last inversion of each set and a more detailed image of the color scales used can be found in Figures 9 and 10.

#### Transient Inversions of Cable A Dipole-Dipole Data

Every inverted pseudosection is from a dipole-dipole data file collected on Cable A, and the start times range from the first through ninth day of the study. Since the first file is used as a template for the later ones and the wettest files had the best data quality, the first three inversions in the set were performed in reverse (from the youngest, wettest file to the oldest, driest file). After four days of wetting, data quality improved and the remaining inversions were performed forward in time from drier to wetter.

# Plate B-1

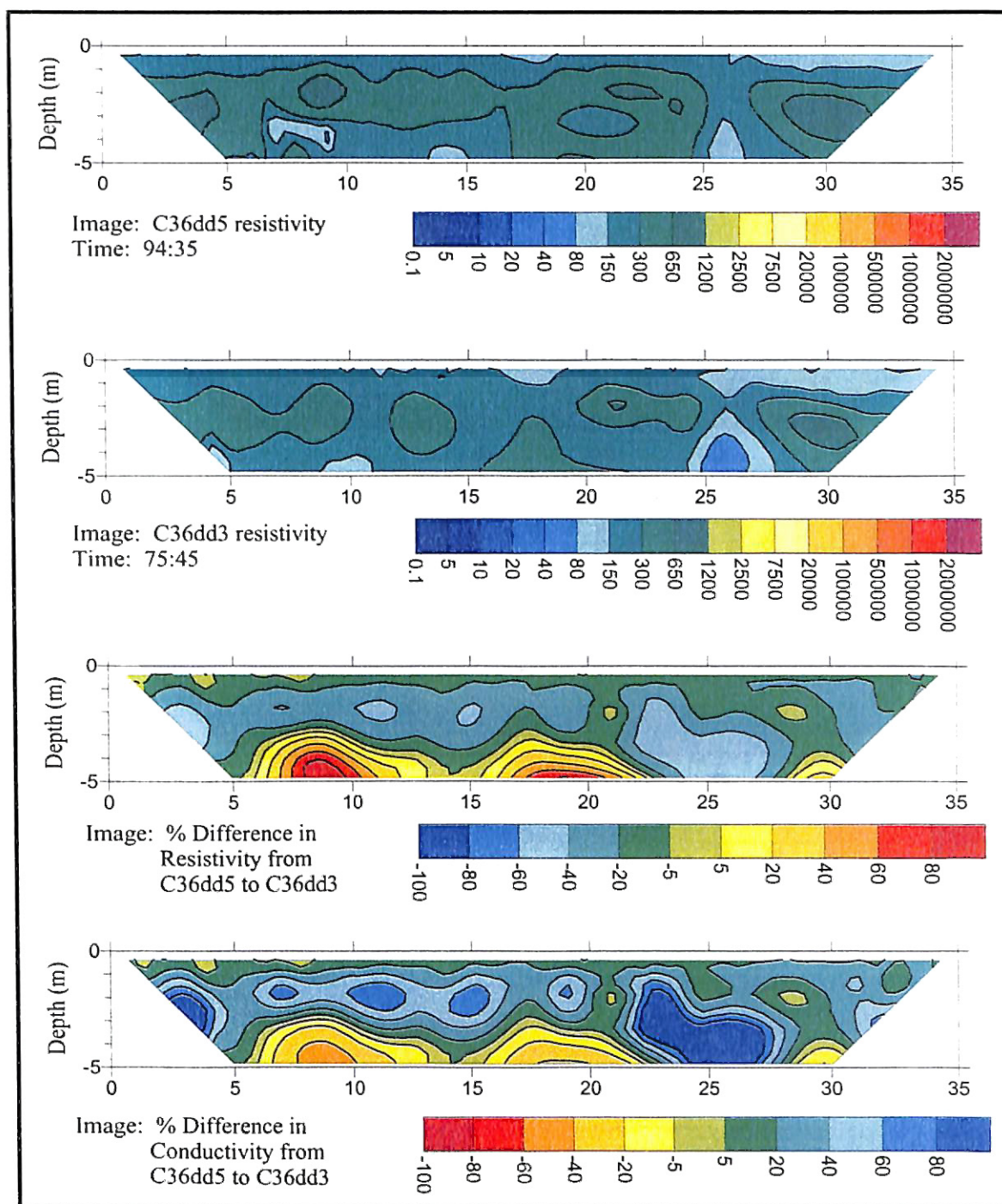


# Plate B-2

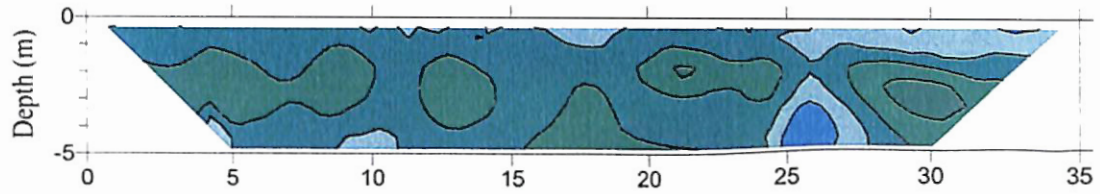


Image: C36dd3 resistivity  
Time: 75:45

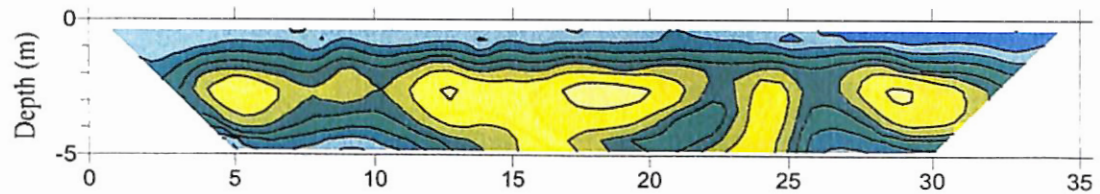


Image: C36dd2-9 resistivity  
Time: 19:20

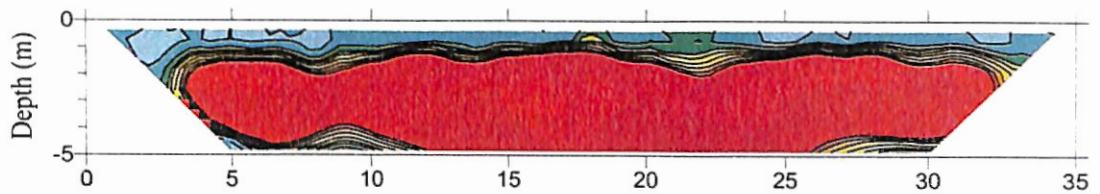
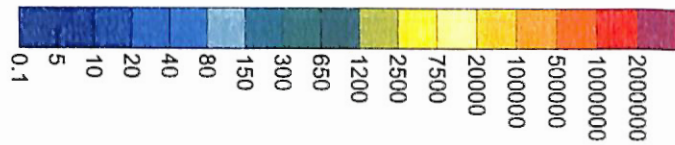


Image: % difference in  
resistivity from  
C36dd3 to C36dd2-9

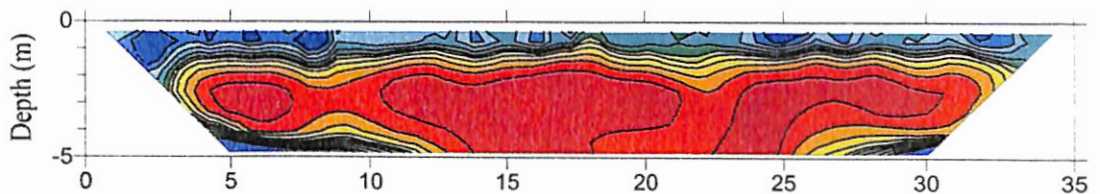
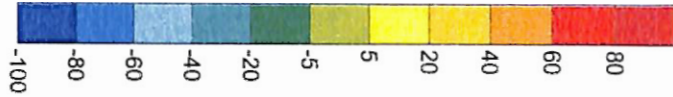
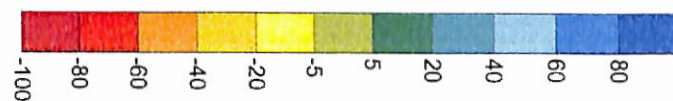


Image: % difference in  
conductivity from  
C36dd3 to C36dd2-9





# Plate B-3

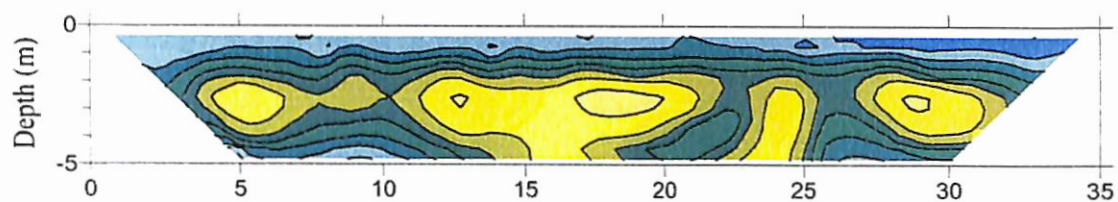


Image: C36dd2-9 resistivity

Time: 19:20

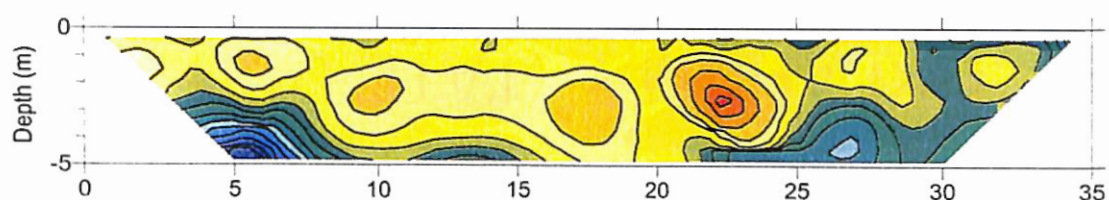


Image: C36dd2 resistivity

Time: 0:15

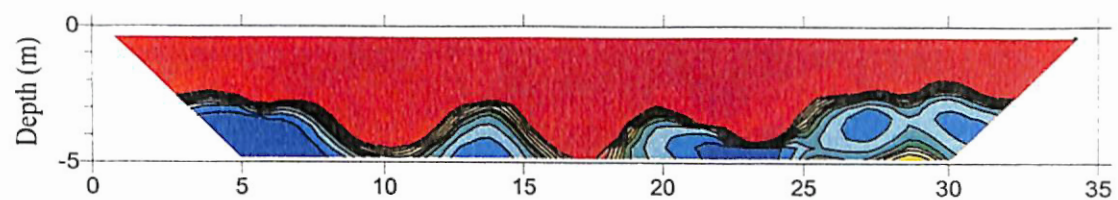
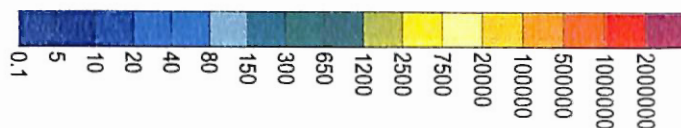


Image: % difference in  
resistivity from  
C36dd2-9 to C36dd2

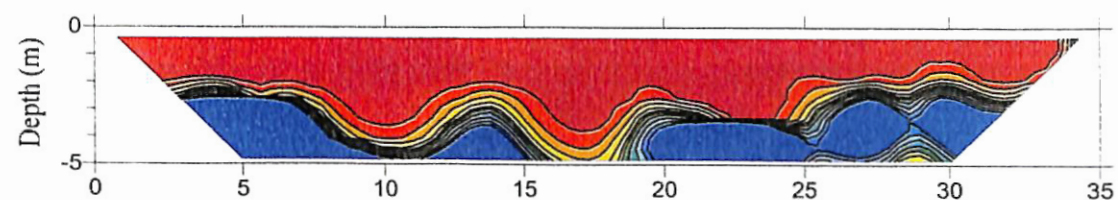
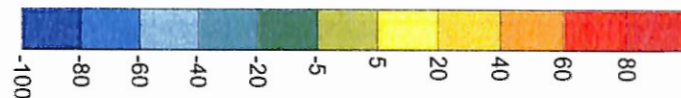


Image: % difference in  
conductivity from  
C36dd2-9 to C36dd2



# Plate B-4

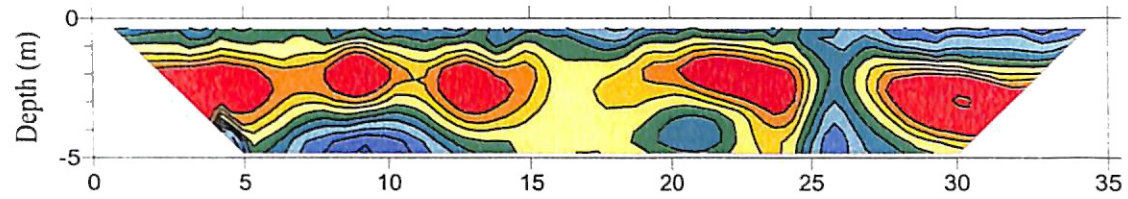


Image: C36dd5 resistivity  
Time: 94:35

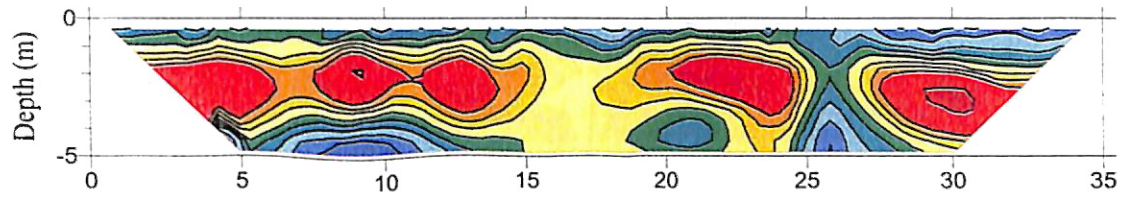


Image: C36dd8 resistivity  
Time: 115:25

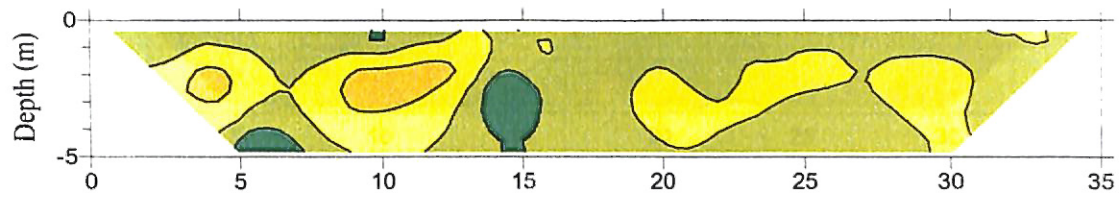


Image: % Difference in  
resistivity from  
C36dd5 to C36dd8

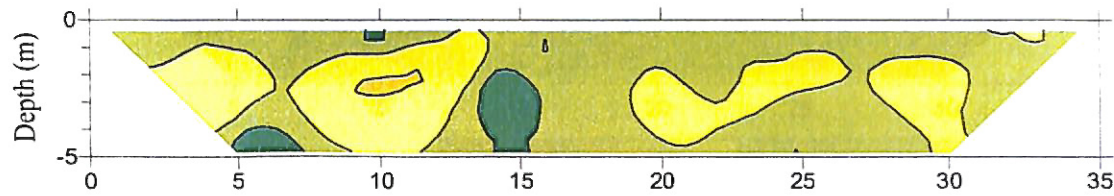


Image: % Difference in  
conductivity from  
C36dd5 to C36dd8





Plate B-5

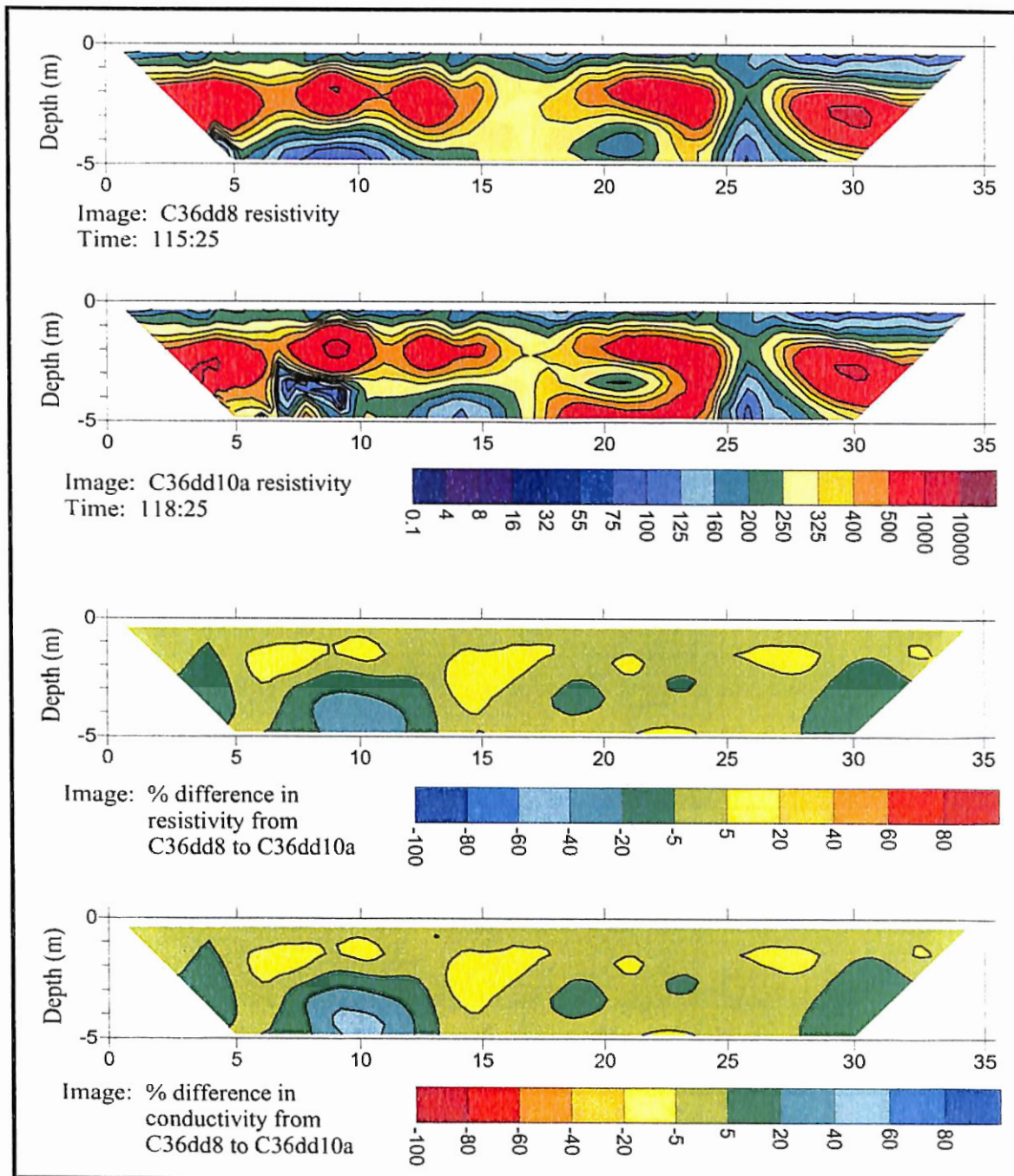


Plate B-6

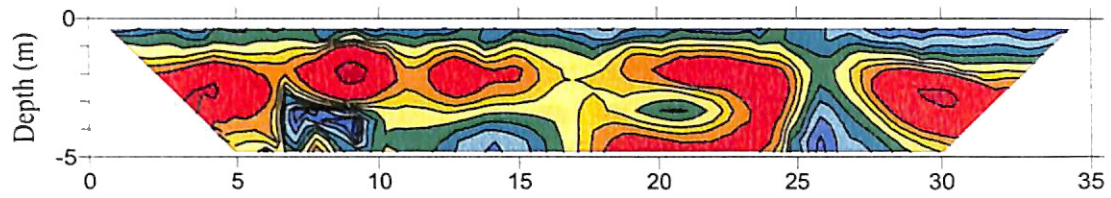


Image: C36dd10a resistivity  
Time: 118:25

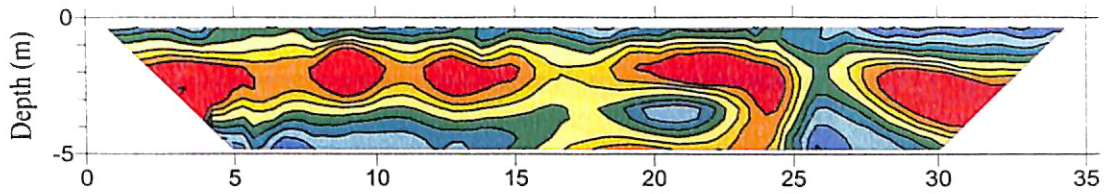


Image: C36dd10c resistivity  
Time: 119:55

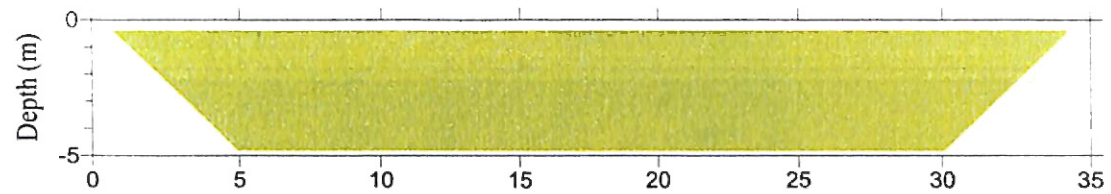
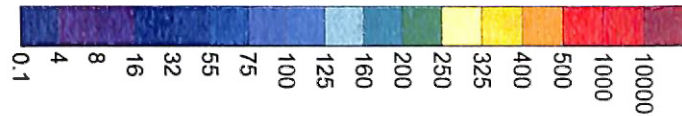


Image: % difference in  
resistivity from  
C36dd10a to C36dd10c

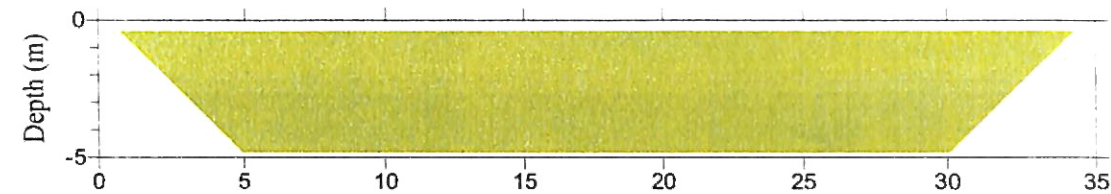


Image: % difference in  
conductivity from  
C36dd10a to C36dd10c





Plate B-7

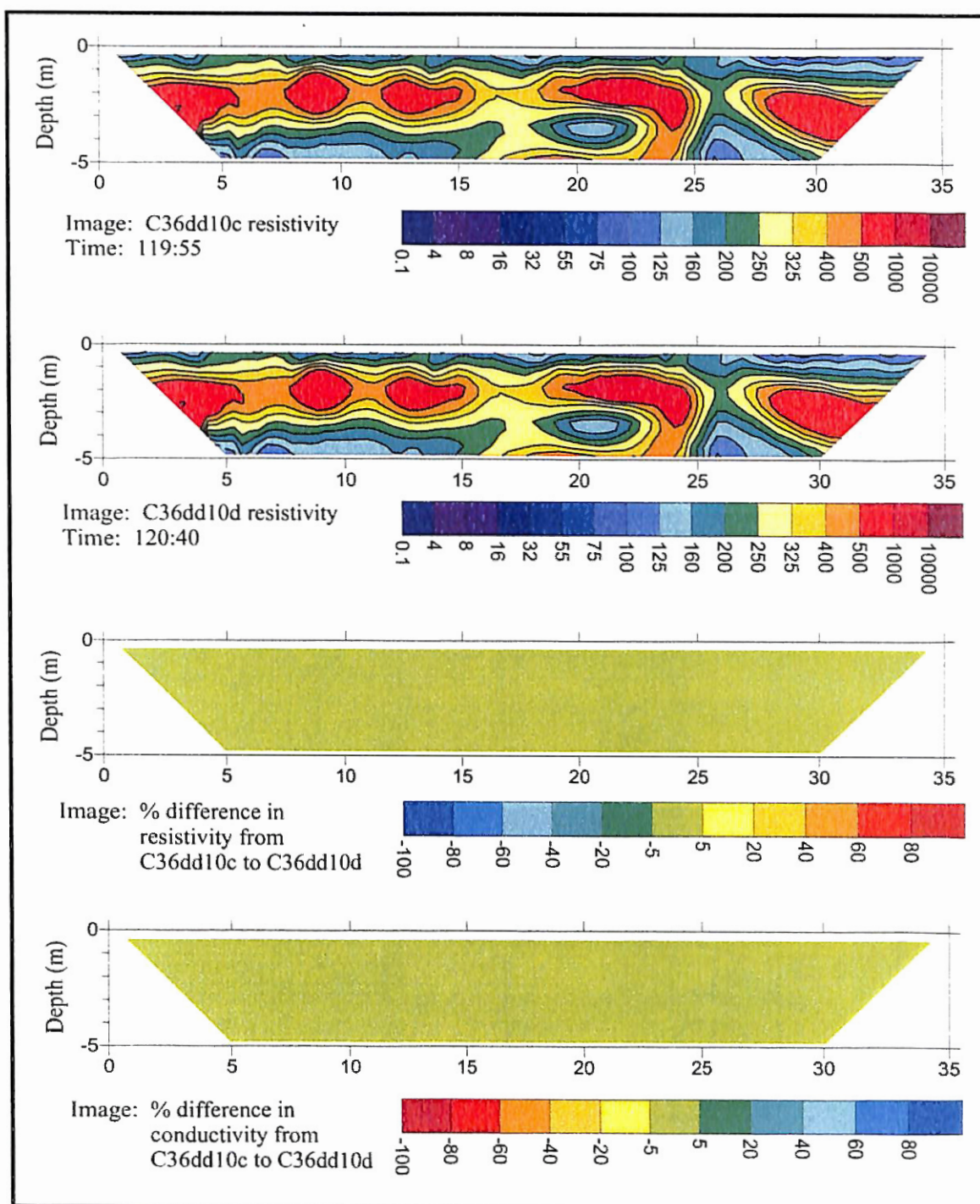


Plate B-8

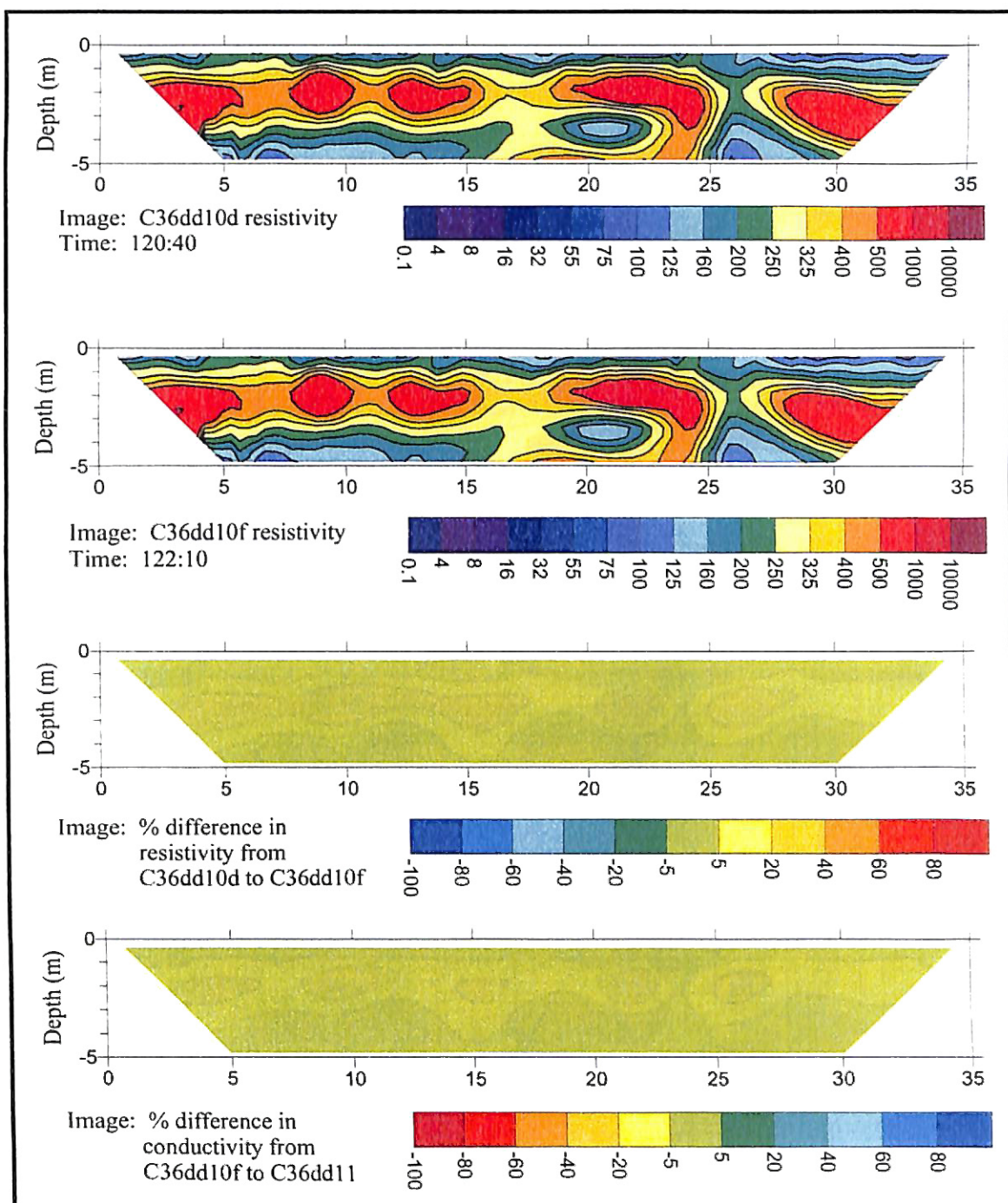
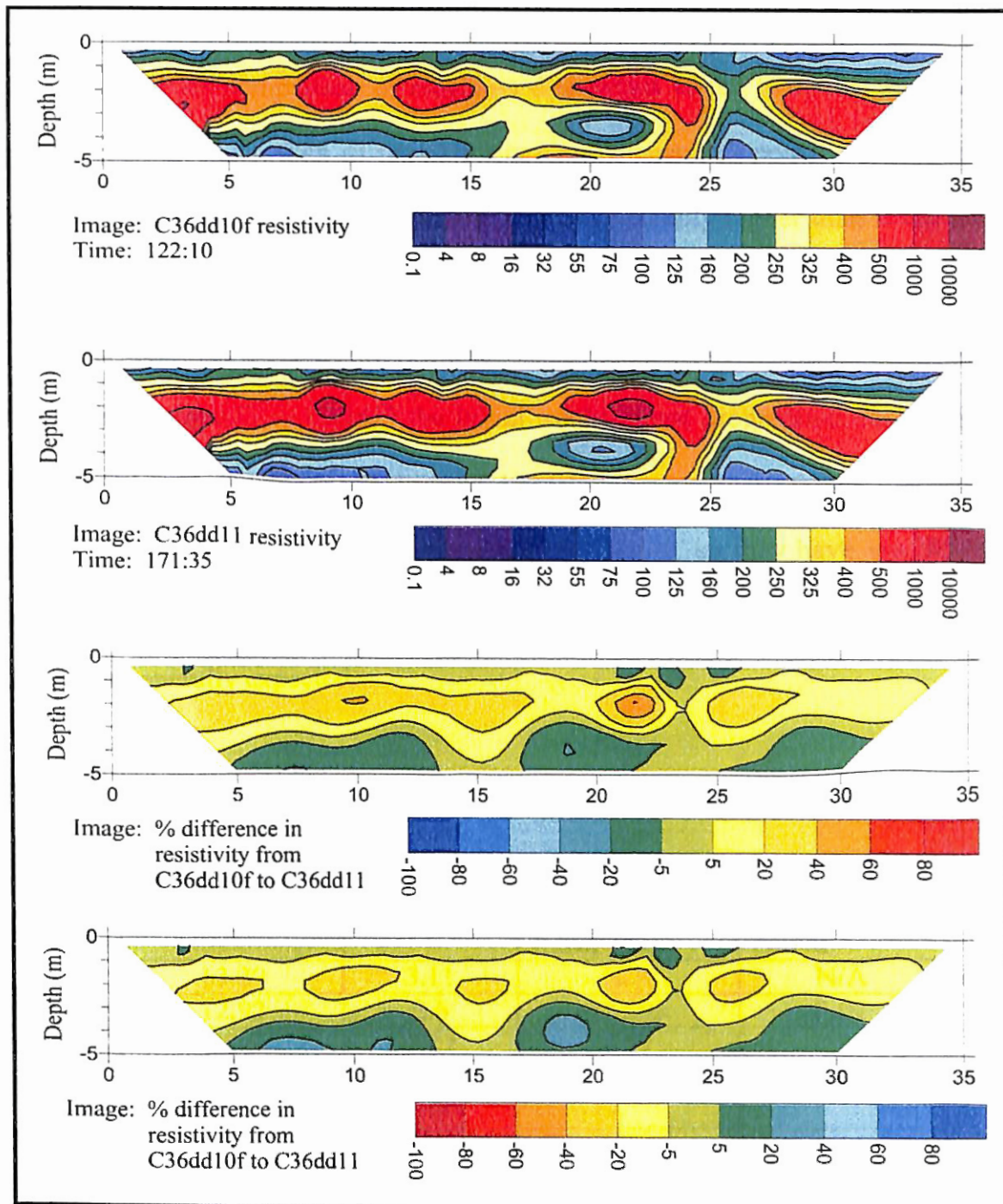




Plate B-9





### Cable A Dipole-Dipole Transient Data Error Statistics

Each data file was sparingly trimmed prior to transient inversion. Since transient analysis is a direct comparison of matching data points in the two files analyzed, it is better to keep as much data as possible since any unmatched points are automatically trimmed. This means that initial error statistics are generally higher than if the file were trimmed by the usual procedure.

The transient inversion error statistics reflect how well the two files match. For example from C36dd5 to C36dd3 the initial wetting front progression caused dramatic electrical changes and the RMS error of 122.93% is a product of that. Whereas, the C36dd10 files are close together in time, and are similar, so they have low RMS error percentages. Transient inversions cannot be trimmed, so this can produce error statistics higher than generally expected.

<b>File Name</b>	<b>Inverted RMS Error (%)</b>	<b>Inverted L2 Norm</b>	<b>Transient Inverted RMS Error (%)</b>	<b>Transient Inverted L2 Norm</b>
C36dd5	13.29	3.11	N/A	N/A
C36dd3	12.92	2.6	122.93	3.02
C36dd2-9	16.6	7.22	8.77	1.48
C36dd2	22.55	20.38	63.5	47.92
C36dd5	13.29	3.11	N/A	N/A
C36dd8	19.15	5.42	5.2	0.67
C36dd10a	17.26	3.79	8.31	1.44
C36dd10c	17.59	5.27	1.77	0.25
C36dd10d	17.48	5.26	1.39	0.05
C36dd10f	17.33	5.17	1.03	0.04
C36dd11	16.86	3.73	5.2	0.46

### Transient Inversions of Cable B Pole-Pole Data

Each of the following files was taken on Cable B with infinity electrodes IEE and IEW. This data series was better than any other statistically. Each file collected an identical number of data points, and no trims were necessary on any file.

Plate B-10

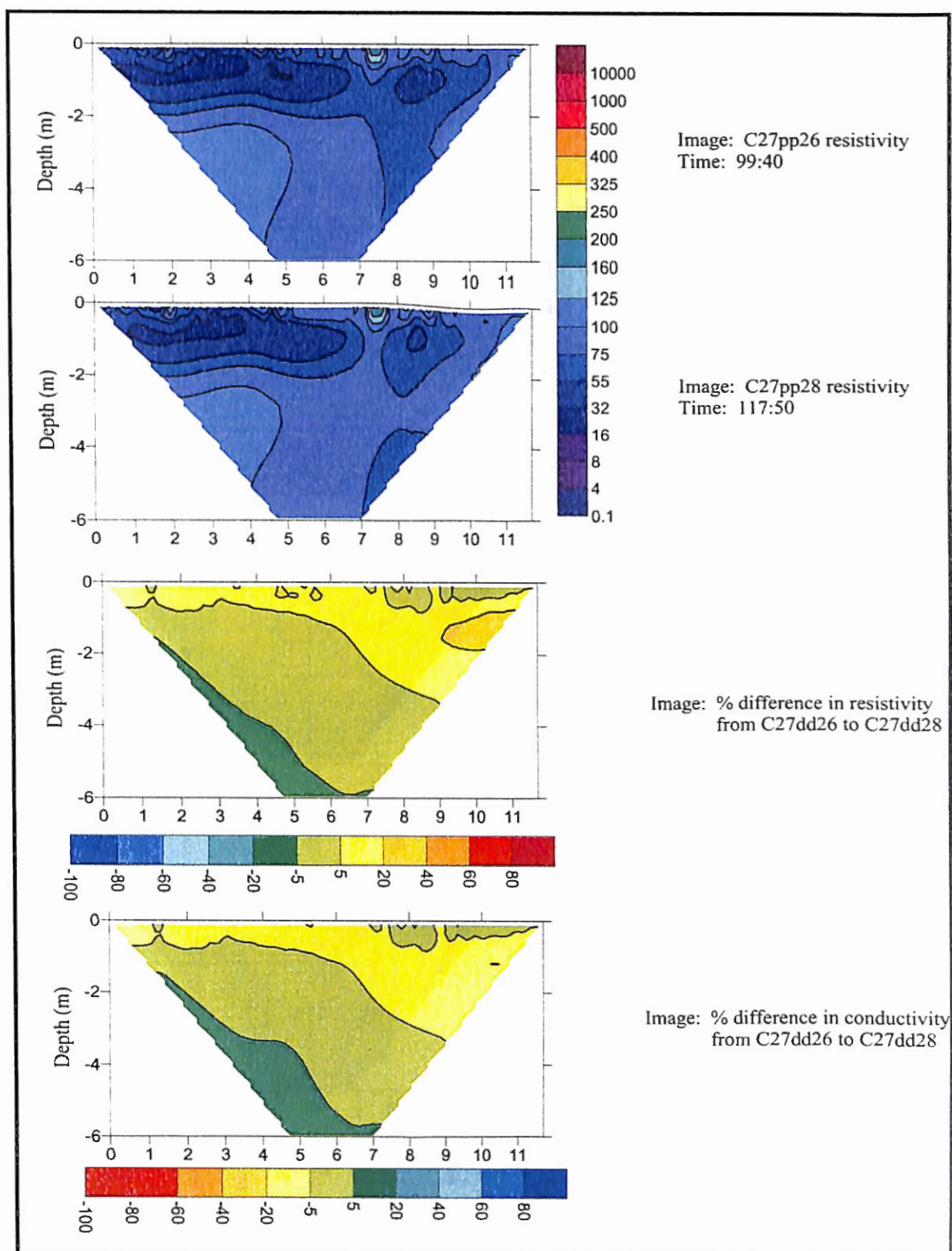
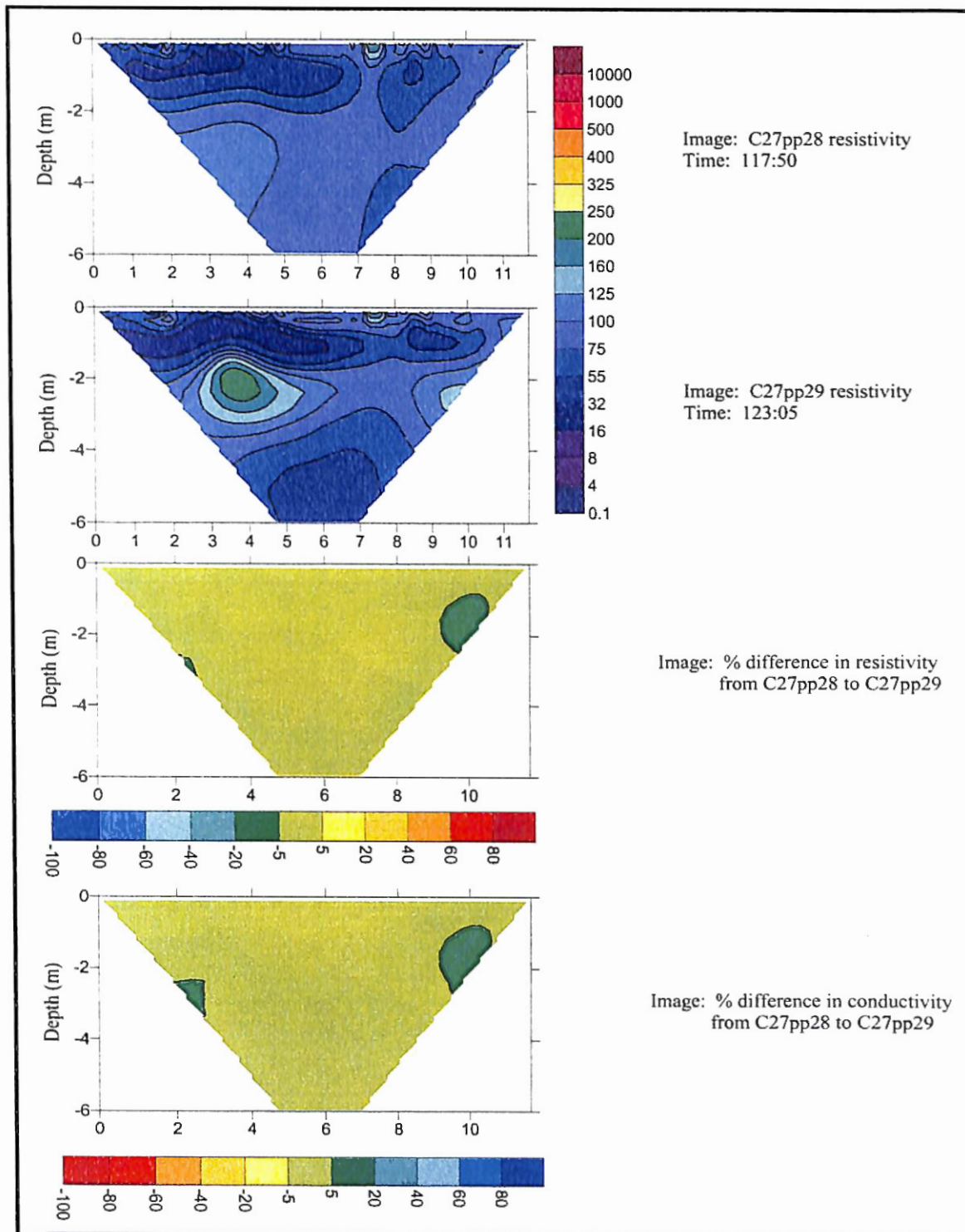


Plate B-11



# Plate B-12

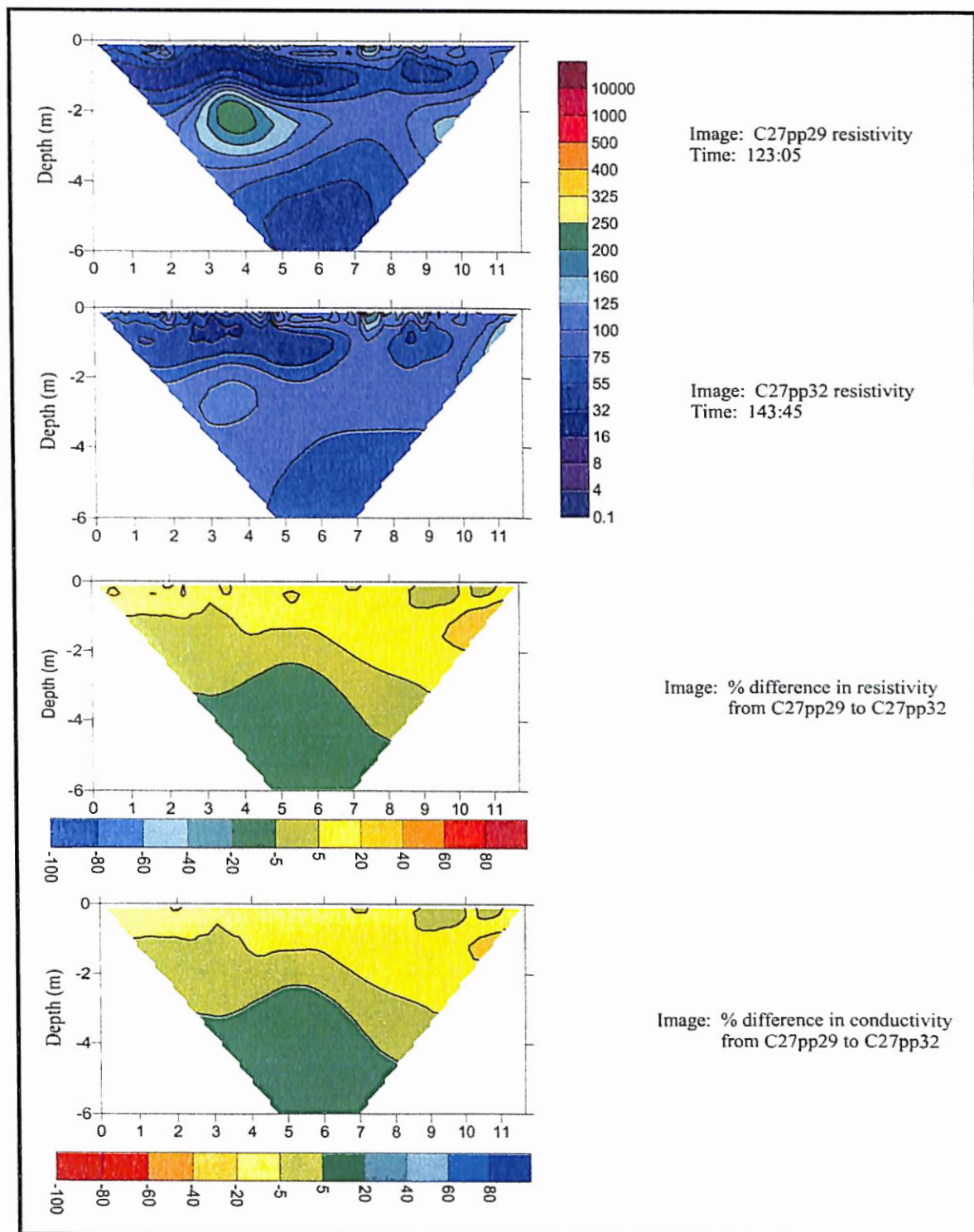




Plate B-13

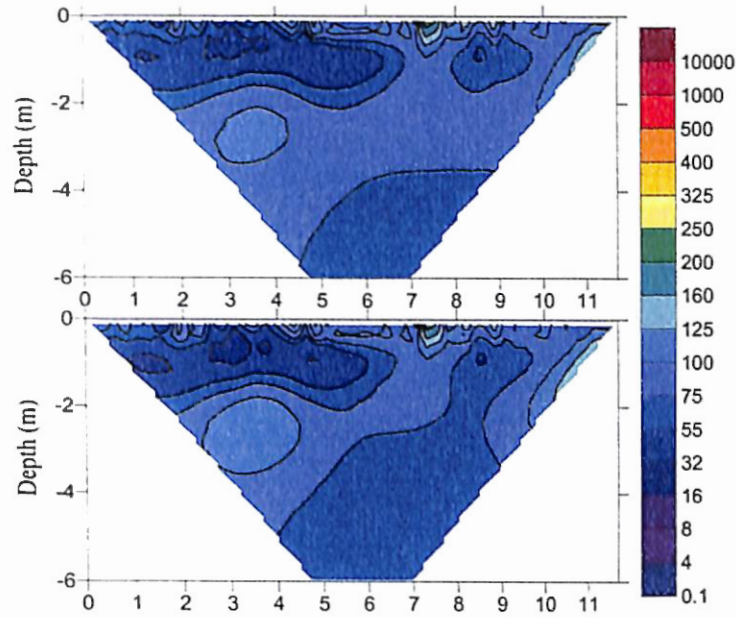


Image: C27pp32 resistivity  
Time: 143:45

Image: C27pp34 resistivity  
Time: 146:55

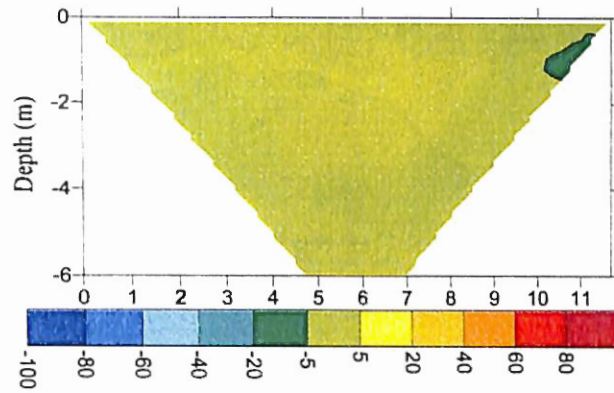


Image: % difference in resistivity  
from C27pp32 to C27pp34

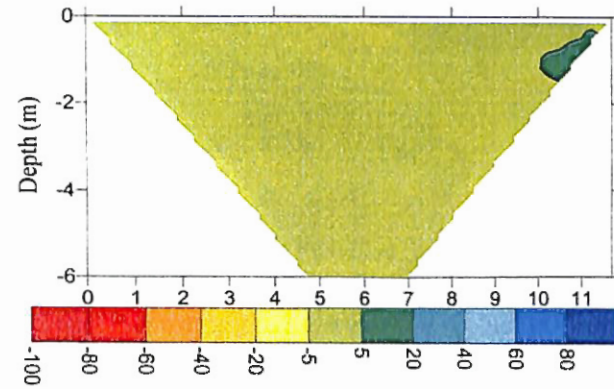


Image: % difference in conductivity  
from C27pp32 to C27pp34

Plate B-14

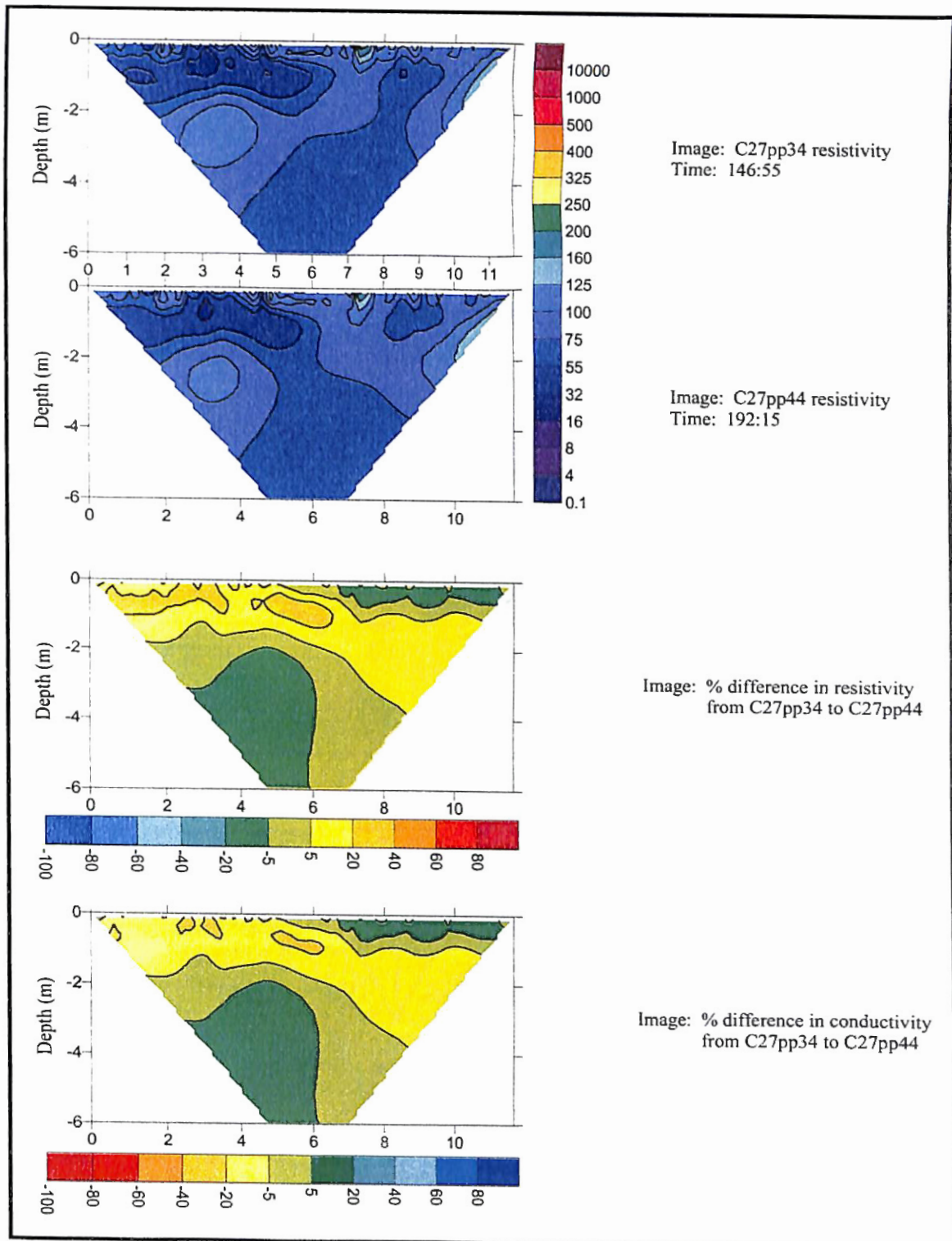
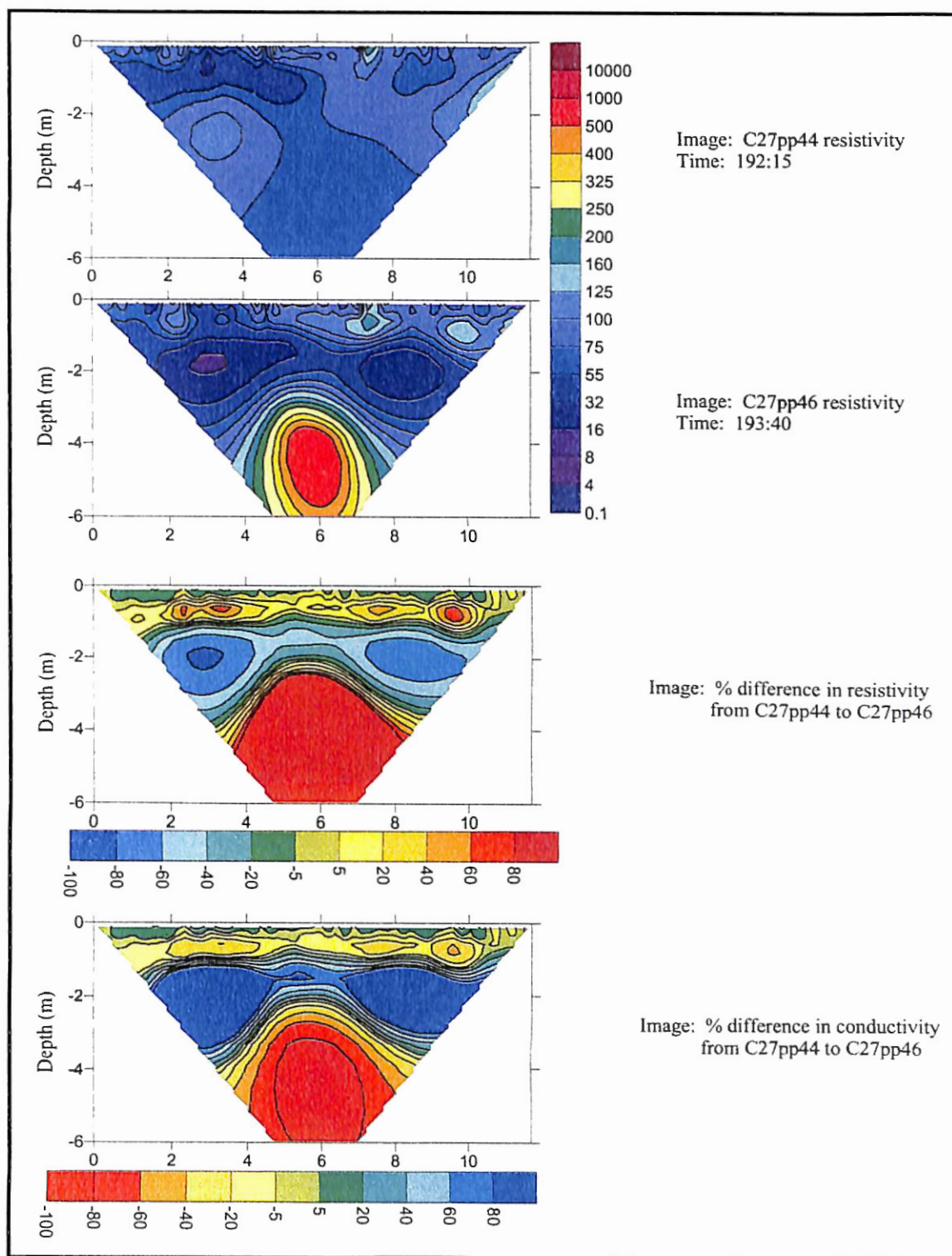


Plate B-15





#### Cable B Pole-Pole Transient Data Error Statistics

<b>File Name</b>	<b>Inverted RMS Error (%)</b>	<b>Inverted L2 Norm</b>	<b>Transient Inverted RMS Error (%)</b>	<b>Transient Inverted L2 Norm</b>
C27pp26	8.31	0.99	N/A	N/A
C27pp28	9.88	0.78	2.09	0.36
C27pp29	8.65	0.82	1.48	0.25
C27pp32	10.59	1.03	2.74	0.58
C27pp34	9.38	0.82	2.07	0.47
C27pp44	8.21	0.99	4.37	0.98
C27pp46	5.18	0.79	4.2	1.16

#### Transient Inversions of Cable A Pole-Dipole Data

Each of the following files was collected on Cable A using the infinity electrode IEE. Sensitivity for each of these files was greater than 0.01 to a depth of 7 meters.

Plate B-16

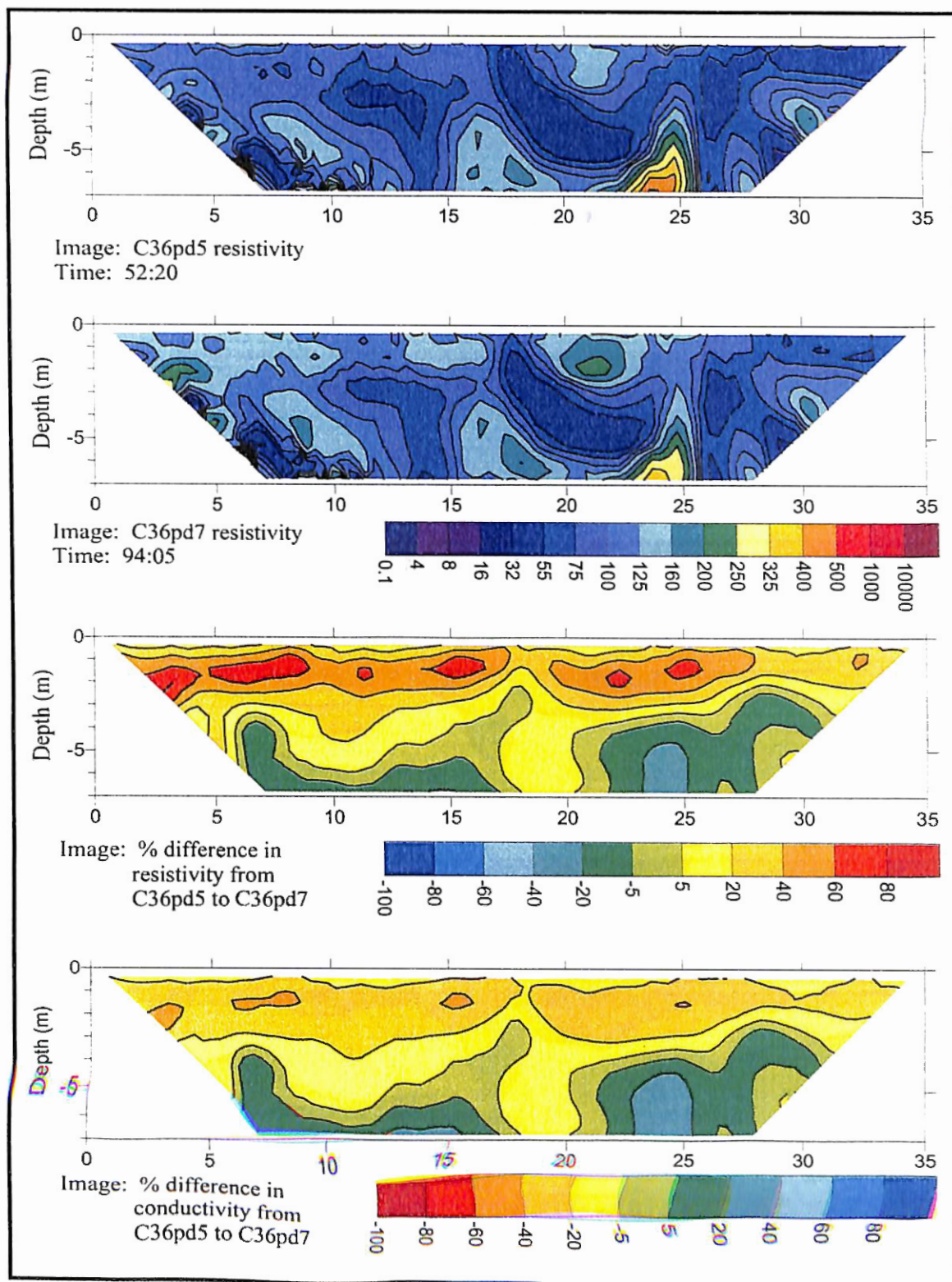


Plate B-17

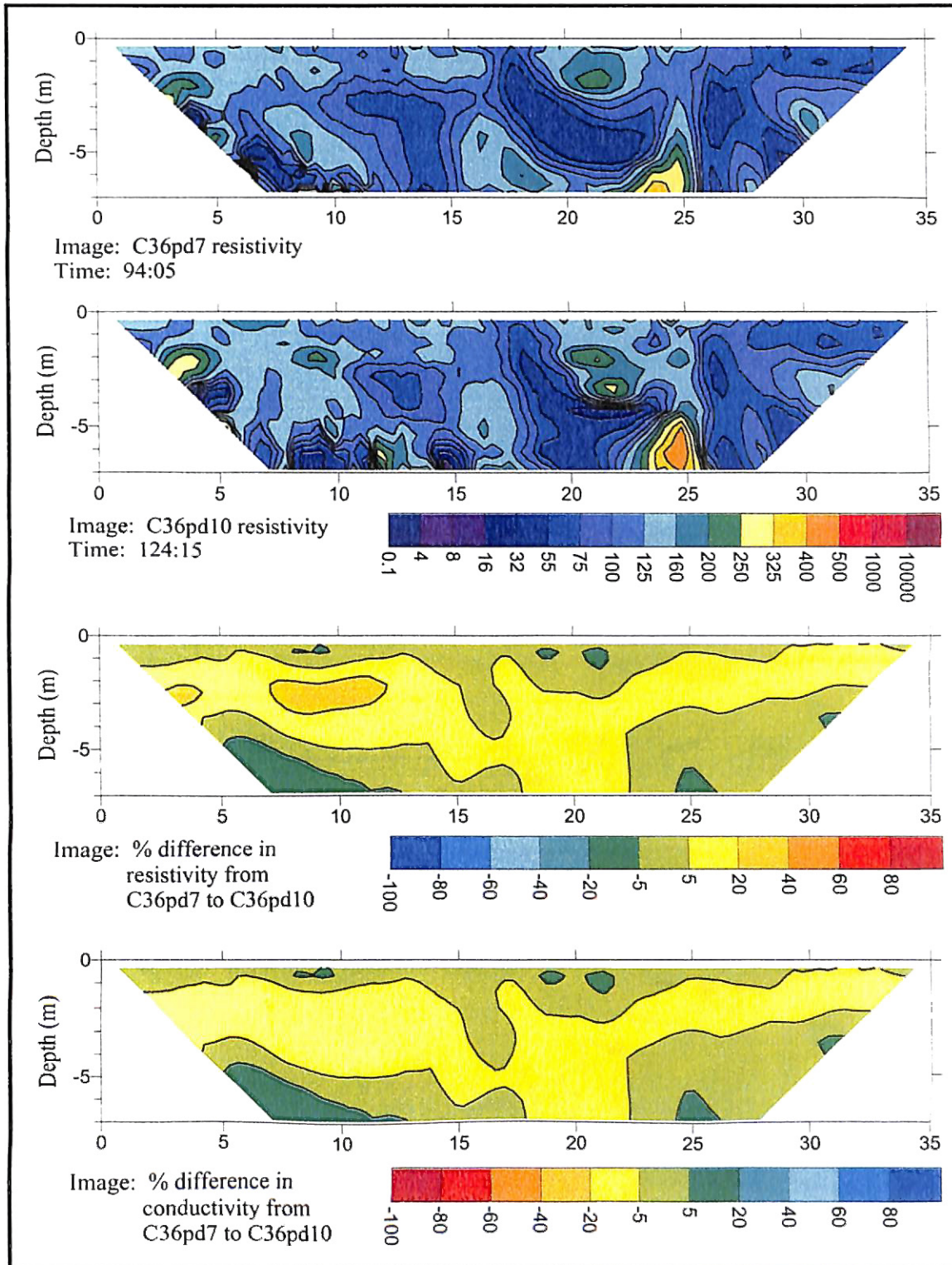
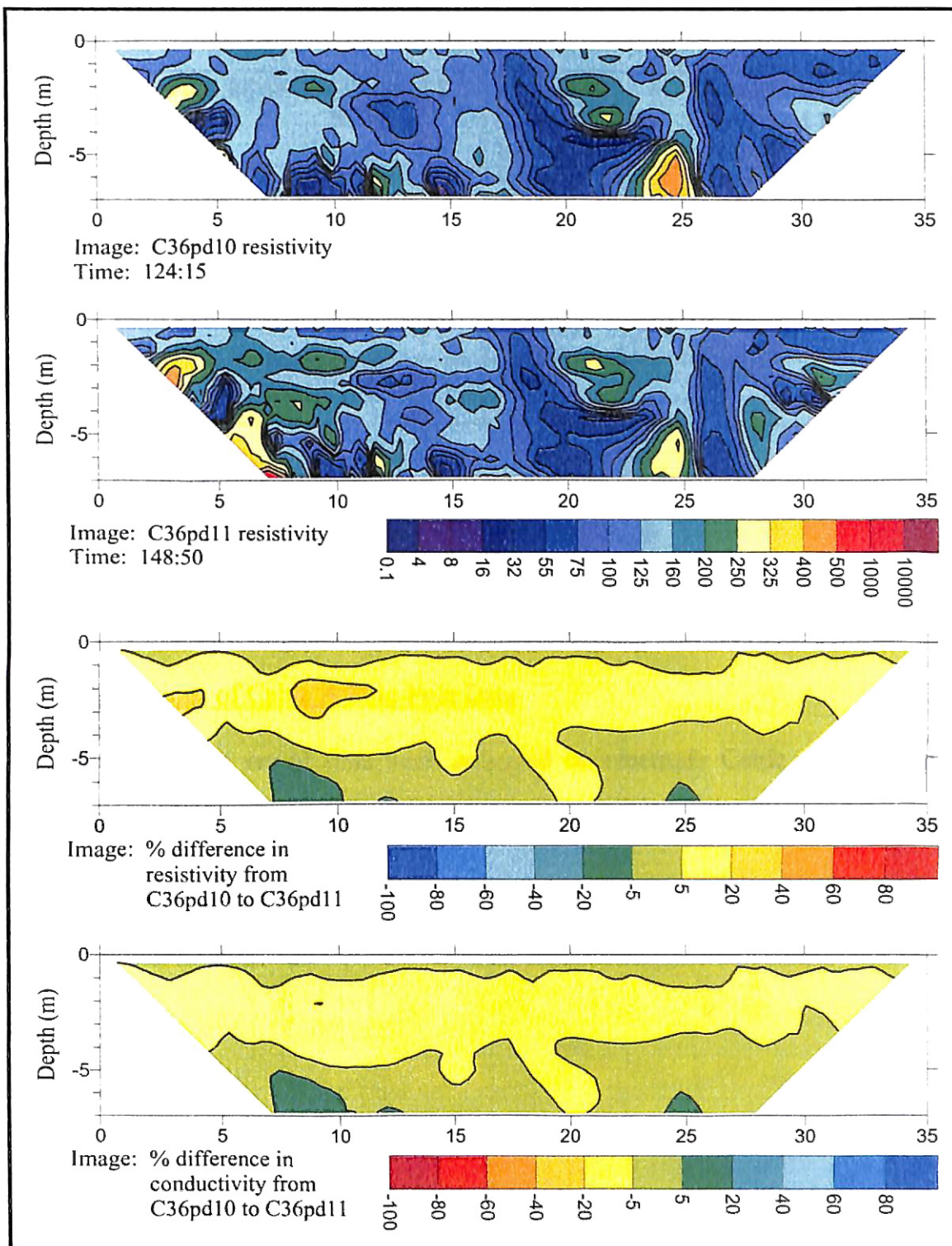




Plate B-18



### Cable A Pole-Dipole Transient Data Error Statistics

<b>File Name</b>	<b>Inverted RMS Error (%)</b>	<b>Inverted L2 Norm</b>	<b>Transient Inverted RMS Error (%)</b>	<b>Transient Inverted L2 Norm</b>
C36pd5	16.07	1.88	N/A	N/A
C36pd7	17.82	1.82	10.54	1.95
C36pd10	22.6	3.69	39.67	1.21
C36pd11	17.16	2.19	10.26	0.86

### Transient Inversions of Cable A Pole-Pole Data

The following set of files were collected on electrode Cable A using infinity electrodes IEE and IEW. Sensitivity plots were used to blank the files to a depth of 15 meters.

Plate B-19

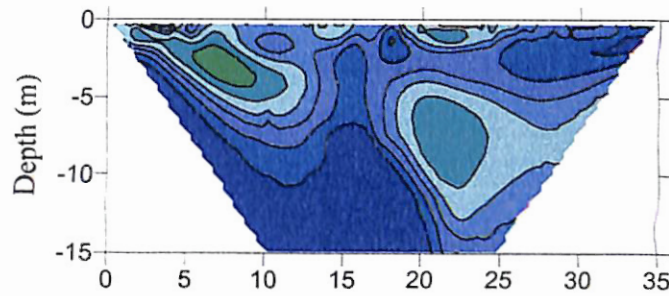


Image: C36pp12 resistivity  
Time: 93:30

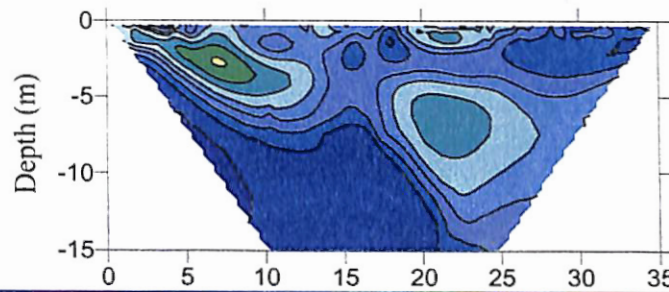


Image: C36pp13 resistivity  
Time: 100:00

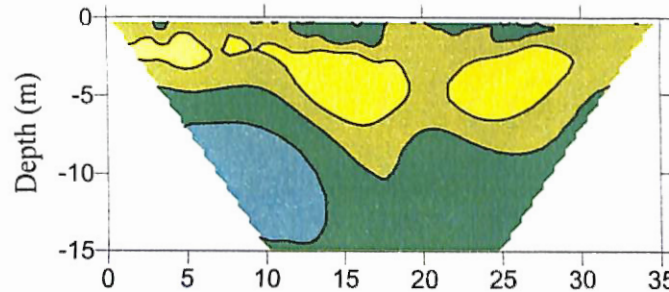
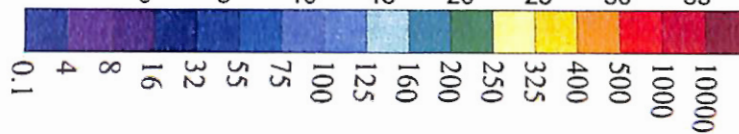


Image: % difference in  
resistivity from  
C36pp12 to  
C36pp13

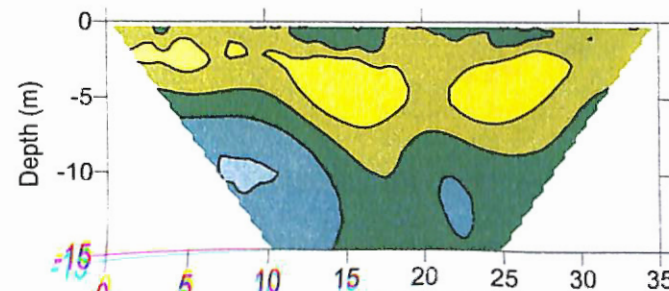


Image: % difference in  
conductivity from  
C36pp12 to  
C36pp13

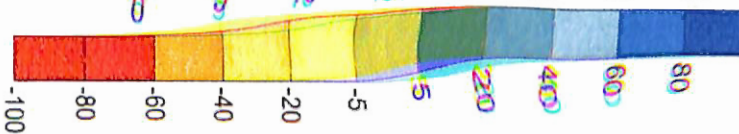




Plate B-20

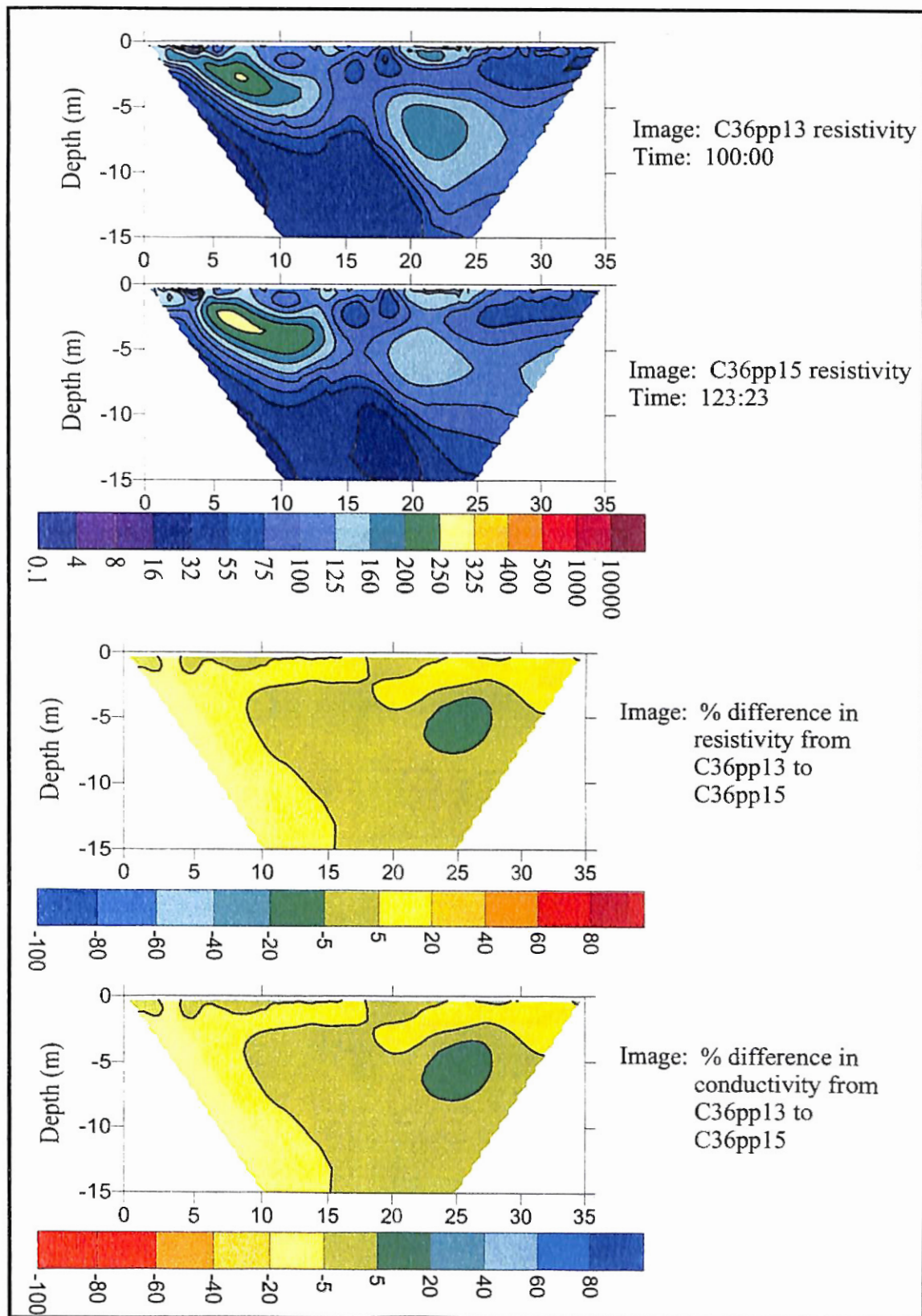


Plate B-21

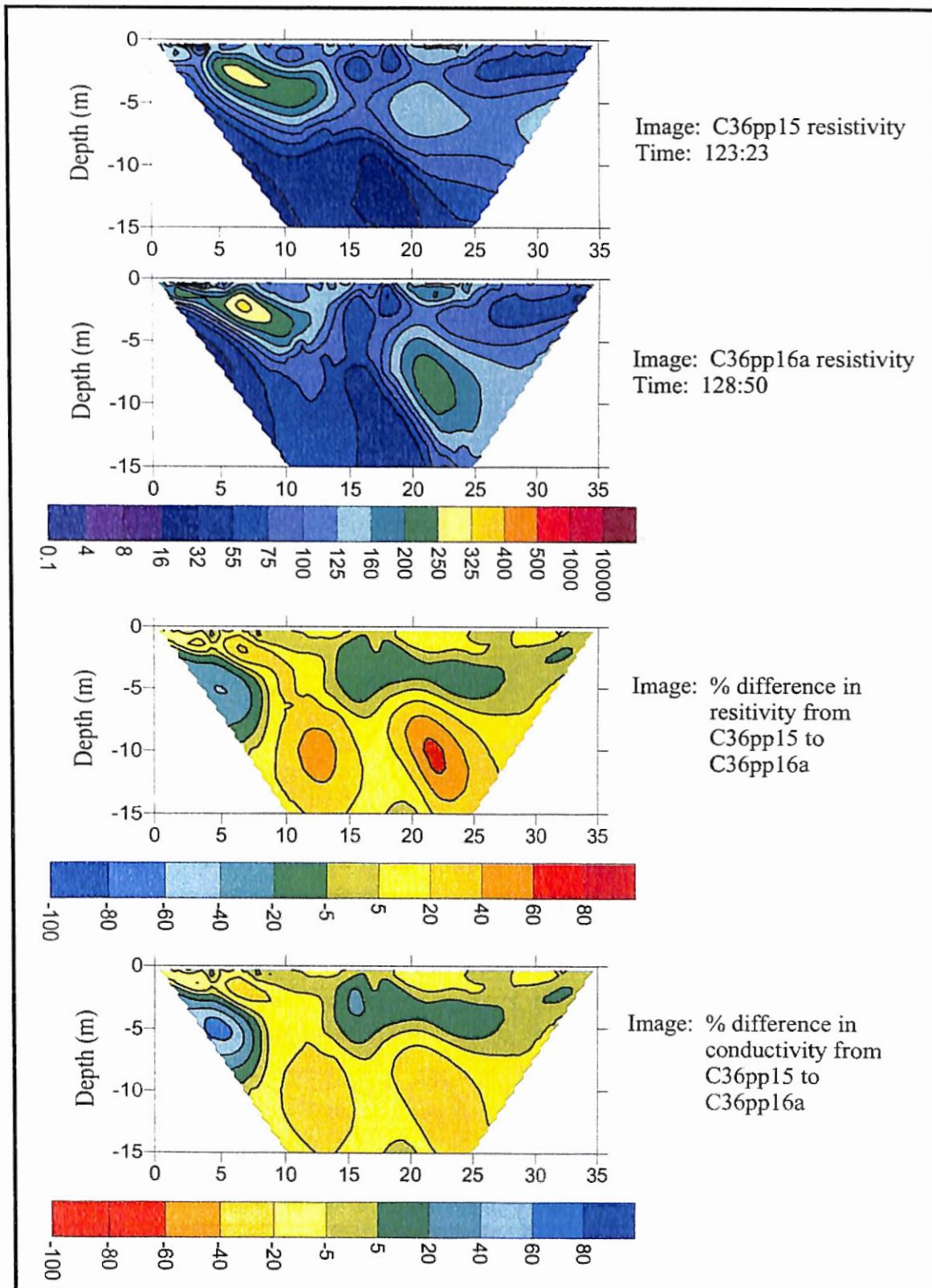




Plate B-22

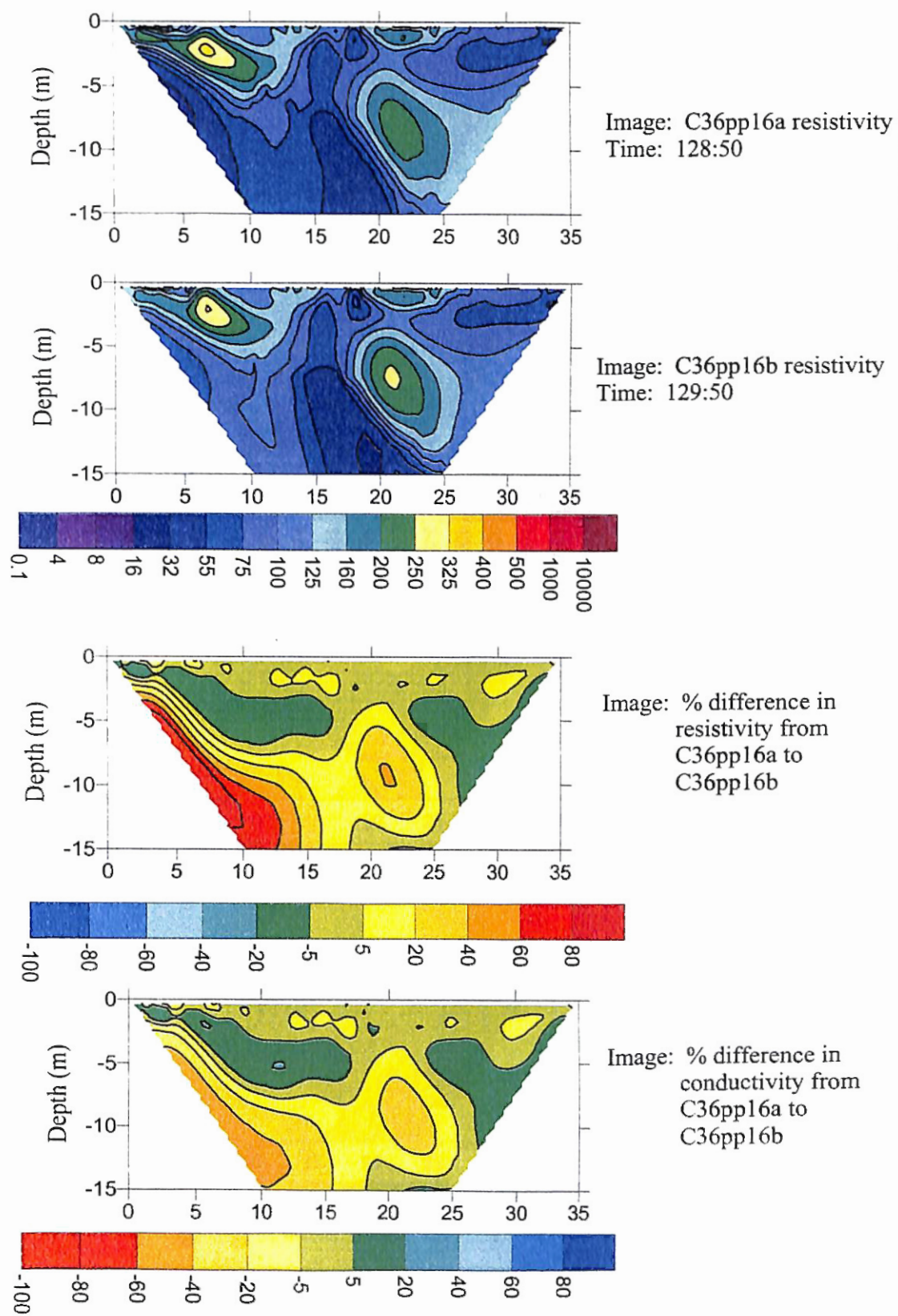


Plate B-23

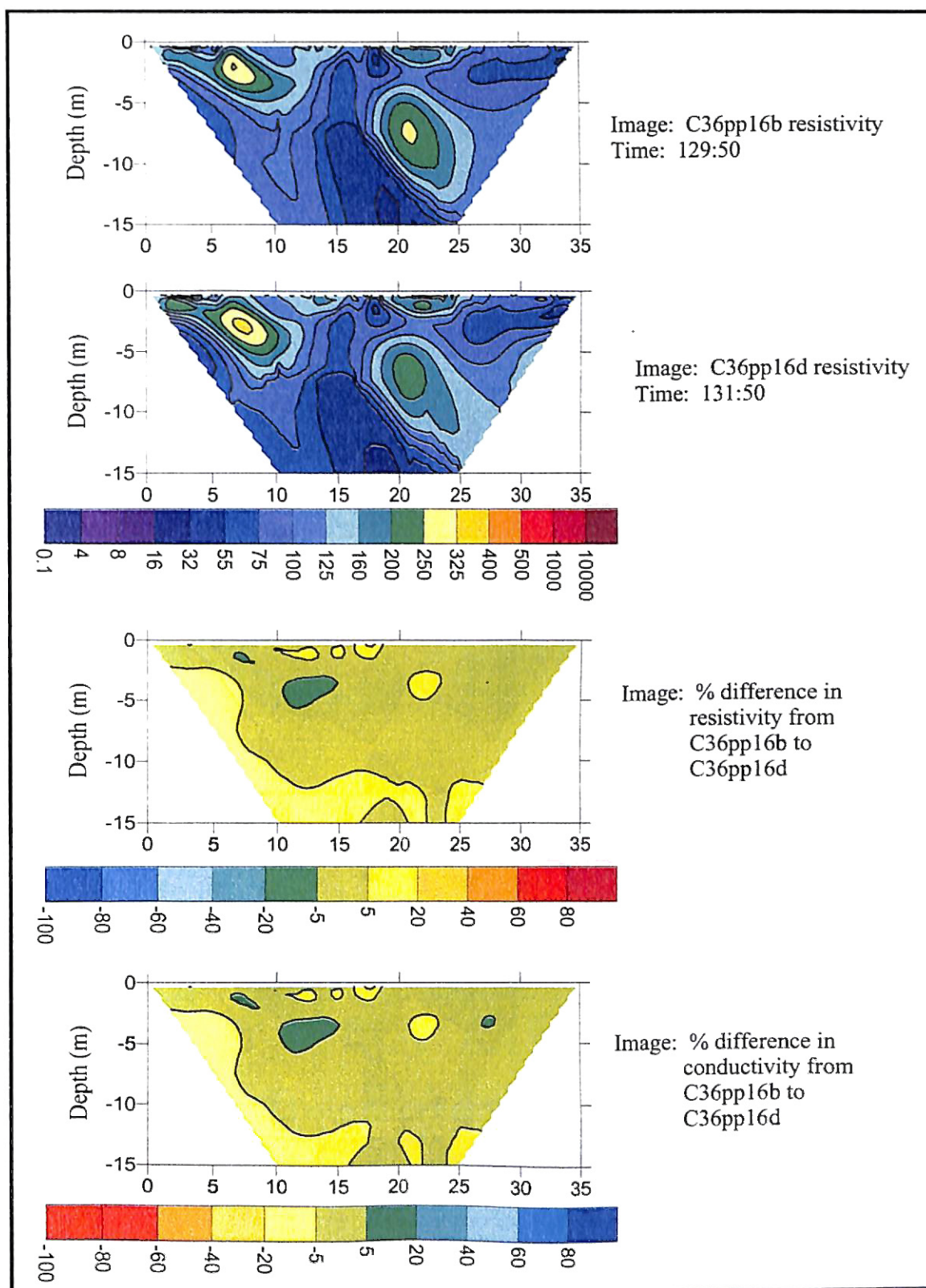


Plate B-24

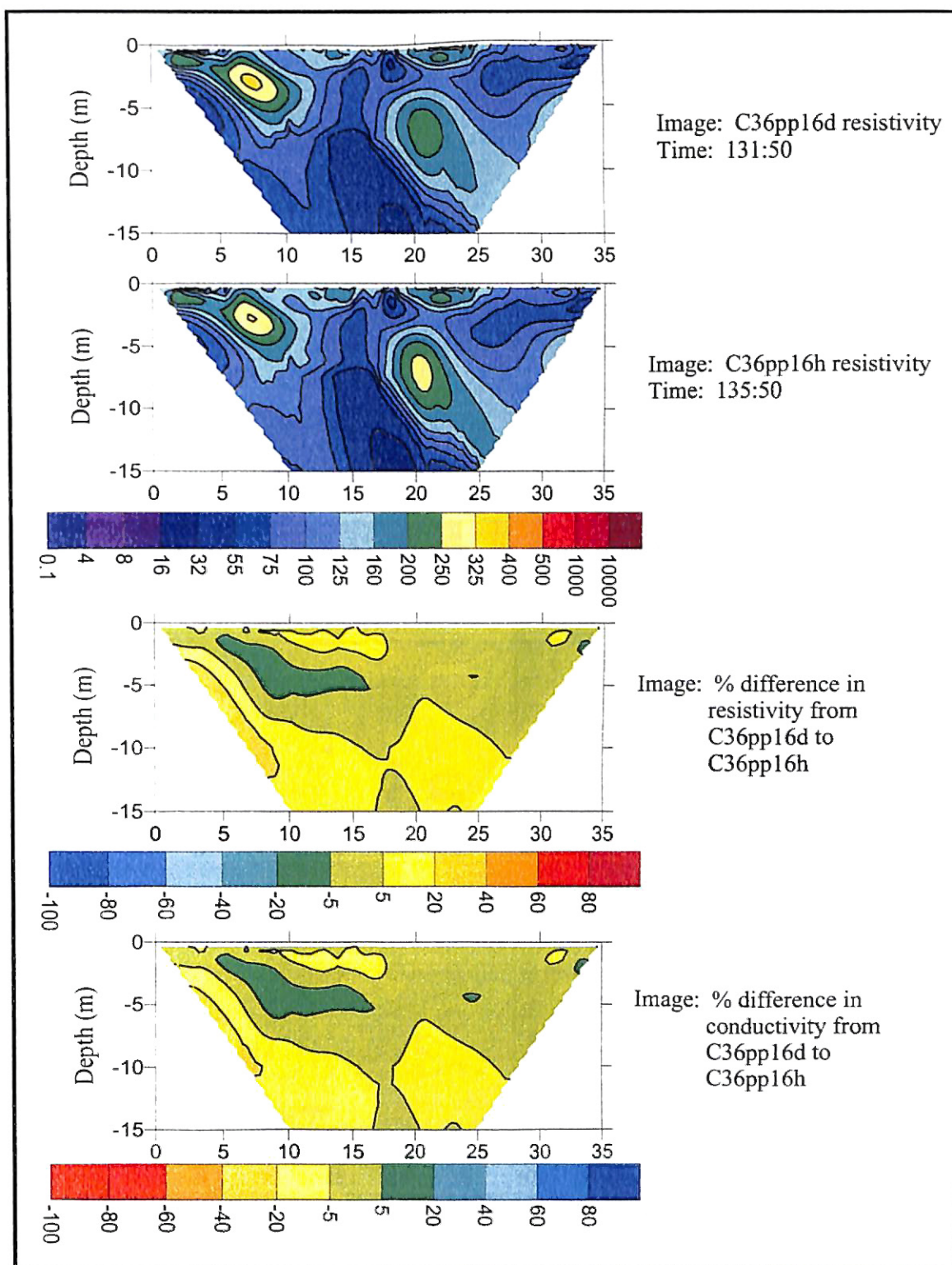




Plate B-25

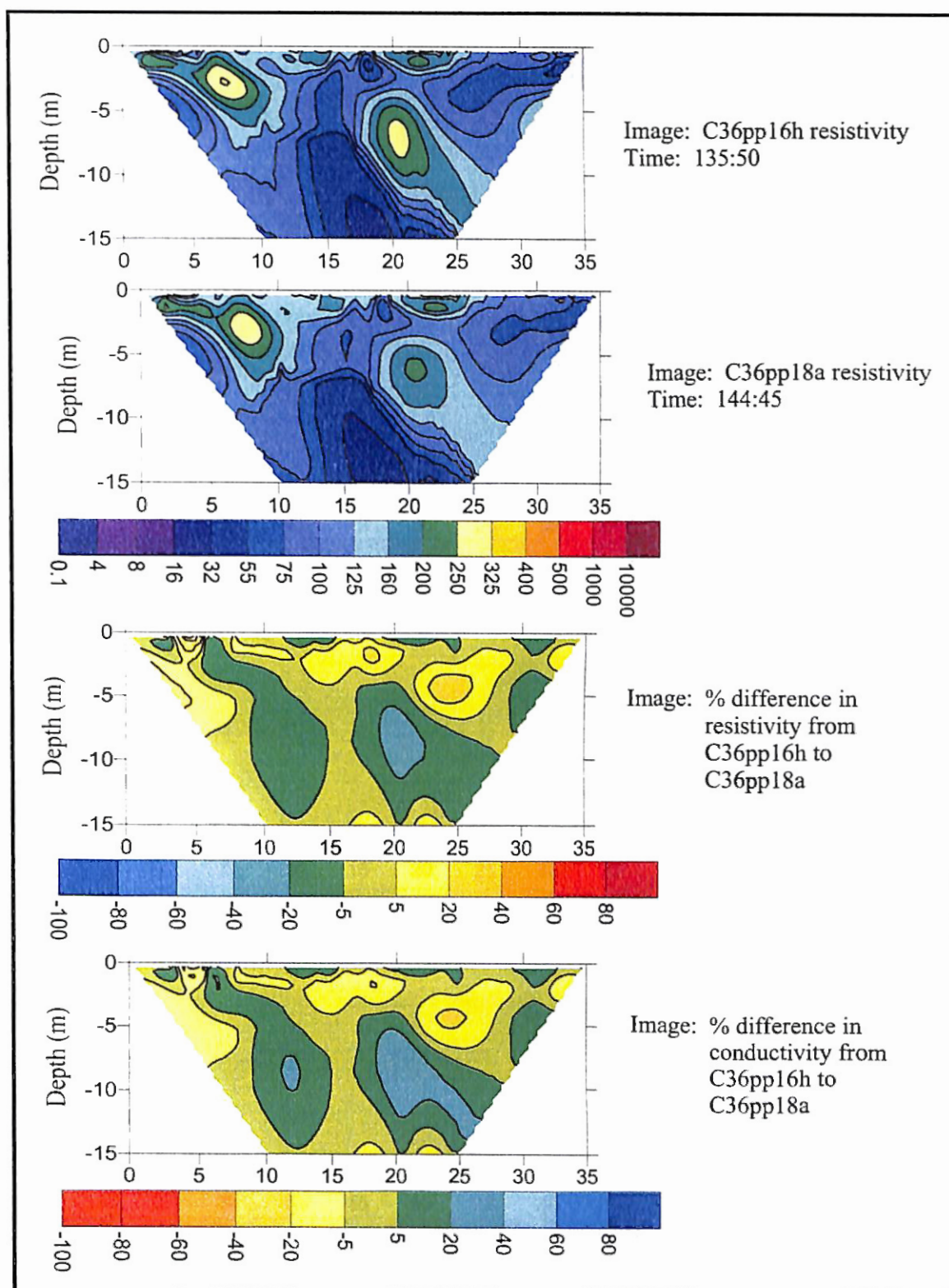


Plate B-26

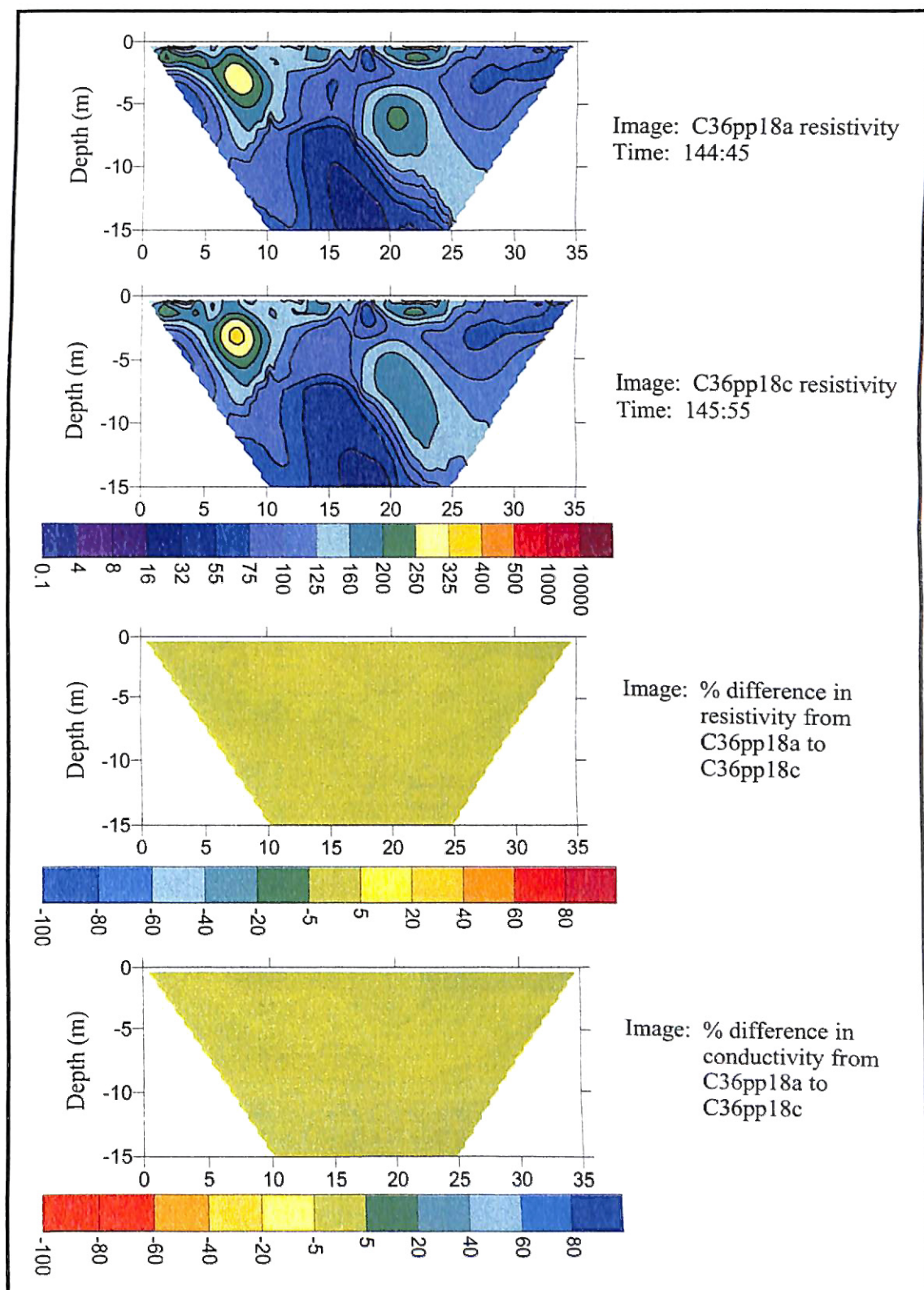


Plate B-27

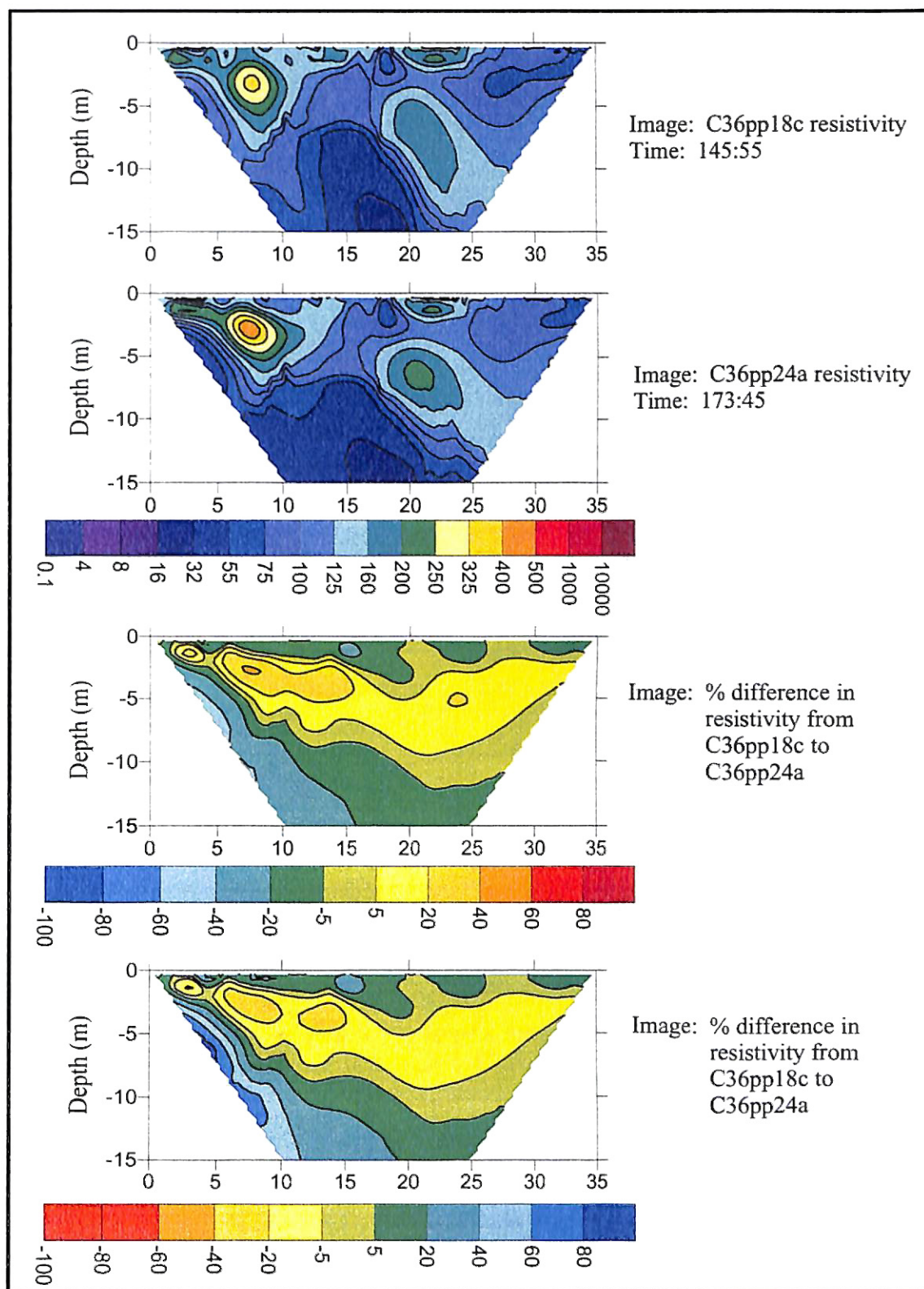




Plate B-28

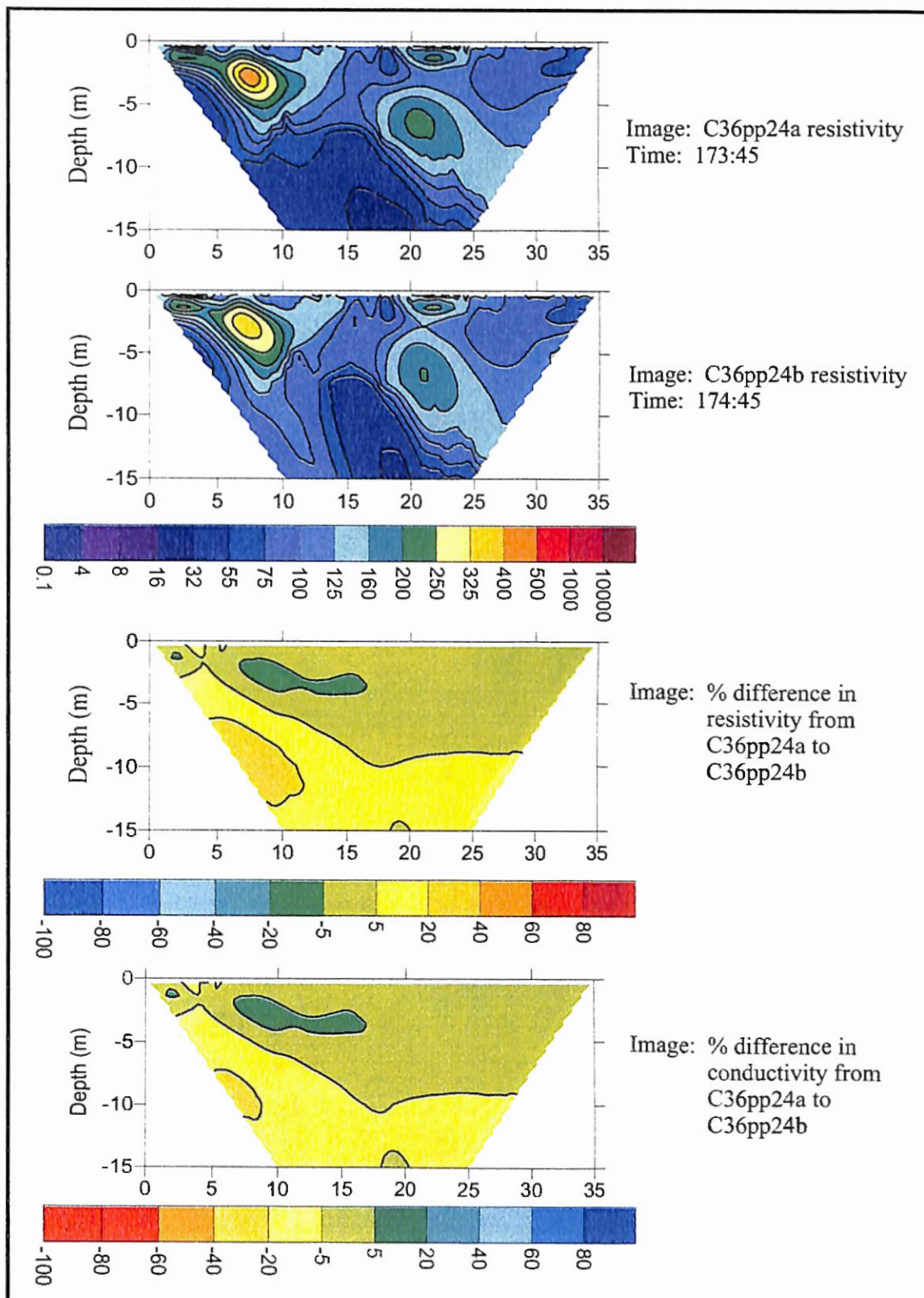




Plate B-29

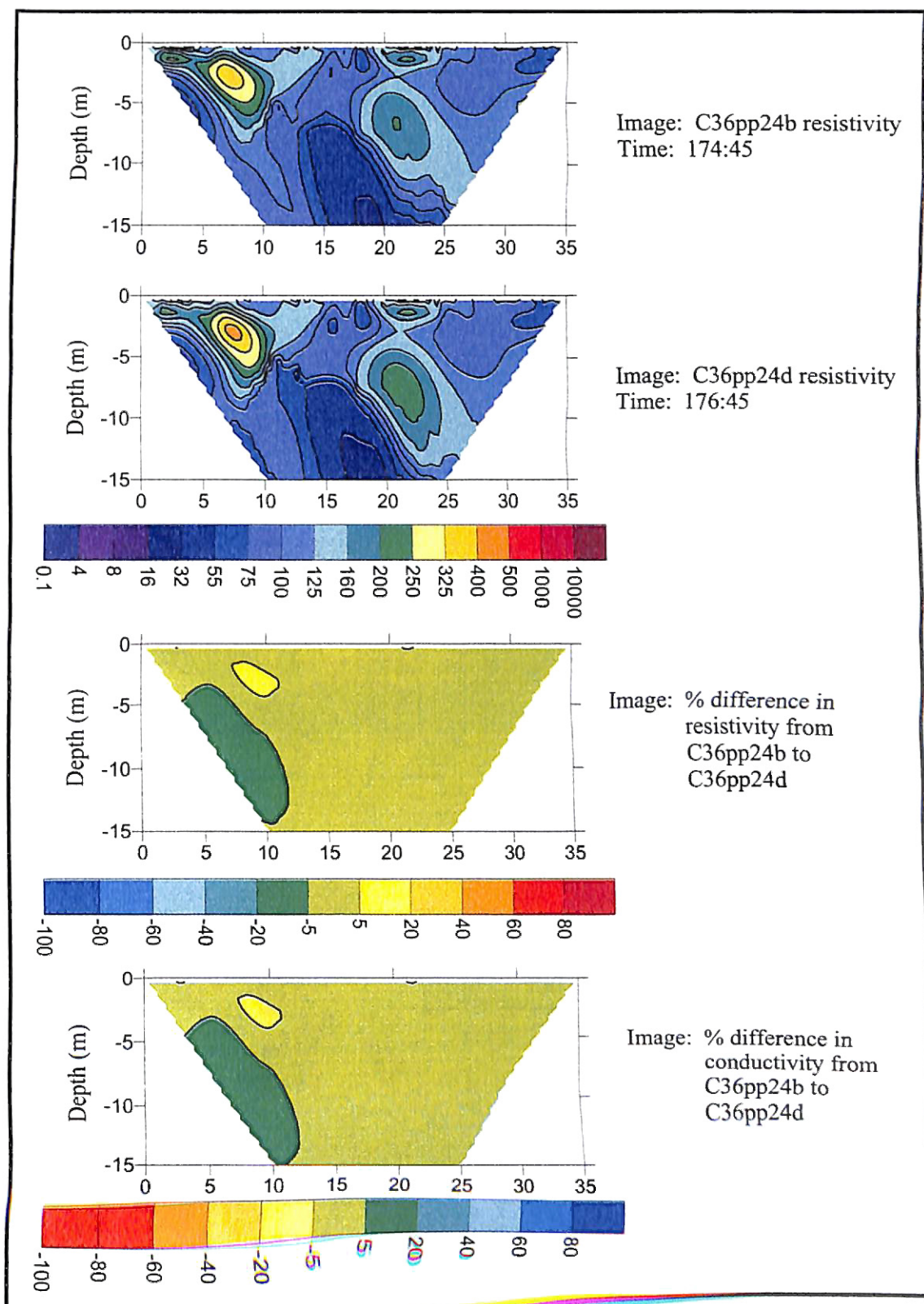


Plate B-31

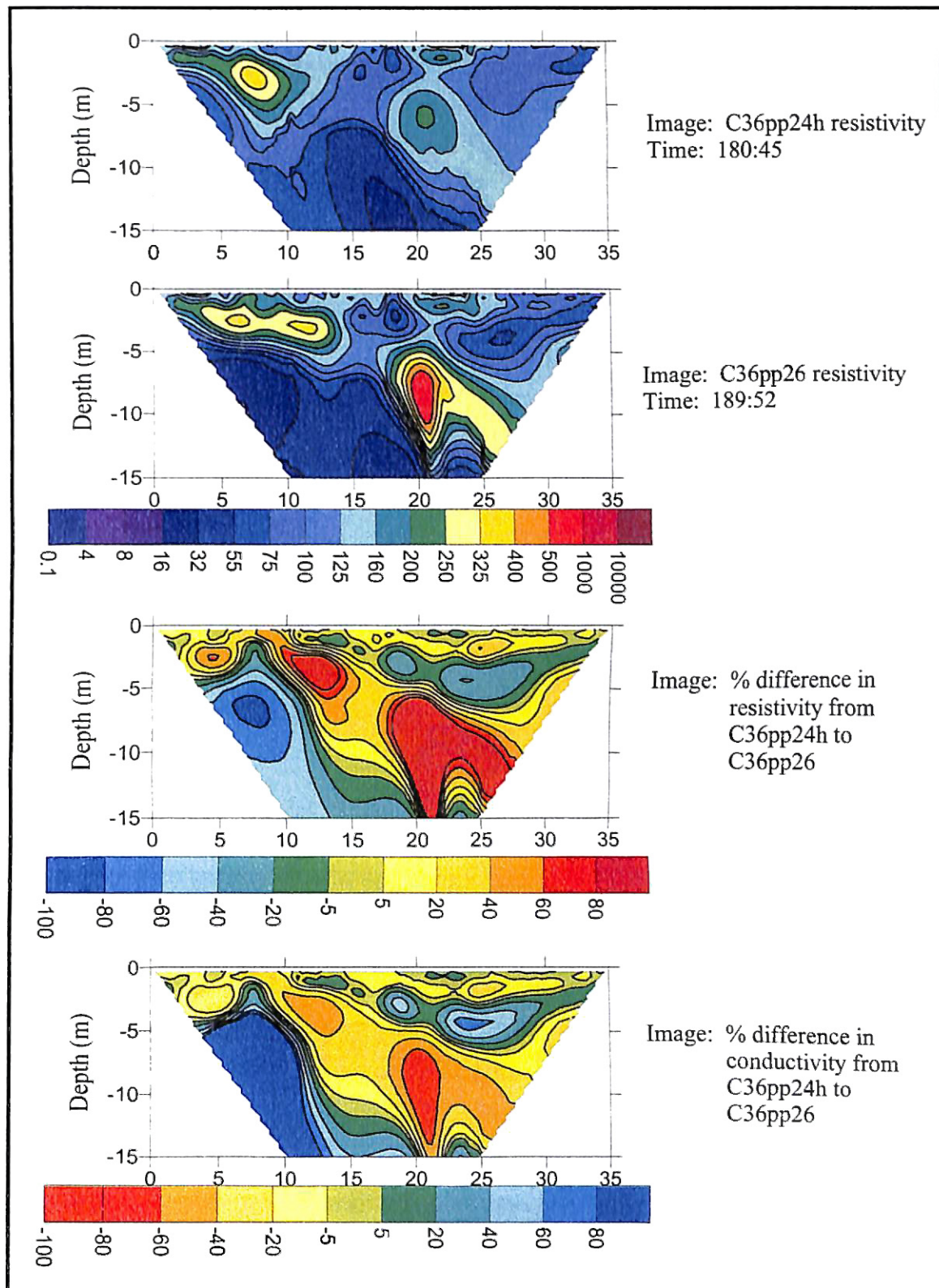


Plate B-30

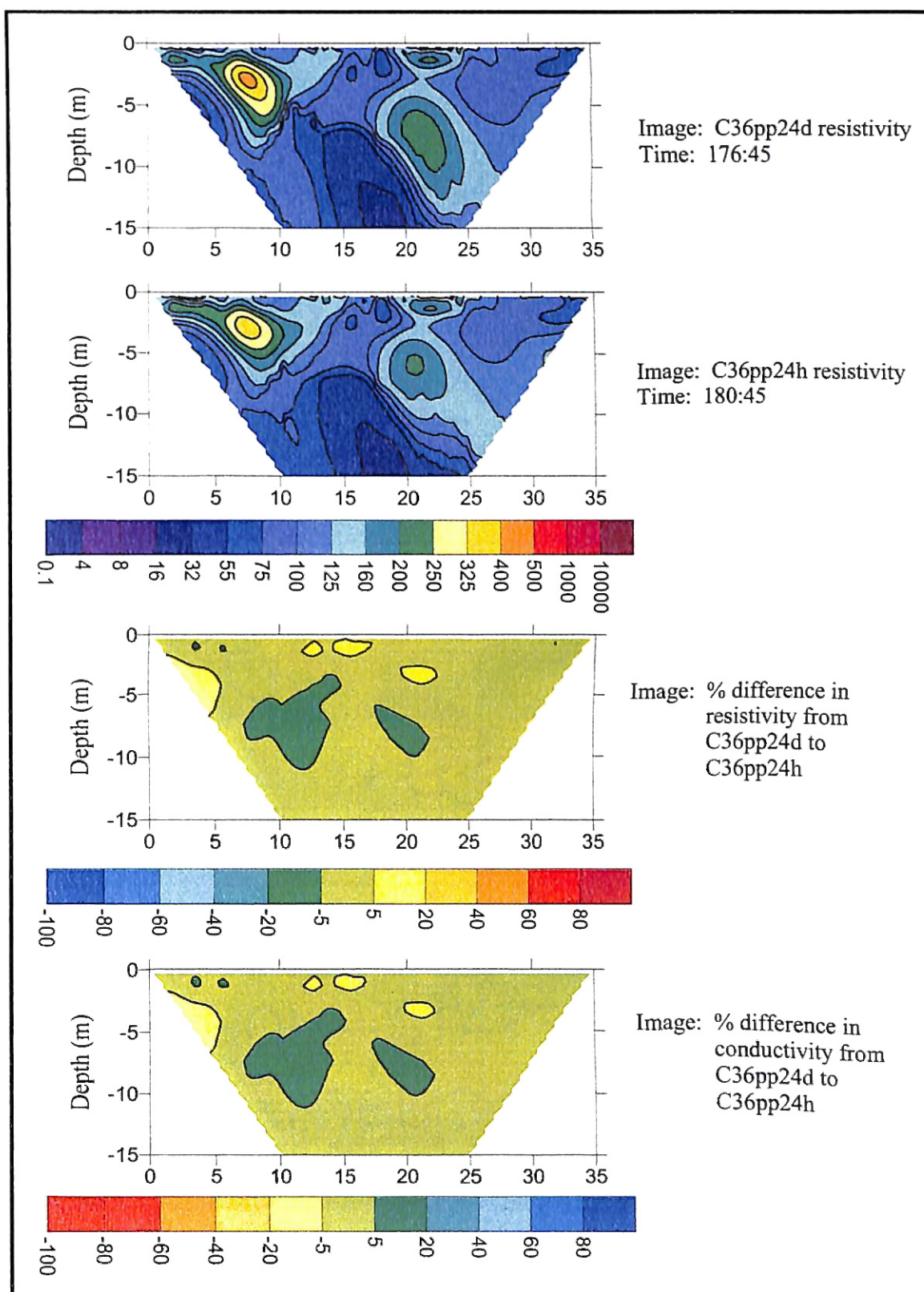
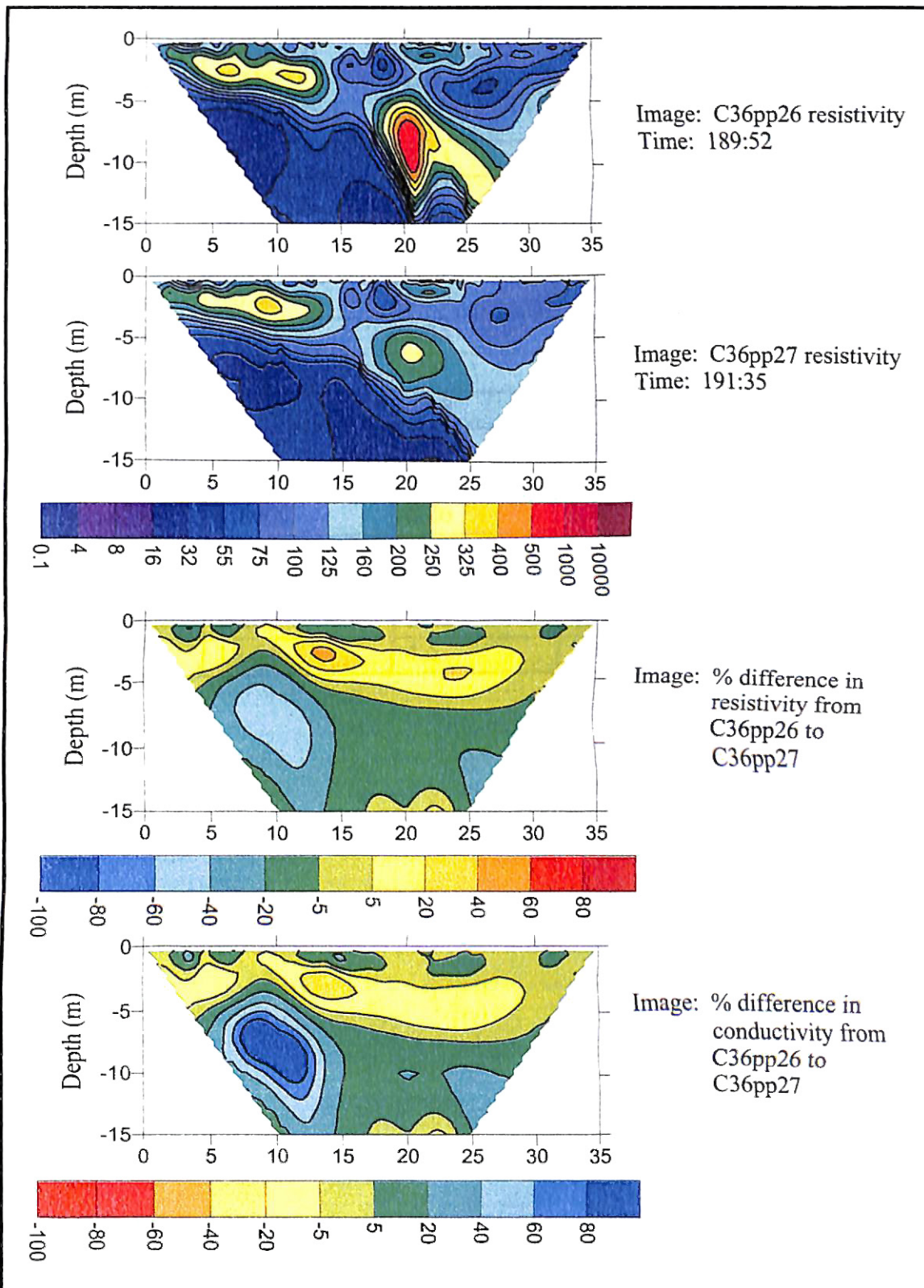




Plate B-32



Cable A Pole-Pole Transient Data Error Statistics

<b>File Name</b>	<b>Inverted RMS Error (%)</b>	<b>Inverted L2 Norm</b>	<b>Transient Inverted RMS Error (%)</b>	<b>Transient Inverted L2 Norm</b>
C36pp12	21.14	9.83	N/A	N/A
C36pp13	19.13	8.54	2.86	0.69
C36pp15	20.35	9.3	2.41	0.46
C36pp16a	23.73	10.92	4.68	0.75
C36pp16b	20.46	6.56	3.52	1.24
C36pp16d	21.56	6.86	2.81	1.05
C36pp16h	22.45	7.4	2.5	0.41
C36pp18a	20.13	6.38	3.89	1.0
C36pp18c	19.73	6.17	1.16	0.17
C36pp24a	21.15	6.41	4.3	0.73
C36pp24b	19.67	6.26	2.76	1.11
C36pp24d	20.84	6.35	1.72	0.46
C36pp24h	21.1	6.68	2.69	1.05
C36pp26	20.05	5.42	13.28	2.66
C36pp27	19.64	4.67	4.44	1.28

VITA

①

Julie Ann Turrentine

Candidate for the Degree of

Master of Science

Thesis: USING TRANSIENT ELECTRICAL RESISTIVITY TO CHARACTERIZE  
AN ACTIVE HEAP LEACH SITE

Major Field: Geology

Biographical:

Personal Data: Born in Ft. Smith, Arkansas, On August 17, 1980.

Education: Graduated from Stigler High School, Stigler, Oklahoma in May 1998.  
Received Bachelor of Science degree in Geology from Oklahoma State  
University, Stillwater, Oklahoma in December 2001. Completed the  
requirements for the Master of Science degree with a major in Geology at  
Oklahoma State University in May 2004.

Experience: Employed by Oklahoma State University, Department of Geology as  
an undergraduate and graduate research assistant and teaching assistant,  
2001 to present.

Professional Memberships: Geological Society of America, Oklahoma State  
University Geological Society, American Association of Petroleum  
Geologists